
UNIVERSITÀ DEGLI STUDI DI PADOVA

SCUOLA DI SCIENZE
Dipartimento di Fisica e Astronomia
"Galileo Galilei"

CORSO DI LAUREA MAGISTRALE IN FISICA

---

# Gamma-ray emission from molecular clouds with the Cherenkov Telescope Array and the cosmic ray spectrum in the Galaxy

---

*Autore:*
Giada PERON

*Relatore esterno:*
Prof. Felix AHARONIAN

*Relatore interno:*
Prof. Roberto TUROLLA

*Corelatori esterni:*
Prof.ssa Sabrina CASANOVA
Dr.ssa Roberta ZANIN

Anno accademico 2016/2017

# *Abstract*

**Gamma-ray emission from molecular clouds with the Cherenkov Telescope Array and the cosmic ray spectrum in the Galaxy**

In this work we calculate the diffuse emission from molecular clouds (MCs) in the Galaxy at very high energy (from hundreds of GeV to hundreds of TeV). We present the results from the analysis of the simulated emission of these sources as it will be detected by the incoming imaging Cherenkov telescope detector, the Cherenkov telescope array (CTA) and we estimate the capabilities of such measurements to constrain the cosmic ray spectrum in the cloud. Molecular clouds are regions of the Galaxy, typically a few tens of parsec in size, where the density of cold molecular gas is often orders of magnitude higher than that of the diffuse interstellar medium. The MCs high gas density enhances the gamma-ray emission produced through the hadronic channel by cosmic ray nuclei interacting with the ambient gas. The gamma-ray emission from MCs depends only upon the total mass and the distance of the cloud. Assuming to know them from radio observations, one can thus test the cosmic ray spectrum far away from the Earth, in regions of the Galaxy, where no direct measurements of the cosmic ray spectrum can be carried out. MCs serve then as cosmic ray barometers.

# Summary

Cosmic rays (CR) have been known for more than a hundred years, but some aspects of the physics of these high energy particles are still mysterious. While their composition is pretty common: electrons, protons and a minority of heavier particles, their energy distribution is astonishing. Direct measurements of the cosmic ray spectrum have been carried out with air balloons and satellites in the Earth vicinity and showed that these particles energy extends from hundreds of MeV ($\equiv 10^6$ eV) to $\sim 1$ PeV ($\equiv 10^{15}$ eV). Which are the mechanisms and the astronomical objects responsible of their acceleration, is not known. Supernova remnants have been proved to accelerate particles but up to a maximum energy of $\sim 100$ TeV. Other mechanisms must be involved in the acceleration of higher energy particles: star formation regions or the black hole at the center of the Galaxy may be involved, but this has to be demonstrated. Another noteworthy fact is that the spatial distribution of cosmic rays at Earth appears to be very isotropic. This suggests the idea that these particles, after being accelerated, propagate in the Galaxy, where they undergo continuous deflections because of the magnetic fields of the interstellar plasma. We expect then to find a pretty uniform distribution of cosmic rays all around the Galaxy, the so called *sea* of Galactic cosmic rays. Nevertheless our information on CR are limited to the detections performed in our neighborhood. A priori we can't neither assume that a CR sea exists, nor that it is characterized by the same energy density we measure in our *local* environment ($\rho \sim 1$ eV/cm$^3$ ). A complete knowledge of the Galactic cosmic rays distribution would provide crucial constraints on the origin of these particles and on the physics of their exceptional accelerators, giving the unique chance to explore processes in a range of energy impossible to achieve in any terrestrial laboratory.

Probes can't go much further than the solar system, so direct measurements are limited to our ambient. A new extraordinary chance to probe the *Galactic* cosmic rays spectrum however is embedded by gamma ray astrophysics. This discipline explores the astrophysical radiation at the highest extreme of the electromagnetic spectrum. Usually one divides $\gamma$ photons into Low Energy (LE) photons $\sim$ MeV, High Energy (HE) photons $\sim$ GeV and Very High Energy (VHE) photons $\sim$ TeV. Cosmic rays produce gamma radiation when they interact with the interstellar matter: for example CR protons that hit protons of the interstellar medium give birth to an instable $\pi^0$ that quickly decay in $\gamma$ rays. The energy of the released photons will depend on the energy of the parent particles: roughly it will have the 10% of the primary energy, so the measurements of these HE gamma rays spectrum may lead us to the knowledge of cosmic rays spectrum at even higher energies.

To enhance the chances of production of gamma rays, one should look for big concentration of gas. Molecular clouds (MCs) for this purpose are a perfect target. They are massive (up to $10^7$ $M_\odot$) clumps of molecules, mostly $H_2$, concentrated in a restricted space ($\sim$ 10-100 pc). Assuming a certain spectrum for primary proton, the resulting gamma-ray flux from molecular clouds depends only on their mass and

on their distance. MCs are traced with radio survey of the CO emission. Last year a catalog of clouds was released, based on the survey of the Harvard-Smithsonian Center for Astrophysics. This catalog contains 1064 MCs, some of which are very massive and close enough to be detectable with the upcoming $\gamma$-ray instruments.

The gamma ray signal can arrive to us practically undeflected from each region of the Galaxy. These particles originate from non-thermal processes, hence there are not many classes of objects in the Galaxy that produce them. Object like supernova remnants, pulsars or micro-quasars can accelerate particles that consequently radiates in this energy band. Non thermal radiation can rise from the diffuse gas too: atomic hydrogen is spread all around the Milky Way and can generate $\gamma$ photons in the same way as its molecular counterpart; electronic contribution via inverse Compton scattering can be important as well.

The the signal from molecular clouds is very faint at high energy ($\sim$ 1% C.U. at 1 TeV), due to the power-law like shape of spectrum. This is why in order to investigate their emission features one needs the best available instrumentation. The *Fermi*-LAT telescope studied some examples of these objects, but its analysis was limited to very close or very massive ones, and didn't result conclusive. The incoming Cherenkov Telescope Array (CTA) with its huge collecting area, will have a better sensitivity and will open up new chances of testing the cosmic ray sea with molecular clouds at higher energies. CTA in fact is expected to provide a unique view of the high energy sky from some tens GeV to hundreds TeV with an angular resolution that can reach 0.05°at 1 TeV. This will lead to the discovery of many new sources and hopefully will put some constraints on the uppermost part of the CR spectrum.

We performed some simulations of a cloud of the considered catalog, assuming different parent protons spectra and we analyzed the resulting datasets. It was chosen to start with the *best* cloud, namely n. 877, that resulted to be the most promising in terms of mass and distance and found itself in a position rather free from other sources of gamma rays. We tested the hypothesis of a spectrum that resembles the local one, and the hypothesis that spectrum in other part of the Galaxy could be harder (with different spectral indexes), for the presence of some acceleration mechanisms. Interesting to note that if the real observations will tell us that the Galactic cosmic ray spectrum is instead steeper or lower than the local one, we will have to conclude that the Earth is in a very special position in the Galaxy. Besides we tested the ability of CTA to recognize the presence or absence of a high energy cutoff in the CR proton spectrum. This is of central importance in the understanding of the mechanism of acceleration and of the nature of the accelerators.

It resulted that CTA will be definitely able to distinguish between spectra of different slopes. In particular we found that already 20 hours of observation will be enough to recognize a hard power law spectrum, of slope 2.4 or 2.6, while to recognize a steeper spectrum, like the AMS one ($\alpha \sim 2.85$), more observation hours are needed. For what concerns the cutoff spectra that we tested, it emerged that a cut off feature in the parent spectrum up to 500 TeV is recognizable by CTA in the gamma spectrum, while for higher energies cutoff systematic errors (that we accounted to be 15 %) prevent us to distinguish this feature.

Although this was a preliminary approach, and our methods must be improved, we believe that CTA will provide a detailed overview on the gamma ray emission of molecular clouds, from which we will derive crucial constraints on the Galactic

cosmic rays spectrum. For this reason we will then to continue with this study and extend this analysis to as many MC as possible.

# Riassunto

I raggi cosmici sono noti da più di un secolo, ma alcuni aspetti della fisica di queste particelle di alta energia rimangono ad oggi un mistero. Da un lato la loro composizione è piuttosto comune: elettroni, protoni e una minoranza di nuclei più pesanti, dall'altro la loro distribuzione in energia è impressionante. Misure dirette dello spettro dei raggi cosmici sono state condotte con l'uso di palloni aerostatici in atmosfera e di satelliti in orbita attorno alla Terra e hanno mostrato che l'energia di queste particelle si estende dalle centinaia di MeV ($\equiv 10^6$ eV) fino a $\sim 1$ PeV ($\equiv 10^{15}$ eV). Quali siano i meccanismi e gli oggetti astrofisici responsabili della loro accelerazione, ancora non è del tutto chiaro. É stato provato che i resti di supernova accelerano particelle, ma arrivano al massimo ad un'energia di $\sim 100$ TeV, occorre quindi invocare alri meccanismi per spiegare lo spettro osservato. Regioni di formazione stellare, o il buco nero al centro della Galassia potrebbero essere possibili acceleratori, ma non è ancora stato dimostrato. Un altro fatto degno di nota è che la distribuzione spaziale dei raggi cosmici risulta altamente isotropica. Questo suggerisce l'idea che queste particelle, dopo essere state accelerate, si propagano nella Galassia, dove subiscono continue deflessioni a causa dei campi magnetici dei plasmi interstellari. Ci aspettiamo quindi che i raggi cosmici seguano una distribuzione piuttosto uniforme, il cosiddetto *mare* dei raggi cosmici galattici. Tuttavia le informazioni che abbiamo sui raggi cosmici, sono limitate alle osservazioni condotte nelle vicinanze della Terra. A priori non possiamo né assumere che esista un mare dei raggi cosmici, né che sia caratterizzato dalla stessa densità di energia ($\rho \sim 1$ eV/cm$^3$) che misuriamo qui, nelle vicinanze della Terra. Una completa conoscenza della distribuzione dei raggi cosmici nella Galassia porrebbe dei vincoli decisivi sull'origine di queste particelle e sulla fisica dei loro acceleratori, e darebbe un'irrepetibile opportunità di esplorare la fisica di processi ad energie impossibili da raggiungere in laboratori terrestri.

Le sonde non possono spingersi molto più in là del sistema solare, quindi misure dirette sono limitate alla nostra regione. Tuttavia una nuova straordinaria opportunità di testare lo spettro dei raggi cosmici galattici è rappresentata dall'astrofisica gamma. Questa disciplina studia la radiazione astrofisica all'estremo più alto dello spettro elettromagnetico. Di solito si considerano tre fasce di fotoni gamma: quelli di bassa energia $\sim$ MeV, di alta energia $\sim$ GeV e di energia molto alta $\sim$ TeV. I raggi cosmici producono radiazione gamma interagendo con il mezzo interstellare: per esempio un protone dei raggi cosmici che colpisce un protone del mezzo interstellare dà vita a un $\pi^0$ instabile che decade rapidamente in raggi gamma. L'energia dei fotoni prodotti dipenderà dall'energia iniziale dei protoni: all'incirca il 10% dell'energia dei primari. La misura dello spettro dei raggi gamma ad alta energia porta quindi alla conoscenza dello spettro dei protoni a energie ancora più elevate.

Per aumentare la probabilità di osservare raggi gamma prodotti in questo modo, si

cercano zone con un'alta concentrazione di gas. Le nubi molecolari, a tal proposito, sono il target ideale. Queste sono delle massicce (fino anche a $10^7$ $M_\odot$) concentrazioni di molecole, per lo più $H_2$, ristrette in una regione di 10-100 pc. Assumendo un certo spettro per i protoni primari, il flusso di una nube dipende solo dalla sua massa e dalla sua distanza da noi. Le nubi molecolari vengono tracciate dalle osservazioni radio delle emissioni del CO. Lo scorso anno è stato pubblicato un catalogo di nubi molecolari, basato sulle osservazioni dell Harvard Smithsonian Center of Astrophysics. Questo catalogo contiene 1064 oggetti, alcuni dei quali sono molto massivi e abbastanza vicini da essere osservabili con la futura strumentazione gamma.

I fotoni gamma possono arrivarci, praticamente indisturbati da qualsiasi regione della Galassia. Queste particelle si originano in processi non-termici, perciò non ci sono molte classi di oggetti nella Galassia che siano in grado di produrli. Oggetti come resti di supernova, pulsar, micro-quasar possono accelerare particelle che di conseguenza irradiano in questa banda di energia. Radiazione non termica può essere generata parimenti anche dal gas diffuso: l'idrogeno atomico è distribuito in ogni parte della Via Lattea e può produrre fotoni $\gamma$ nello stesso modo della sua controparte molecolare, che è concentrata principalemente nelle nubi. Il contributo elettronico, via scattering Compton inverso può essere altrettanto importante.

Il flusso gamma delle nubi molecolari è piuttosto debole ad alte energie ($\sim$ 1% C.U. a 1 TeV), a causa della forma a power law dello spettro. Perciò per studiare le caratteristiche della loro emissione sono necessari i migliori strumenti. *Fermi*-LAT ha studiato alcune nubi molecolari, ma la sua analisi si è limitata a oggetti molto vicini o estremamante massicci, e comunque è risultata inconcludente. Il venturo Cherenkov Telescope Array (CTA) con la sua enorme estensione avrà una sensibilità mai raggiunta prima e aprirà così nuove possibilità di testare il mare dei raggi cosmici ad alta energia per mezzo delle nubi molecolari. Si prevede che CTA offrirà un'insuperabile vista del cielo ad alta energia, da qualche decina di GeV fino a centinaia di TeV, con una risoluzione angolare che può raggiunger i 0.05 °a 1 TeV. Questo permetterà di scoprire molte nuove sorgenti, e porrà dei vincoli ad alta energia allo spettro dei raggi cosmici.

Abbiamo condotto delle simulazioni di una nube del catalogo sopracitato, assumendo diversi spettri per i protoni primari e abbiamo analizzato gli eventi prodotti. É stato scelto di cominciare con il candidato *migliore*, cioè la nube n.877, che è risulata essere la più promettente in termini di massa e distanza e si trova in una posizione piuttosto libera da altre sorgenti di raggi gamma. Abbiamo testato il caso in cui lo spettro dei primari ricalchi lo spettro locale e il caso in cui invece lo spettro sia più *hard* (con diversi indici spettrali), per la presenza, per esempio di qualche acceleratore. Interessante da sottolineare che se le osservazioni ci diranno che lo spettro dei raggi cosmici galattici è in realtà più *steep* o comunque inferiore dello spettro locale, dovremmo concludere che la Terra si trova in una posizione molto particolare della Galassia. Inoltre abbiamo testato le capacità di CTA nel riconoscere un cutoff nello spettro dei primari. Questo è di fondamentale importanza per la comprensione dei meccanismi di accelerazione e della natura degli acceleratori.

La nostra analisi ci ha permesso di concludere che CTA sarà effettivamente in grado di distinguere spettri con diverse pendenze. In particolare abbiamo trovato che già 20 ore saranno sufficienti per riconoscere uno spettro di indice 2.4 o 2.6, mentre per riconoscere uno spettro più steep, come quello locale ($\alpha \sim 2.85$) è necessario più

tempo. Per quanto riguarda gli spettri con cutoff, è emerso, da uno studio qualitativo, che un ipotetico cutoff nello spettro dei primari è riconoscibile fino a 500 TeV, mentre per i cutoff a più alta energia, gli errori sistematici (che abbiamo valuato contare per il 15 %) impediscono di riconoscere cutoff a più alta energia.

Anche se questo è stato un lavoro preliminare, e i nostri metodi vanno migliorati, siamo fiduciosi che CTA potrà fornire una dettagliata panoramica dell'emissione gamma delle nubi molecolari, dalla quale si potranno ricavare importanti informazioni sullo spettro dei raggi cosmici nella Galassia. Per questa ragione, continueremo con questo studio ed estenderemo quest'analisi a quante più nubi molecolari possibili.

# Contents

# List of Figures

# Chapter 1

# Cosmic rays

With the term *cosmic rays* (CR) one refers to high energy particles that have been observed at the top of the atmosphere and come from still unsure sources outside the solar system. The reason to believe that these particles are of extra-solar origin is that their spatial distribution appears from Earth to be uniform at a very high level[1]. The particles that belong to CR are mainly protons and other nuclei (98%) whilst the remaining 2 % is made out of leptons. Usually one distinguishes between *primary* and *secondary* particles, such as the nuclei of the (Li, Be, B) group as well as anti-particles like positrons, albeit in small part. Secondaries result from the interactions of the primaries with the interstellar medium, the thermal plasma or with low-frequency photon fields ( [Schlickeiser, 2013], [Longair, 2011]). Observed CR are distributed in a very wide range of energy up to $10^{19}$ eV. The CR spectrum have been measured by many experiments with increasingly better accuracy but is still being improved nowadays, especially with the advent of $\gamma$-ray astronomy, that allows us to derive information on the primaries by the analysis of the secondaries (see for example [Aharonian et al., 2013]).

While the energy spectrum of the cosmic rays can be known with pretty good accuracy, at least in the Earth vicinity, the origin of the high energy of these particles is still matter of debate. Many authors ([Longair, 2011], [Cardillo et al., 2014]) accept supernova remnants as the main factories of cosmic particles, but there are many arguments that make people believe that they are not the only contributors, especially at energies above few hundred TeVs ([Aharonian, 2004], [Lingenfelter, 2017]).

In section 1.1 we describe the main features of the spectrum of these particles as derived from direct experiments and from $\gamma$-rays observations. A short paragraph explains how to derive the relation between the primaries and the secondaries spectrum. Section 1.2 presents briefly the main candidates as CR accelerators, and the evidences in favor or against each of them. Finally in 1.4 the main constraints that we would like to achieve with the incoming Cherenkov telescope array are discussed.

## 1.1 CR spectrum

The CR spectrum is the distribution in energy of cosmic rays. It is measured as the number of CRs detected per unit area, time, solid angle and energy. The knowledge of the spectrum is the key to the understanding of the accelerating mechanisms of these particles and of their origin. Many measurements of the cosmic rays spectrum

[1] Except for a minor component associated with solar activity.[Schlickeiser, 2013]

have been carried out since their discovery in 1912 by the pioneering air balloon experiment of Victor Hess [F. Hess, 1912] and now data beyond 100 TeV are available. Despite of this it is useful to stress out that the CR flux has always been measured from the Earth's vicinity and in principle there is no reason to assume that the cosmic rays have the same properties all around the Galaxy. Therefore is more correct to distinguish between the well measured *local* CR spectrum and the unknown *global* CR spectrum of the Galaxy.

### 1.1.1 The local CR spectrum

The local spectrum of CRs is known to have a power-law shape with two main features: one at $10^{15}$ eV (*knee*) and another at $10^{18}$ eV (*ankle*). Particles below the knee are believed to be produced inside the Galaxy, whereas particles of extremely high energy (EHE, i.e. $\gtrsim 1$ PeV) are more likely to be produced by powerful extragalactic objects as AGN, radiogalaxies or clusters of galaxies. Although there is no firm confirmation on their origin, at least for EHE particles there is a certain confidence in saying that they have an extragalactic parenthood. If they were produced within the Galactic disk, significant anisotropies would be expected, in contrast with observations. CRs in fact appear to be homogeneously distributed no matter of their energy. The continuous interactions that CRs suffer during a typical confinement timescale of $t_{esc} \sim 10^7$ years, with the interstellar medium and with the Galactic magnetic fields mix them up and make them lose information of their original direction. This is why they appear to be as a *sea*, uniformly spread, but with potential local enhancement due to some kind of perturbation, like can be the vicinity of an accelerator ([Aharonian, 2004]).

Figure 1.1 shows the plots of the differential energy spectra for different species of nuclei as derived by many experiments and reported by the Particle Data Group booklet [Patrignani et al., 2016]. The fitted form of the energy spectrum in the range from several GeV to somewhere beyond 100 TeV as reported by the same authors is given by:

$$J(E) \approx 1.8 \left( \frac{E}{1\mathrm{GeV}} \right)^{-\alpha} \frac{\text{nucleons}}{\mathrm{cm}^2 \ \mathrm{s} \ \mathrm{sr} \ \mathrm{GeV}} \tag{1.1}$$

here $\alpha = 2.7$ is the differential spectral index. This equation is normalized taking into account all the species. To recover the correct formula for each species one has to know the relative abundance of that element. For example for protons one multiplies for another factor 1.8. Table 1.1 gives an overview of the main nuclei that populate the CRs and reports the abundances of the elements relative to oxygen, whose flux at 10.6 GeV is known to be $I_O = 3.29 \times 10^{-2}$ nucleons $m^{-2}$ $sr^{-1}$ $s^{-1}$.

| Z | Element | F | Z | Element | F |
|---|---|---|---|---|---|
| 1 | H | 540 | 13-14 | Al-Si | 0.19 |
| 2 | He | 26 | 15-16 | P-S | 0.03 |
| 3-5 | Li-Be | 0.40 | 17-18 | Cl-Ar | 0.01 |
| 6-8 | C-O | 2.20 | 19-20 | K-Ca | 0.02 |
| 9-10 | F-Ne | 0.30 | 21-25 | Sc-Mn | 0.05 |
| 11-12 | Na-Mg | 0.22 | 36-28 | Fe-Ni | 0.12 |

TABLE 1.1: Relative abundances, normalized ($\equiv 1$) at the oxygen flux at 10.6 GeV that is 3.29 $\times$ $10^{-2}$ nucleons $m^{-2}$ $sr^{-1}$ $s^{-1}$. Data from [Patrignani et al., 2016]

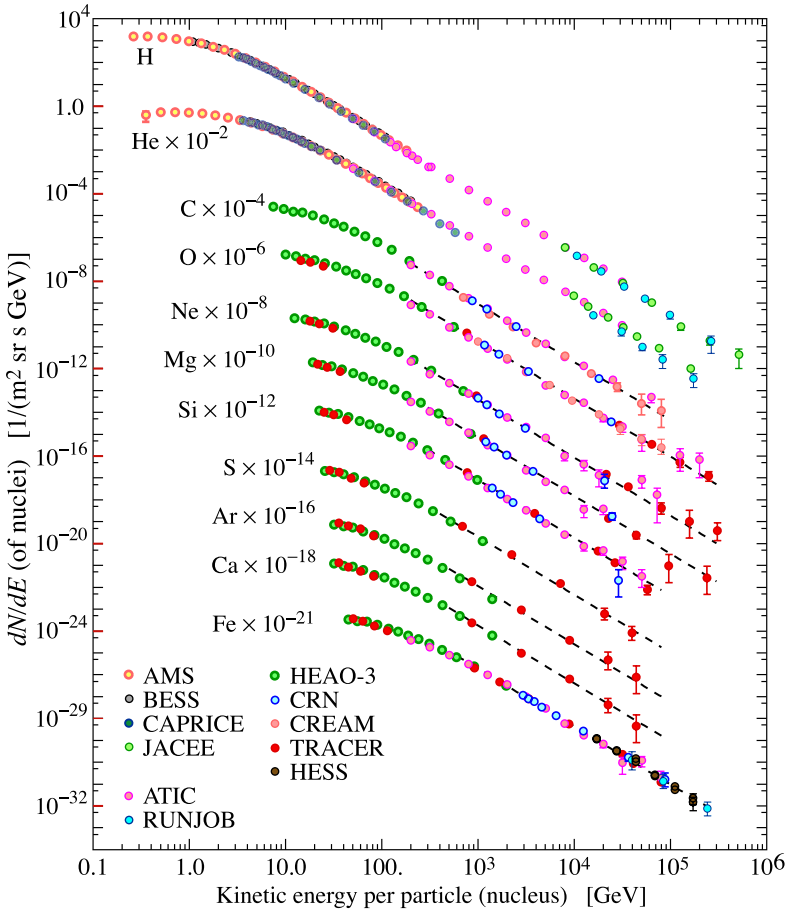


FIGURE 1.1: Intensity of primary nuclei from some hundreds of GeV and up to 100 TeV in units of particle per energy-per-nucleus vs kinetic energy per particle. Note that a scaling factor has been introduced to distinguish each species. Figure from [Patrignani et al., 2016]

**The AMS measurements of the local spectrum**

Recent experiments like ATIC-2[2], CREAM[3] and PAMELA[4] showed that the proton spectrum deviates from a single power law ([Panov et al., 2009], [Yoon et al., 2011] and [Adriani et al., 2011]). The most recent measure comes from the Alpha Magnetic Spectrometer (AMS, [Aguilar et al., 2015]). AMS is a particle detector in space: it is on board of the International Space Station (ISS) and it is basically a silicon scintillator. During a survey of 30 months (from May 2011 to November 2013) AMS measured the spectrum as a function of rigidity. By definition the rigidity of a particle measures its resistance to a magnetic force that deflects the particle from a straight-line. It is measured in units of momentum/charge and is given by:

$$R = \frac{pc}{q} \tag{1.2}$$

where $q$ is the charge of the particle and therefore, if $pc$ is measured in electronvolt, $R$ will be in volt. Considering the definition of energy, as a function of the particle momentum $p$ and mass $m$, a conversion formula can be simply recovered:

$$E = \sqrt{m^2c^4 + p^2c^2} \tag{1.3}$$

$$\begin{aligned} E^2 &= m^2c^4 + \frac{p^2c^2}{q^2}q^2 = m^2c^4 + R^2q^2 \\ \rightarrow R &= \frac{mc^2}{q}\left(\frac{E^2}{m^2c^4} - 1\right)^{1/2} = \frac{mc^2}{q}(\gamma^2 - 1)^{1/2} \\ &= \frac{m_0[eV]}{1\ eV}\frac{(\gamma^2 - 1)^{1/2}}{Z}\left[\frac{eV}{C}\right] \end{aligned}$$

where $\gamma$ is the Lorentz factor that comes from special relativity, $m_0$ is the particle rest mass and $Z$ is the number of charges. For example for a hydrogen nucleus $Z = 1$ and therefore:

$$R = 9.38 \times 10^8(\gamma^2 - 1)^{1/2}\ \mathrm{V} \tag{1.4}$$

For ultra-relativistic particle $\gamma \gg 1$ hence

$$R \approx \frac{E}{q} \approx \frac{1}{Z}\left(\frac{E}{1\ \mathrm{eV}}\right)\ [\mathrm{V}]$$

that explains the linear relation between these two quantities above 10 GeV, as shown by the plot in 1.2 (remember that the proton rest mass is $\approx 1$ GeV and therefore its contribution is negligible at higher energy).

The data collected in the AMS-02 experiment are reported in figure 1.3. It is clear that a single power law with a fixed index cannot fit the measures. At higher energy the spectrum becomes harder and in order to fit it we must assume that the spectral index depends on the energy.

The analytical fit function as given in [Aguilar et al., 2015] is:

[2] http://cosmicray.umd.edu/atic-home
[3] http://cosmicray.umd.edu/cream/
[4] http://pamela.roma2.infn.it/index.php

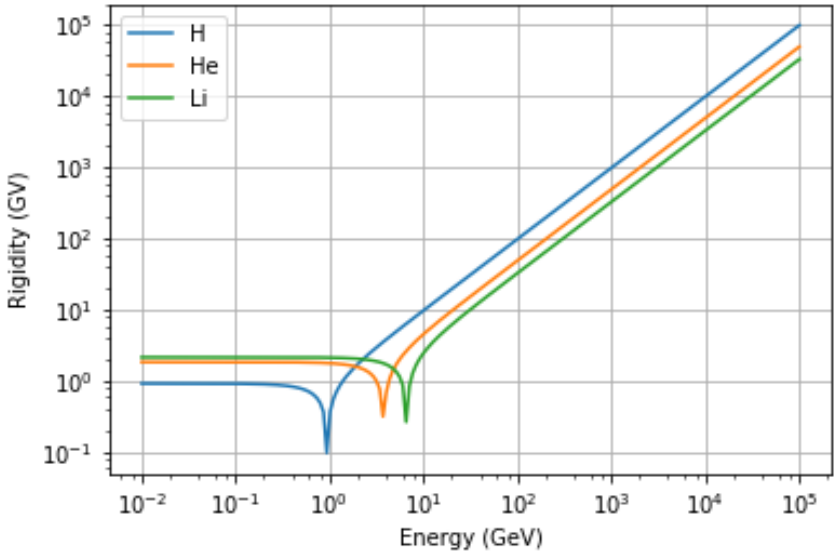


FIGURE 1.2: Relation between rigidity and energy for different ions

$$J(R) = C\left(\frac{R}{45\ GV}\right)^{\gamma}\left[1+\left(\frac{R}{R_0}\right)^{\frac{\Delta\gamma}{s}}\right]^{s} \tag{1.5}$$

here C= 0.4544 $m^{-2}$ $sr^{-1}$ $s^{-1}$ $GV^{-1}$ is the flux normalization, $\gamma$ =-2.849 is the power-law-like spectral index, $\Delta\gamma = 0.133$ measures the hardening of the spectrum. $R_0$= 336 GV is the characteristic rigidity at which occurs the transition of the spectral index and s=0.024 quantifies the smoothness of this transition. AMS measurements, although very precise, cover only a range from 1 GV to 1.8 TV (corresponding to 1.4 GeV to 1.8 TeV and therefore an extrapolation at higher energy is necessary for the purpose of this work. On the other hand measurements of high energy photons will in principle allow us to set precise constraints on the high energy counterpart of this spectrum.

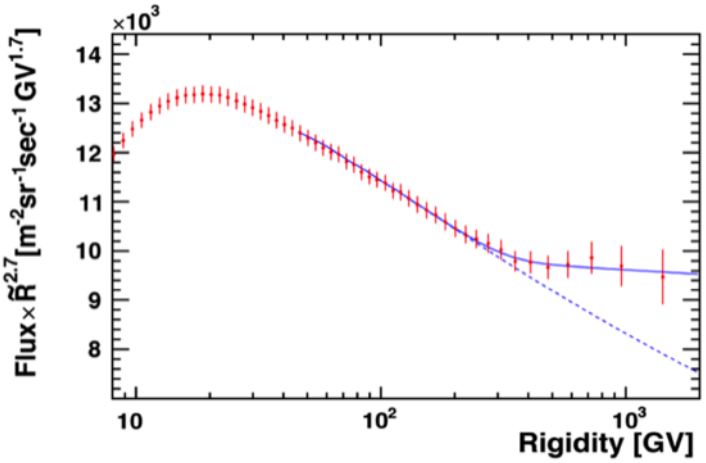


FIGURE 1.3: AMS measurements (red dots with error bars), the the blue solid line is the fitting function as in 1.5, while the dotted line is a power law spectrum, obtained from 1.5 by setting $\Delta\gamma$=0. Figure from [Aguilar et al., 2015]

### 1.1.2 The Galactic CR spectrum and gamma ray astronomy

All available data on cosmic ray spectrum were derived by experiments performed in the Earth's vicinity. As this work aims at showing, there is no reason to assume a priori that these results can be extended everywhere in the Galaxy. There exists a way to test this hypothesis and that makes use of gamma ray astronomy. Our targets are gamma rays produced as the CRs collide with particles in the interstellar medium (ISM), as they can reach us from nearly everywhere in the Galaxy without suffering any significant deflection. Already with the Energetic Gamma Ray Experiments Telescope (EGRET) there were hints that the cosmic ray density may not be uniform all around the Galactic plane [Hunter et al., 1997], but results were not accepted at that time due to the limited resolution of the instrument, that prevented to distinguish if the emission came from the gas or from unresolved gamma-ray sources. *Fermi*-LAT (Large Area Telescope) improved sensitivity made it possible to overcome the problem of resolving emission that comes from the diffuse gas instead of from sources.

Detection and analysis of these photons allow us to reconstruct the spectrum of CRs in the region where they are generated. Galactic gamma rays emissivity was studied by analyzing data from *Fermi*-LAT by many authors like [Yang et al., 2016], [Casandjian et al., 2015] or the *Fermi*-LAT collaboration itself [Ackermann et al., 2012a]. All of them found out that the gamma-ray emissivity deviates from what expected according to the local data both in the spectral index and in the flux normalization. Results from Yang are summed up in figure 1.4 as an example.

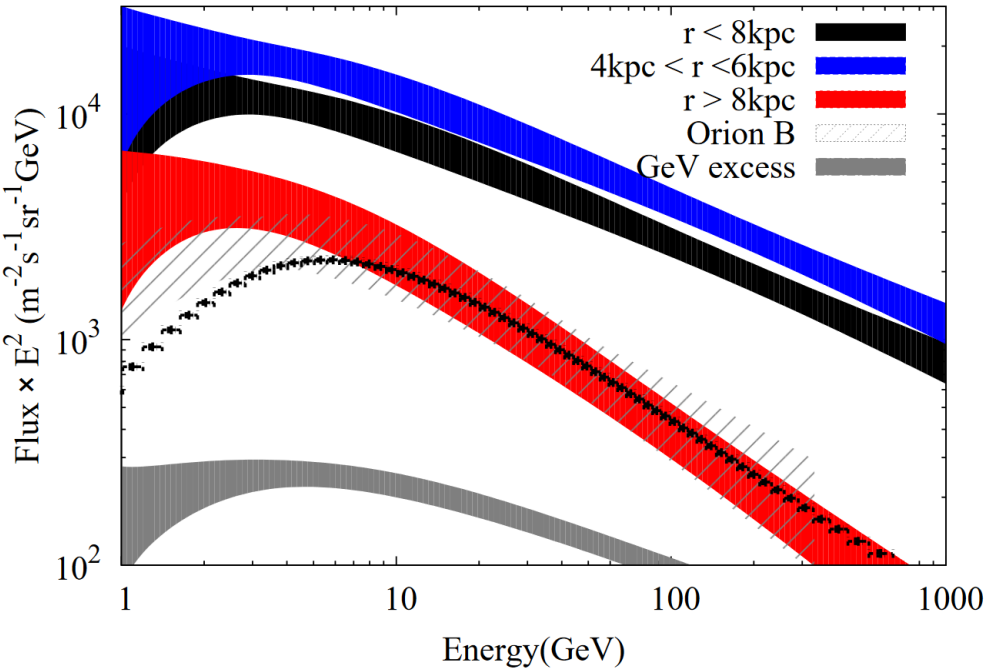


FIGURE 1.4: The CR proton spectra as derived from the $\gamma$ emissivity from diffuse gas in different Galactic ring as computed by [Yang et al., 2016]. The $\gamma$ spectrum as derived from the local AMS spectrum is also shown as black dots. Also are reported the data from Orion B nearby molecular cloud and from the low energy sources called "GeV excess". Figure from [Yang et al., 2016].

The cosmic ray energy density, as derived from gamma observations, appears to increase towards the Galactic center, and at the same time the spectrum becomes harder. A special feature arises between 4 and 6 kpc, where the emission shows a peak.

### Deriving secondaries spectrum

The primaries spectrum can be easily related to the secondaries flux once the differential cross section of the process involved is known, as in [Gaisser et al., 2016]:

$$\frac{dN_j}{dE_j dV dt} = \int dE_i \frac{d\sigma_{i\to j}}{dE_j}(E_i, E_j)\left(\frac{c\rho(\mathbf{r})}{m}\right)\frac{4\pi}{c} J_i(E_i) \tag{1.6}$$

where $i$ and $j$ denote, respectively, the primaries and the secondaries.

For the purpose of this work we assume that the main channel of production of gammas is the decay of $\pi^0$. That is quite reasonable if one considers that proton-proton inelastic collisions give birth to heavy particles, that quickly decay in many pions. We hence assume that our gammas are created according to the chain:

$$p + p \to X \to \pi^0 \to 2\gamma$$

where X is a generic heavy particle (for example the $\Delta(1232)$ baryon).

Reliable experimental data are available for the cross section of production of $\pi^0$ only below some GeVs. For higher energy protons, like the ones that populate the cosmic rays one has to rely on numerical simulation. For this work we chose to use the recent parametrization from [Kafexhiu et al., 2014]. They considered the available data from the Large Hadron Collider (LHC) measurements at low energy and parametrized the behavior of the pp inelastic cross section at higher energies, taking into account different theoretical models of production of pions. The cross section that they give, takes into account both the proton-proton interaction and the pion decay. Their results for different energies are plotted in 1.5.

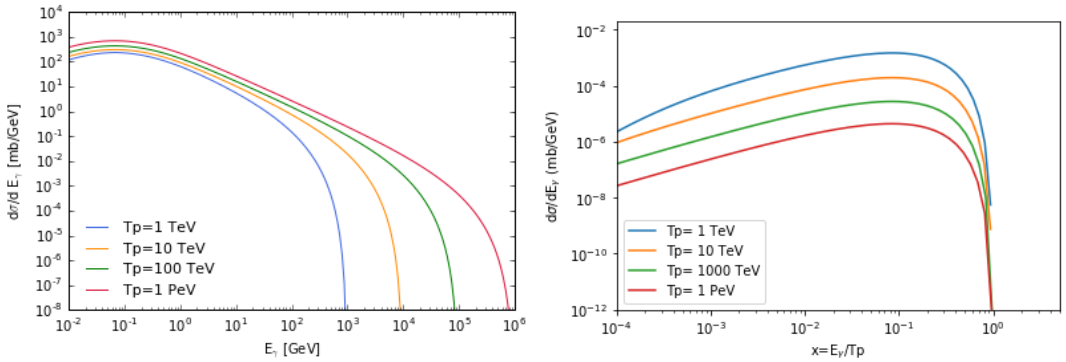


(a) (b)

FIGURE 1.5: Differential cross section for pp $\to$ 2 $\gamma$ process for different kinetic energy of the protons from 100 GeV to 1 PeV. In (b) the energy is normalized to the incoming proton energy. These plots have been realized thanks to python library LibppGam developed by the same authors [Kafexhiu et al., 2014].

It is interesting to see the shape of the differential cross section for different energies of the incoming proton: the differential cross section shows a cutoff at a certain value of energy. This cutoff corresponds to the maximum energy that the photons can have, given a certain energy of the primaries, and is approximately the 10% of the proton kinetic energy. That means that from the measured energy of gamma rays one can roughly infer some lower limits on the energy of the cosmic rays. For example, if a photons with energy of 100 TeV will be detected, this will suggest that the primary particle had an energy around 1 PeV, that would imply the existence of an accelerator of such capability.

## 1.2 CR accelerators

CR nowadays keep on being an intriguing mystery. The first issue of these particles is that we still don't know for sure how they are pushed at those high energies and by what sources. The astronomical objects responsible for imparting them their kinetic energy are named *CR accelerators*. It is widely accepted that Supernova Remnants (SNRs) are the main accelerators of CR, however that does not prevent other objects from being responsible of the CR acceleration. Other objects like pulsars, young stars winds or micro-quasars for example fulfill the energetic requirements to supply the CR power. The question remains then open, especially because the theory of shock acceleration in SNe has not yet been able to solve the so-called 'maximum energy problem', namely to explain the highest energy observed particles of the CR. More detailed and precise studies on gamma-ray emission will be definitely helpful to come over this big enigma. Clouds in particular may results decisive in findng out the "guilty party" of the acceleration of CR. If by chance in fact a passive cloud occurs to be in the vicinity of an accelerator its spectrum will bear the imprint.

### 1.2.1 Supernovae

Supernovae mark the end of massive (M > 8 $M_\odot$) stars. When the nuclear burning comes to the synthesis of the elements of the iron group (Fe, Co, Ni), nuclear reactions are no more able to balance the self-gravity of the star. The star undergoes then an inevitable collapse that ends in a violent explosion that frees a huge amount of energy and matter. The powerfulness of these events is the basic argument in favor of SNe as CR accelerators, and was proposed since the very beginning of the developing of this field already by Baade and Zwicky [Baade and Zwicky, 1934]. This hypothesis is supported by the consideration that the total power released in Galactic SN explosions is largely sufficient to maintain the entire CR population of our galaxy. A rough estimation as given in [Aharonian et al., 2013] of the CR power can be:

$$\mathcal{P}_{CR} \sim \left(\frac{1\ \mathrm{eV/cm^3}}{t_{esc}}\right) V_{Gal} = \frac{1.6 \times 10^{-12}\mathrm{erg/cm^3} \times 4 \times 10^{66}\mathrm{cm^3}}{20\ \mathrm{Myr}} \sim 10^{40}\mathrm{erg/s} \quad (1.7)$$

where $t_{esc}$ is the escaping time and it is derived from considerations on the $^{10}$Be population of the CR; $V_{Gal}$ instead is the Milky Way volume computed as the volume of a disk of radius 15 kpc and height 200 pc, whereas the CR energy density is derived from local measurements. This power can be supplied very easily by SN explosions,

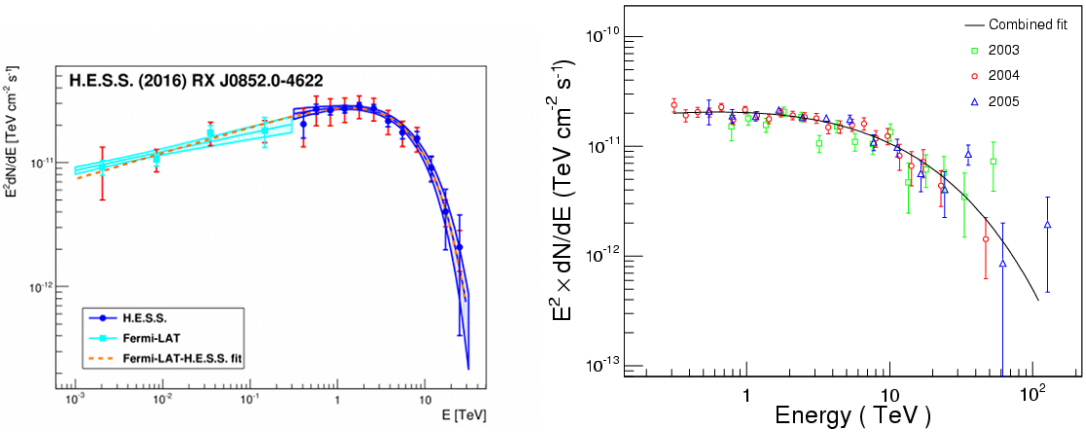


(a) (b)

FIGURE 1.6: Spectrum of two famous young supernova remnants. In (a) RX J0852.0-4622, known also as Vela junior; in (b) RX J1713.7-3946, the first resolved source in the gamma sky. From [HESS Collaboration et al., 2016] and [Aharonian et al., 2007]

considering that a 10 $M_\odot$ star will release, exploding, on average $10^{51}$ erg of kinetic energy[5] and that SN explosion rate is estimated to be $\sim 2$ century$^{-1}$ in the Galaxy[6].

Moreover several young supernova remnants (SNRs) were discovered to be TeV-emitters (RX J1713.7-3946 [Aharonian et al., 2007], Tycho [Acciari et al., 2011], Vela junior [HESS Collaboration et al., 2016]) and there appeared to be a correlation between mid-aged SNRs and GeV emission of the surrounding gas (for example around SNR W44 [Uchiyama et al., 2012]). This conforms with the scenario in which particles are accelerated by the SN explosion and then migrate and populate the surroundings before being mixed up in the so-called CR 'sea'. However even if it is clear that SNRs emit $\gamma$-rays up to 100 TeV, it is not yet clear if this emission is of hadronic or leptonic origin and therefore one can not reach certain conclusions on the primaries energy. Moreover, the so-called 'Diffusive Shock Acceleration' (DSA) mechanism nicely explains the transfer of energy from the SN explosion to the particles[7], but makes for SNR difficult to be a continuous injectors of PeV particles, as computed by [Bell et al., 2013]. Furthermore, all spectra of young SNRs show a clear cutoff at few TeV, meaning that SNRs observed until now can, at most, accelerate CRs at hundreds of TeV, as figure 1.6 clearly show.

### 1.2.2 PeVatrons

The current paradigm of CRs advocates that the observed particles with energy up to $10^{15}$ eV are accelerated inside our own Galaxy. This is suggested by considerations on homogeneity of CRs and on their composition, as discussed by [Blasi, 2013]. If

[5]Rough estimations of SN power can be performed assuming that the star releases gravitational energy due to the collapse from an average radius of 10 $r_\odot$ to the typical white dwarf radius $\sim 100$ km. These estimations suggest that the explosion releases $\approx 10^{53}$ erg, of which the most is employed to blow away the envelope and to produce the observed luminosity, whereas $\sim 10^{51}$ erg are left as kinetic energy of the ejected particles. See for example [Kippenhahn et al., 1990].

[6]Estimates on SN explosion rate have been performed independently by [Diehl et al., 2006]. exploiting the aluminum emission and by [Keane, 2011] from considerations on the massive stars birthrate.

[7]For more details we refer to [Drury, 1983] and [Hillas, 2005]

the hypothesis of a Galactic origin of CRs up to $10^{15}$ eV is true, there must be some objects able to accelerate particles up to 1 PeV within our Milky Way. In analogy to the TeVatron, (an artificial accelerator in Illinois that can reach the TeV regime), these accelerators were named *PeVatrons*. None of the known SNR seems to be a PeVatron, since no compatible emission has been detected (remind figure 1.6). That suggests the need to seek a new class of accelerating objects.

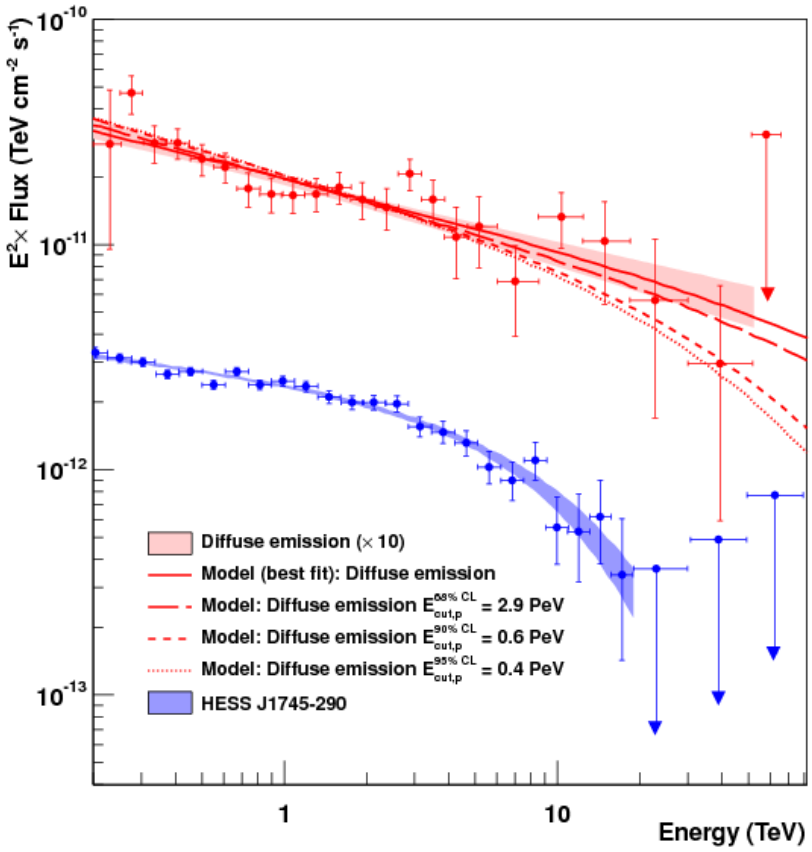


FIGURE 1.7: The diffuse spectrum detected by HESS in the central region of the Galaxy, compared with the one of the unidentified source HESS J1745-209. The colored bands indicate the $1\sigma$ confidence intervals of the fits. For the diffuse component different models are tested, as described in the figure legend. Figure from [Abramowski et al., 2016]

The High Energy Stereoscopic System (H.E.S.S.) array observed $\gamma$-ray emission at energy close to one hundred of tera-electronvolt coming from the Galactic center region [Abramowski et al., 2016]. At these energies the leptonic component is disfavored[8], so there is no confusion on the hadronic origin of the radiation. In this case, the parent protons must have had energy close to 1 PeV. The identification of the source of this emission is not yet clear, but on the other hand the radial dependent profile of the emission suggests that it should be some object located in the Galactic Center. The unidentified TeV source HESS J1745-290 appears to be in the center of

[8]This is because at 100 TeV the severe losses due to inverse Compton scattering and synchrotron radiation prevent electrons to propagate further from the accelerator.

this diffuse emission, so it is believed to be related to that. Its spectrum however contradicts it: while the diffuse emission extends to several tens of TeV, the spectrum of HESS J1745 dies around 10 TeV (see figure 1.7). It is not know which is the low energy counterpart of HESS J1745, but a plausible candidate is the central supermassive black hole, Sagittarius A* (Sgr A*). Sgr A* now has a relatively modest activity, but it had a much higher accretion rate in the past. This could explain the observed VHE particles: the common believing is hence that it injected in the diffuse gas energetic particles, while now it is no more able to produce them.

### 1.2.3 Star forming regions

SNRs alone can hardly explain the entire observed spectrum of CRs, above all in the region around the PeV knee. Many authors suggest [Higdon and Lingenfelter, 2005], [Binns et al., 2008] that another powerful acceleration mechanism could be the interaction of massive star winds with multiple shocks initiated by SN explosions. OB associations, namely open clusters of massive stars, are the perfect places where to find both massive powerful stars and SN events. It is commonly known in fact that massive stars end their life with a core collapse supernova explosion. Deep studies of the millimeter, sub-millimeter and infrared emissions of star forming regions (SFRs) in giant molecular clouds have shown that there is a spatial and temporal correlation between OB star forming regions and supernovae events, meaning that these stars don't migrate significantly during their life.

It has been calculated [Higdon and Lingenfelter, 2005] that $\sim$ 75 % of SN explosion occurs within a *superbubble*, e.g. a big cavity (> 150 pc) in the hot ($\sim 10^6$ K) tenuous ($5 \times 10^{-3}$ cm$^{-3}$) plasma, leftover of a former SN explosion. The hotness and tenuousness of this material makes the acceleration easier and acceleration of protons to PeV energies can be realized in a much easier way than in SNR. Multi-TeV gamma rays observations of some massive stellar clusters as Westerlund 1 [Ohm et al., 2013] for example support this scenario with superbubbles acting like high energy particles accelerators. Unfortunately this is not the case of PeV-particles that were observed coming from the Galactic center, since in that region the SN explosion rate is not sufficient. Nevertheless SFR proved themselves to be a very efficient accelerators.

## 1.3 CR dynamics

The high energy of observed cosmic rays implies that they are *non-thermal* particles: that means that they are not in thermal equilibrium with the medium where they are produced. While thermal particles follow a Maxwellian distribution, that depends only on the temperature, in general the distribution of non-thermal particles $f(E, \mathbf{r}, t)$ depends on the energy, the position and on the time. The transport mechanism of cosmic rays is then a key point of their physics.

After they have left the source, CRs propagate in the interstellar medium, that is filled with a collisionless, high conductive, magnetized, tenuous plasma made mostly of electrons and protons. The energy density of CR ($\sim 1$ eV/cm$^3$, as measured from Earth) is often comparable to the one of the surrounding medium, that means that CRs influence the local electromagnetic fields and can't be taken as "test particles". This complicates further the already difficult task of propagation within plasmas. A

plasma can be defined as a gas that contains a considerably amount of charge particles so that their collective Lorentz force influences the medium itself. The dynamics of plasma requires then knowledge of magnetohydrodynamics. In this medium, Alvén waves and magnetosonic waves generate easily, yielding to a non linear problem.

In the general case, the evolution of the CR distribution is described by the cosmic rays transport and acceleration equation:

$$\begin{aligned}\frac{\partial f_a}{\partial t} - S_a(\mathbf{x},\mathbf{p},t) = &\frac{\partial}{\partial z}\kappa_{zz}\frac{\partial f_a}{\partial z} + \frac{\partial}{\partial X}\left[\kappa_{XX}\frac{\partial f_a}{\partial X} + \kappa_{XY}\frac{\partial f_a}{\partial Y}\right] \\ &+ \frac{\partial}{\partial Y}\left[\kappa_{YY}\frac{\partial f_a}{\partial Y} + \kappa_{YX}\frac{\partial f_a}{\partial X}\right] && spatial\ \ diffusion \\ &+ \left[U + \frac{1}{4p^2}\frac{\partial(p^2 v A_1)}{\partial p}\right]\frac{\partial f_a}{\partial z} && spatial\ \ convection \\ &+ \frac{1}{p^2}\frac{\partial}{\partial p}\left(p^2 A_2 \frac{\partial f_a}{\partial p}\right) && momentum\ \ diffusion \\ &+ \left[\frac{p}{3}\frac{\partial U}{\partial z} + \frac{v}{4}\frac{\partial A_1}{\partial z}\right]\frac{\partial f_a}{\partial p} && momentum\ \ convection\end{aligned} \tag{1.8}$$

that determines the evolution of the isotropic part of the distribution of cosmic rays $f_a$ in a reference system comoving with the plasma. It takes into account: a source term $S_a$, that counts for the particles created during the propagation; the transport terms, both through diffusion and through convection and the acceleration terms. $\kappa_i j$ is the spatial diffusion tensor, $A_1$ is the adiabatic deceleration rate, $A_2$ the momentum diffusion coefficient. For more details refer to [Schlickeiser, 2013].

An analytical solution of the cosmic transport equation doesn't exist. In order to solve it, one must recover to numerical calculation and software like DRAGON[9] or GALPROP[10]. In particular the latter uses a simplified but efficient model of flat halo diffusion. In this model it is assumed that all the CR sources are embedded in a thin disk and that the diffusion over a scale of hundred parsecs is isotropic.

The particles observed from Earth appear to belong to the sea of cosmic rays, seen the high level of isotropy they manifest. On the other hand, when observing $\gamma$-rays, that carry information of in-situ cosmic rays, it may be important to consider deviation from the average energy density. In this context knowledge of the transport mechanism from the source to the target can be fundamental both to interpret the observation and to understand the nature of the accelerators.

## 1.4 Constraints on cosmic rays features at high energy

As a conclusion of this brief overview one can easily infer that CR still remain an open field of studies. The new branch of gamma-ray astronomy made great progresses, by extending the energy and spatial range of analysis. Gamma rays in fact are a signature of higher energy particles and reaches us practically undeflected from

[9] https://github.com/cosmicrays, [Maccione et al., 2011]
[10] https://galprop.stanford.edu/index.php, [Strong et al., 2009]

all over the Galactic disk. *Fermi*-LAT and H.E.S.S., the first from the space and the other from the ground, provided a lot of informations but remained limited by their instrumental characteristics. CTA will have a better sensitivity and will cover the highest energy range ever, as it will be able to detect emission up to 100 TeV with a very good sensitivity. The combination with molecular clouds, as explained in the following chapters, will make the analysis more and more precise, since it will allow to localize with a certain accuracy the region where the primary CRs gave birth to the secondaries.

By making use of CTA in the analysis of $\gamma$-ray emitters, with a special look on passive molecular clouds, we are willing to:

- test the spectrum of the 'sea' of cosmic rays up to 1 PeV and to compare it with the local one;
- prove or discard the Fermi observed radial profile of CR density;
- search for the existence of a spectral cutoff, and from that make theoretical deduction on the nature of CR accelerators
- look for a correlation between $\gamma$-emission and possible CR accelerators, so to determine their distribution.

# Chapter 2

# Molecular clouds

Molecular clouds (MCs) are regions of relatively dense cold interstellar gas, typically $n \sim$ 100-1000 particle/cm$^3$, that extend in size around few tens of parsecs (1 pc $\simeq$ 3.08 $\times 10^{16}$ m). The outer layers of these regions act as a shield against UV radiation, hence the inner part is kept very cold (T $\sim$ 10-20 K). This makes it possible to have matter in the form of molecules. Hydrogen is the most abundant element, primarily in the form of molecular hydrogen $H_2$, but also its atomic phase is present, especially in the outer layers where molecules of the *shield* absorb radiation and dissociate. Other molecules that can be found in molecular clouds are carbon monoxide (CO), water ($H_2O$), hydrogen cyanide (HCN) and formaldehyde ($CH_2O$). Differently from $H_2$ these last are more likely to be found in the inner parts, since their formation process needs many passages. and each of them needs a cold steady environment. The latter are many times less abundant than $H_2$: for example a typical ratio CO:$H_2$ is estimated to be roughly 1:10000.

MCs in first approximation are then dense conglomerate of hydrogen so they are a perfect place to produce gamma-rays via proton-proton collision; these reaction is very effective and moreover is very easy to model, since it depends only on the cloud mass and distance (2.11). As a matter of fact already the first $\gamma$ satellite COS-B (ESA, 1975-1982) detected gamma ray emission coming from the nearby molecular cloud $\rho$-Ophiuchi.

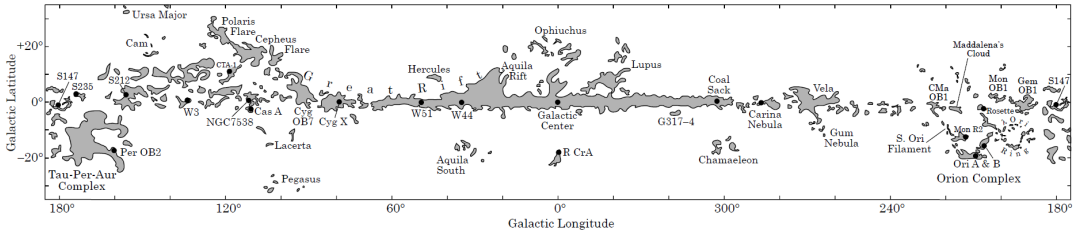


FIGURE 2.1: Location of the main molecular cloud complexes of the Galaxy. Image from [Dame et al., 2001]

Recently a new catalog [Rice et al., 2016] of 1064 Galactic MCs based on the $^{12}$CO survey [Dame et al., 2001] of the Harvard-Smithsonian Center for Astronomy (CfA) at the Cerro Tololo Inter-America Observatory (CTIO) has been released. The carbon monoxide is believed to be the best tracer of molecular hydrogen $H_2$, the main constituent of MCs, that is instead practically invisible.

This chapter is dedicated to molecular clouds, with the specific focus on the ones from the already quoted Rice's catalog. The principal features of these objects are

presented in the first section (2.1) as well as the techniques to determine their physical properties. The second section 2.2 explains how molecular clouds can serve to derive informations on the global spectrum of cosmic rays and presents some examples of results already derived with the current gamma-rays instruments.

## 2.1 Characterization of clouds

Molecular clouds are identified among the detected gas as enhancement of the local density. The news of the Rice et al. catalog is that the selection of MCs has been performed by making use of a *dendrogram technique* [Rosolowsky et al., 2008]. This technique exploits the peculiarity of the molecular gas of having a hierarchical structure that spaces from the the low-density gas of the envelope to the dense core where stars form. This hierarchical structure reflects on the pattern of emissions of the spectral lines and hence allows to identify and characterize the clouds.

Physical properties are assigned based on luminosity: for example distance is inferred from the rotational curves from the Doppler signature, while mass is derived by the brightness temperature profiles along the line of sight. The considered catalog contains objects with masses that spans from 0.03 to 115 $M_5$ ($\equiv 10^5$ $M_\odot$) and distances between 0.33 and 17.4 kpc with an angular size in between 2 and 62 arcmin. In figure 2.2 the distribution of the clouds of the catalog in terms of distance and mass is shown. They are also distinguished between northern and southern objects. Clouds in the south belong to the central region (l $<$ 60°or l $>$ 300°) and in general are more massive and far, while the northern ones are smaller and closer, since they belong to the arms.

### 2.1.1 Determination of the distance

MCs are not characterized by a standard size or a standard luminosity, hence the usual 'standard ruler' or 'standard candle' methods can not be applied to them. Nevertheless molecular clouds populate the spiral arm of our Galaxy, hence they are correlated to the rotation of the Milky Way itself. Assuming to know with certainty the rotational curve of the Galaxy, one can measure the velocity of the cloud and link it with a galactocentric position [Roman-Duval et al., 2009]:

$$r = R_\odot \sin(l) \frac{v(r)}{V_r + V_\odot \sin(l)} \tag{2.1}$$

where $R_\odot$ is the galactocentric radius of the Sun ($\approx$ 8.5 kpc), $V_\odot$ is its orbital velocity around the center of the Galaxy ($\approx$ 220 km/s), $v(r)$ is the rotation curve and $V_r$ is the object radial velocity. $V_r$ is inferred from the Doppler shift of emission line; $v(r)$ is parametrized from observations as well, since data deviate significantly from the theoretical models.

Most of galaxies show a flat rotation curve, differently from what expected from their density profiles, as inferred from the luminous components. This can be explained either by assuming the presence of an important component of non-emitting matter, the *dark matter*, or assuming that at larger scales gravity laws get modified (MOdified Newtonian Dynamics, MOND). Milky Way is not exceptional: its rotational curve

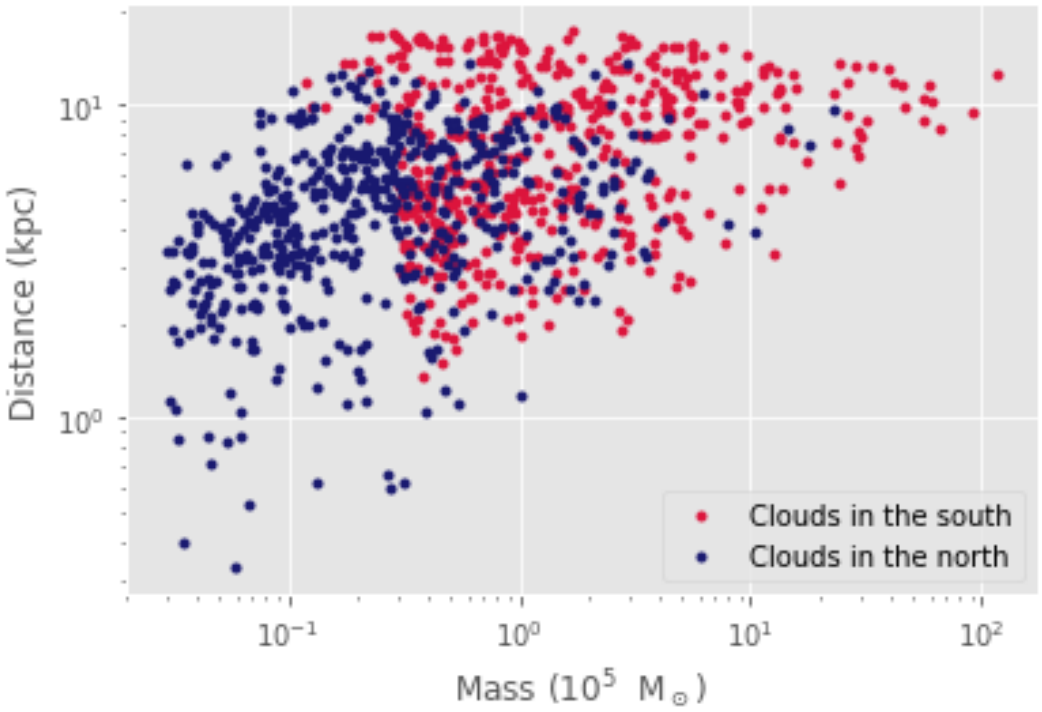


FIGURE 2.2: Distribution of the 1064 MCs of the Rice et al. catalog in mass and distance. Clouds visible from the northern hemisphere are marked in blue, whereas southern ones in red.

was derived by Clemens [Clemens, 1985] from the diffuse gas and is shown in figure 2.3. The points were fitted as a broken polynomial:

$$v(r) = \begin{cases} 3070 \cdot r - 15809 \cdot r^2 + 43890 \cdot r^3 - 68287 \cdot r^4 + 54904 \cdot r^5 - 17731 \cdot r^6 \text{ km s}^{-1} & \text{if } \frac{r}{R_\odot} < 0.09 \\ 325 - 248 \cdot r + 232r^2 - 111 \cdot r^3 + 25 \cdot r^4 - 2 \cdot r^5 \text{ km s}^{-1} & \text{if } \frac{r}{R_\odot} < 0.45 \\ -2342 + 2507 \cdot r - 1024 \cdot r^2 + 224 \cdot r^3 - 28 \cdot r^4 + \cdots & \\ \cdots + 2 \cdot r^5 - 0.08 \cdot r^6 + 0.001 \cdot r^7 \text{ km s}^{-1} & \text{if } \frac{r}{R_\odot} < 1.6 \\ 235 \text{ km s}^{-1} & \text{elsewhere} \end{cases} \tag{2.2}$$

Many factors like local velocity perturbations, expanding shells, deviations from a circular motion, can affect the estimation of the kinematic distance. Recent measurements of parallax of masers embedded in molecular clouds, helped to improve $v(r)$, tracking with more precision the position of the spiral arms. Rice et al. for the characterization of the clouds in their catalog make use of a software that takes into account the vicinity to these objects as well and generates a probability curve from witch it extracts the distance [Reid et al., 2016].

Once derived the galactocentric distance, however, it still remains an ambiguity on the distance $d$ from us. Two clouds on the same ring may have the same radial velocity. The solution for $d$ in fact yields to:

$$d = R_0 \cos(l) \pm \sqrt{r^2 - R_0^2 \sin^2(l)} \tag{2.3}$$

meaning that at the same r correspond two different position along the line of sight. Moreover when $r = R_0 \sin(l)$ the far and near distances result equal ($d = R_0 \cos(l)$). This

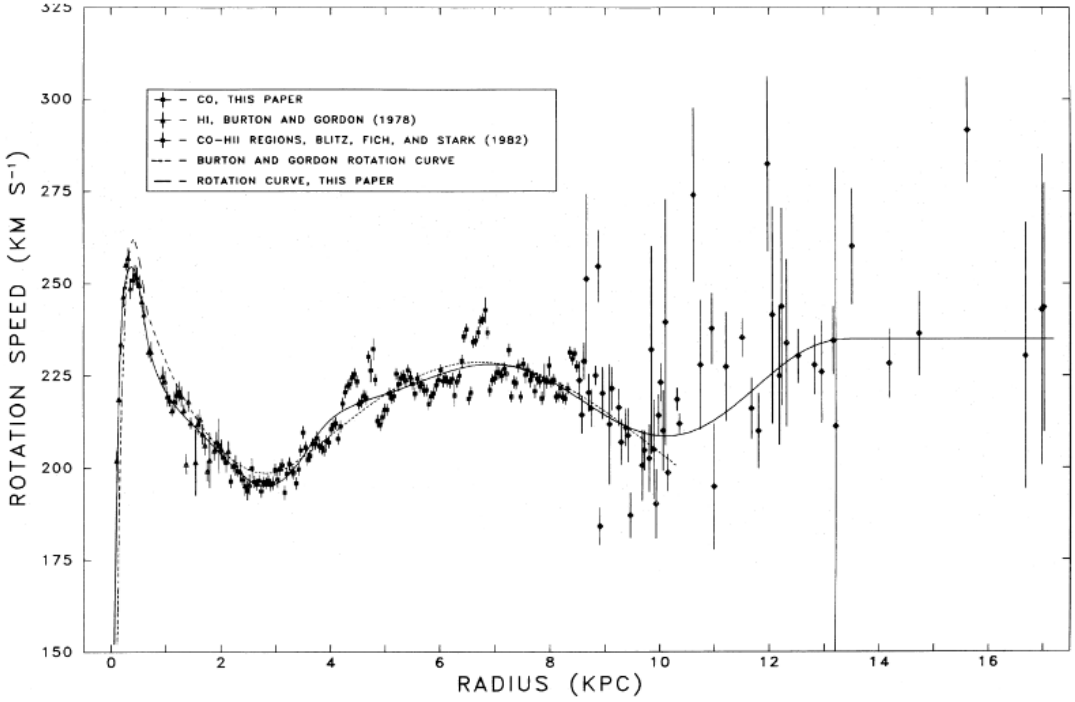


FIGURE 2.3: Rotation curve of the Milky way as in [Clemens, 1985].

problem is known as Kinematic Distance Ambiguity (KDA), and it is an unpleasant issue in the inner galaxy. To deal with it, many techniques have been proposed, for example [Roman-Duval et al., 2009] for MCs makes use of the hot HI in the interstellar medium: if the cloud lies at the near distance it will absorb the emission coming out from the hot gas behind and vice versa; the absorption line should show the same Doppler shift as the cloud spectrum.

### 2.1.2 Determination of the mass

As well as the distance, also the mass of the cloud is determined via its emission features. The question here however is even more delicate, since the major contributor to the cloud mass, namely $H_2$, is practically invisible. In order to estimate the mass, it is necessary to rely on a tracer. CO is the most used tracer of molecular hydrogen but it is not exempt of problems. Assuming to know precisely the conversion factor between the tracer and $H_2$ column density, then derive the mass is pretty easy. Usually it is possible to obtain the *brightness temperature vs. velocity* profile $T_b = T_b(v)$ of the tracer from observations. The brightness temperature is the temperature of an object that has the same brightness (e.g. energy emitted per unit time, area and solid angle) than a black body of that temperature:

$$I_\nu = \frac{2h\nu^3}{c^2} \frac{1}{e^{\frac{h\nu}{kT}} - 1} \tag{2.4}$$

where $h$ is the Planck constant, $\nu$ is the frequency, $k$ is the Boltzmann constant and $c$ the speed of light. On the other hand velocity is related to physical distance as explained in the former section. Once the temperature profile is measured, the abundance of the tracer can be derived from the integral emissivity (W) and, under some assumptions, this quantity can be related to the $H_2$ column density $N(H_2)$, namely the number of protons per unit area. Then having $N(H_2)$ the mass $M$ can be derived integrating over the physical size of the MC:

$$M(H_2) = 2m_p \int N(H_2)\, dA \tag{2.5}$$

where $m_p = 1.67 \times 10^{-27}$ kg is the proton mass, and $dA$ is the surface element. The factor 2 takes into account that the molecule is made of two protons.

### The problem of the CO-to-$H_2$ conversion factor

Molecular hydrogen is the most abundant molecule of the Universe and the major component of molecular clouds. A good knowledge of its distribution and abundance is needed in order to estimate MCs' mass. $H_2$ unfortunately has no directly observable emission. Being formed by two identical atoms it has no permanent dipole moment and hence no corresponding dipolar rotational transitions. Other transitions are rare to occur or need very special environmental condition[1]. On the other hand CO has a permanent dipole moment and can be exited even in the cold MC environment, producing a well visible emission at 2.6 mm. Therefore one usually tries to relate hydrogen abundance to CO emission via expressions like equation 2.6 here:

$$N(H_2) = X_{CO} W(^{12}C^{16}O J = 1 \rightarrow 0) \tag{2.6}$$

where $N(H_2)$ is the molecular hydrogen column density (in cm$^{-2}$) and it is related to the observable integrated intensity $W$ (traditionally in units of K km s$^{-1}$) of $^{12}$CO J=1 $\rightarrow$ 0 transition, via the factor $X_{CO}$. There exist several methods to determine the conversion factor. One of these is to derive $X_{CO}$ from MC $\gamma$-ray emission, that implies however to know exactly the spectrum of primary cosmic rays, that is against the methodology we propose in this work. Another option is to exploit the virial theorem to give an independent estimation of the mass, but there is no proof that MCs are actually in virial equilibrium. A further method is to consider the emission of an optically thin isotopologue of $^{12}$CO, for example $^{13}$CO. By comparing the emission of the two isotopologues it is possible to infer the absorption coefficient and to relate it to the hydrogen total column density. Lastly it is possible to make use of dust emission, whose optical depth should in principle be proportional to the gas density. Modeling of dust absorption coefficient however are feasible only within 1-2 kpc. At the end despite the biggest uncertainties, it is commonly assumed that the conversion factor should be close to:

$$X_{CO} \approx 2 \times 10^{20} \text{ K km s}^{-1} \tag{2.7}$$

according to the discussions in [Bolatto et al., 2013].

Moreover it must be stressed that is not even clear if it is possible to assume a constant $X_{CO}$ all around the Galaxy. $H_2$ and CO, in fact, follow a different formation process that strongly depends on environmental metallicity. That could imply a spatial dependence of $X_{CO}$ that in principle could vary even within the same size of a cloud.

## 2.1.3 Gamma-ray emissivity

Molecular clouds have been proved to be $\gamma$-ray emitters [Aharonian, 1991] and their emission should reflect their ambient CR spectrum. We assume in fact that MCs are passive emitters, that means that the $\gamma$ emission that they produce, is the result of the interaction between high energy cosmic rays and the protons that populate the cloud in the reaction: $p + p \rightarrow \pi^0 \rightarrow 2\gamma$. The $\gamma$-ray emissivity, is calculated from the proton spectrum as in 1.6 like:

$$\phi_\gamma(E_\gamma) = 4\pi n \int J(Ep) \frac{d\sigma_{pp\rightarrow\gamma}}{dE_\gamma} \, \mathrm{d}E_p \tag{2.8}$$

[1]The lowest energy transitions of $H_2$ are its purely rotational quadrupole transitions but these are too weak owing to their long spontaneous decay lifetimes: $\tau_{decay} \sim 100$ yrs. The two lowest para and ortho transitions have upper level energies and are only excited in gas with T > 100 K [Bolatto et al., 2013]

Here $\phi_\gamma(E_\gamma)$ measures the number of secondaries produced per cubic centimeter per second per unit energy interval and $n$ is the numerical density of protons. We assumed a uniform distribution of interstellar matter and a uniform distribution of cosmic rays with an energy spectrum independent of the position.

In order to relate 2.8 and the observed flux at Earth $F_\gamma(E_\gamma)$, consider that by definition:

$$\phi_\gamma = \frac{\mathrm{d}N_\gamma}{dV\ dE_\gamma\ dt} \tag{2.9}$$

and

$$F_\gamma(E_\gamma) = \frac{\mathrm{d}N_\gamma}{dA\ dE_\gamma\ dt} \tag{2.10}$$

So it is sufficient to integrate in $dV$ and to divide for the area of interest that, if the emission is isotropic, corresponds to the area of the sphere centered on the cloud and with the cloud distance ($d$) as a radius. Then:

$$\begin{aligned} F_\gamma(E_\gamma) &= \int \frac{dV}{4\pi d^2}\ \phi_\gamma(E_\gamma, \mathbf{r}) = \\ &= \int \frac{\rho}{m_p} dV \frac{1}{\cancel{4\pi} d^2 \cancel{4\pi}} \int J(Ep) \frac{d\sigma_{pp\to\gamma}}{dE_\gamma}\ \mathrm{d}E_p = \\ &= \frac{M^{[m_p]}}{d^2} \int J(Ep) \frac{d\sigma_{pp\to\gamma}}{dE_\gamma}\ \mathrm{d}E_p \end{aligned}$$

Where $M^{[m_p]} \equiv \frac{M}{m_p}$ is the total mass of the cloud in unit of the proton mass.

It is common to express each quantity as a function of $M_5 \equiv M/10^5\ M_\odot$ and $d_{\mathrm{kpc}} \equiv d/1\ \mathrm{kpc}$ that are typical values for the clouds. Then it will be:

$$F_\gamma(E_\gamma) = 1.25 \times 10^{19} \frac{M_5}{d^2_{kpc}} \int J(Ep) \frac{d\sigma_{pp\to\gamma}}{dE_\gamma}\ \mathrm{d}E_p \tag{2.11}$$

So we see that for MCs the ratio $\frac{M_5}{d^2_{kpc}}$ is a key parameter. The more massive and close the cloud is, the higher will be the measured flux. The plots in 2.4 show the expected flux for clouds with different $\frac{M_5}{d^2_{kpc}}$ parameter.

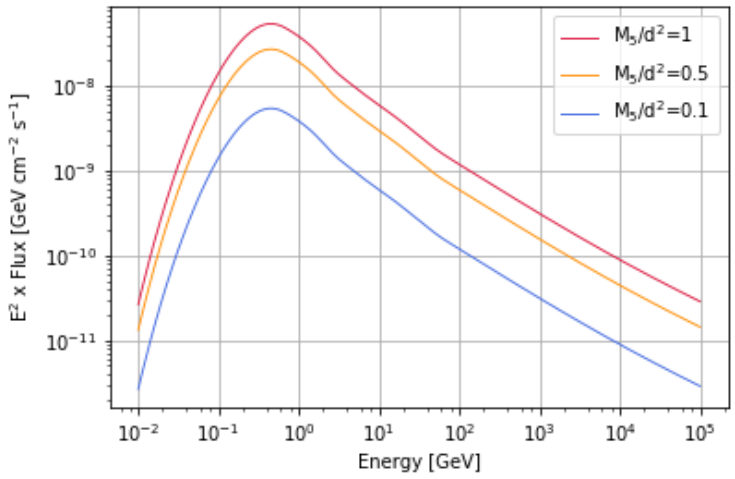


FIGURE 2.4: Differential gamma ray flux expected for a molecular cloud with $M_5/d^2_{kpc}$ = 1, 0.5, 0.1 assuming AMS spectrum for protons as in [Aguilar et al., 2015] and [Kafexhiu et al., 2014] parametrization for the differential cross section.

### 2.1.4 Star formation

If the mass of a cloud, or a part of it, exceeds a certain limit, known as *Jeans mass*, it inevitably undergoes a gravitational collapse. The energy released heats up the medium, until the temperature of the gas is sufficient to allow hydrogen burning (T $\sim 10^6$ K). This, in a very simplistic way, is how a star is born. Molecular clouds are the nurseries where new stars come to light. A common distinction is made between normal clouds, that can form only small star, and giant molecular clouds (GMCs) of masses $\sim 10^6$ $M_\odot$ that are able to give birth to all kind of stars. The former are more interesting in order to study the 'sea' of cosmic rays, whereas the latter ones are more likely to host an accelerator in their inner part, as discussed in §1.2.

Of the sample of Giant Molecular Cloud of [García et al., 2014] $\sim$ 85% of molecular clouds show star formation activity. Evidences of the formation process can be deduced from the observations in the infrared waveband. New born stars emit in the UV, that is absorbed from the cold gas and dust, that then re-emit in the far infrared (FIR). As suggested by [Luna et al., 2006], the formation rate of massive stars (MSFR) can be related to the FIR luminosity of the clouds as:

$$\dot{M} = 6.5 \times 10^{-10} \left( \frac{L_{FIR}}{L_\odot} \right) \mathrm{M}_\odot \ \mathrm{yr}^{-1} \ . \tag{2.12}$$

That allows to estimate the average efficiency of star formation in molecular clouds. It turned out, from Garcìa's calculation that the MSFR in GMC is on average of $\sim 0.41\ L_\odot/M_\odot$, but there are region where it reaches 0.58 $L_\odot/M_\odot$. MSFR in molecular clouds is a factor 2 bigger than the average rate of the Galactic plane ($\sim 0.21\ L_\odot/M_\odot$). Nonetheless the percentage of gas that participate to star formation, on average seems to be limited to the 3 %, suggesting that maybe a model that include only gravitational collapse is too simple.

## 2.2 Molecular clouds as CR 'barometers'

In the past attempts to make significant studies with molecular clouds have always been considered unfeasible due to the faintness of the gamma-emission together with the limitation of the instrumentation sensitivity. Studies of clouds emission limited themselves to two extreme cases: (i) nearby molecular clouds [Ackermann et al., 2012a], [Yang et al., 2014] or (ii) very massive molecular clouds of the Sagitarius B complex [Yang et al., 2015]. The release of the Rice et al. catalog, with its brand new technique of individuation of clouds, together with the improved instrumental capabilities that will be achieved with CTA, however, opened up new chances for this analysis. It turned out in fact that in the Galaxy there are several giant molecular clouds, some of them that even reach $10^7$ $M_\odot$. The main advantage in dealing with clouds is that, being dense region of gas (mainly hydrogen) they enhance the chances of interaction for cosmic rays and therefore for production of gammas. Moreover the hadronic channel here dominates on the leptonic one, since $H_2$ peaks in the region of the cloud, whereas electrons are spread along the entire line of sight. Clouds are then perfect objects to investigate the spatial features of cosmic radiation: studies on the diffuse gas emission have already been performed by the *Fermi*-LAT collaboration [Ackermann et al., 2012b], but clouds allow to make a finer investigation on the topic. MC being limited to 10-100 pcs in size allow us to understand the CRs features in a restricted area and are perfect then to test the 'sea' of cosmic rays all around the Galaxy. They will serve then, as suggested in Casanova's article [Casanova et al., 2010], as cosmic 'barometers' since they will allow to derive information of cosmic ray energy density (that has the same units as pressure from which the term 'barometers').

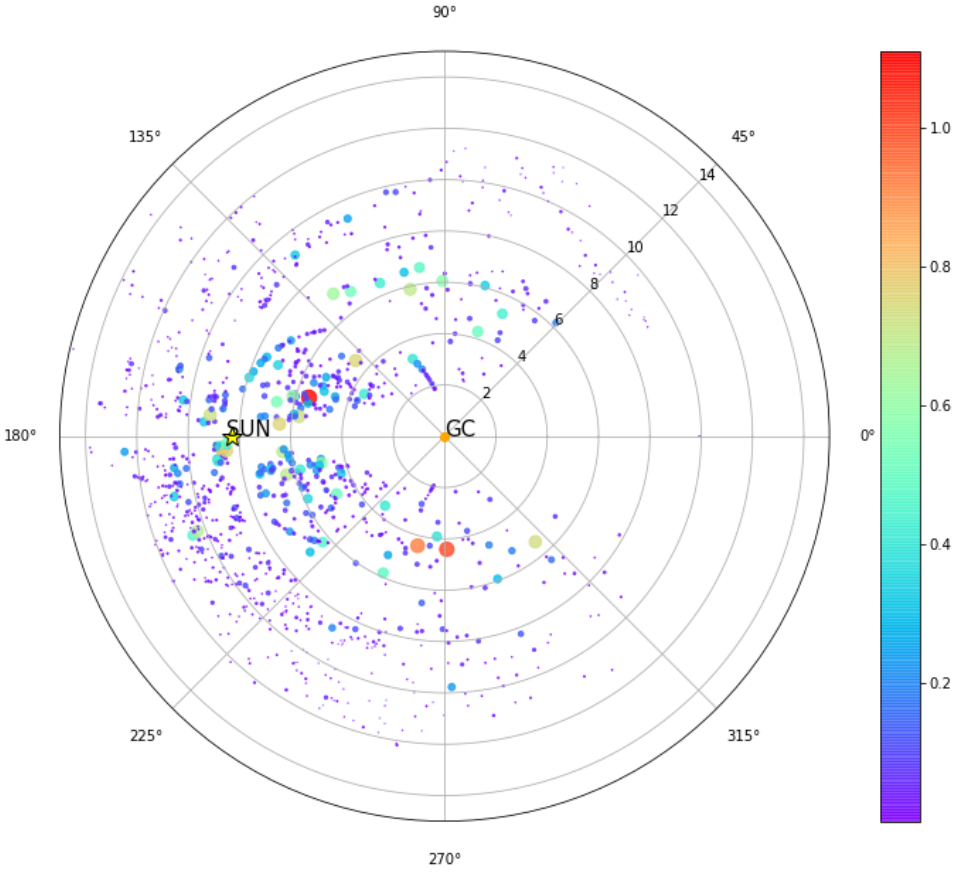


FIGURE 2.5: Galactic distribution of the clouds of the [Rice et al., 2016] catalog. Colors and size of the markers are scaled with the $M_5/d^2_{kpc}$ parameter. The numeration of the rings represents the distance in kpc from the Galactic Center (GC)

### 2.2.1 Nearby molecular clouds

The Gould belt region is a nearby ring-like structure of young stars and star forming regions. Its center is located 100 pc away from the Sun and its perimeter includes the Sun itself, so that the nearest object of the belt is just 12 pc away. Its main objects are big molecular clouds as Orion, $\rho$-Ophiuchi, Taurus [Poppel, 1997]. An analysis of the gamma-ray flux outcoming from these clouds was performed by making use of *Fermi*-LAT data in [Yang et al., 2014]. Yang et al. had the same aim of this work: to probe the cosmic ray spectrum by means of molecular clouds. From their analysis it emerges a noteworthy correspondence with the local cosmic ray spectrum measured by the PAMELA collaboration, at least at energies higher than 10 GeV. Surprisingly most of these clouds are in fact characterized by a $\Gamma$=2.85 spectral index, despite their known star formation activity. The analysis of these so close objects however suffers from uncertainties related both to the big angular extension, that affects the sensitivity, and to the distance, that for nearby objects has an error comparable to the value itself ($\sigma_{dist} \sim 1$ kpc).

### 2.2.2 Molecular clouds in the Central Molecular Zone

On the other side stands the central molecular zone (CMZ), a region within about 300 pc from the Galactic Center, that hosts a high concentration of molecular gas. Its total mass in molecules is estimated to be $3 \times 10^7$ $M_\odot$ [Jones et al., 2012]. In this region is embedded Sagittarius B2, that with its estimated mass of 1.5 $\times 10^7$ $M_\odot$, is up to now the most massive

molecular cloud in the Milky Way. Despite its distance from us, the high mass of this cloud, together with the small angular size made possible the detection of its gamma-ray emission with *Fermi* and the consequent derivation of the ambient proton spectrum. Again the analysis of *Fermi*-LAT data showed a good correspondence with the local spectrum.

The analyses performed on the *Fermi* data of these objects then suggests the actual existence of the *sea* of cosmic rays. This is in disagreement with the results that comes out from the diffuse gas, that want the cosmic ray density to increase towards the Galactic center.

# Chapter 3

# Main sources of gamma rays

As already pointed out molecular clouds, as dense restricted region of gas, make it possible to localize with a certain precision the high energy protons of the cosmic rays. This key property permits to explore the CR spectrum in regions different from our local environment.

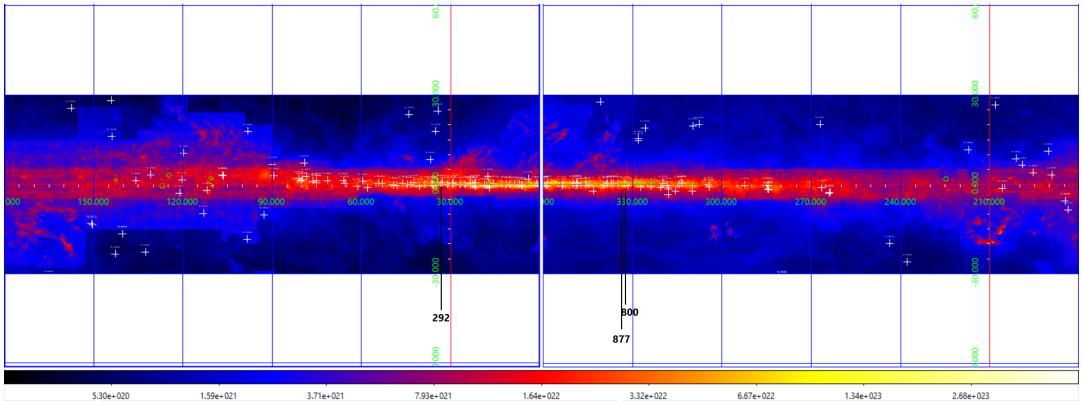


FIGURE 3.1: Bidimensional map of the $H_2$ + HI column density derived from [Dame et al., 2001] CO data cubes and the HI4PI [Bekhti et al., 2016] data survey. White crosses label TeV sources from Chicago TeV-catalog [Wakely and Horan, 2008]. The three most massive clouds of the [Rice et al., 2016] catalog are highlighted by a black arrow

Anyway in order to constrain the radiation that comes from the clouds, we have to be able to distinguish between the gamma emission that truly comes from our clouds and the emission that comes from the several other possible sources of gammas. In this chapter we explore the main sources of gamma rays, starting from diffuse hydrogen, that is spread all around the Galaxy both in the molecular and in the atomic phase, and emits as a passive emitter, just as our clouds do, because of the interactions with high energy protons. As well as protons, also electrons that populate the cosmic rays interact with the ISM and produce gamma-rays via the inverse Compton (IC) scattering or bremsstrahlung radiation; although these processes give less contribution at high energies, the leptonic component remains a nasty problem, since it is not possible to track with precision the distribution of electrons and consequently their contribution to the gamma-ray emission.

Besides these passive emitters stand the 'active' TeV-emitters. Astronomical objects like pulsars and their nebulae, supernova remnants, binary stars systems, star forming regions, starbursts, and active galaxies are producers of high energy photons and hence are sources of background.

Finally a non negligible component of background comes from the atmosphere. Gammas can be produced as interaction of cosmic radiation and the particles in the Earth atmosphere.

These ones are not distinguishable from cloud originated radiation, and are not predictable. Therefore they are usually treated with statistical methods.

## 3.1 The diffuse gamma emission

This section presents the main sources of diffuse gamma emission and their relative importance at VHE. We present the main mechanisms that make the gas radiate at high energies. The hadronic component is considered, mostly in the form of hydrogen, as well as the leptonic counterpart. A minor, but still present contribution to the diffuse emission may derive from the emission of unresolved sources.

### 3.1.1 The diffuse hydrogen component

Most of the gas in the interstellar medium is composed of hydrogen both in its molecular or in its atomic phase (see [Tielens, 2005] for a complete review). As well as the one in the clouds, the diffuse hydrogen can interact with the CRs and give birth to gamma photons.

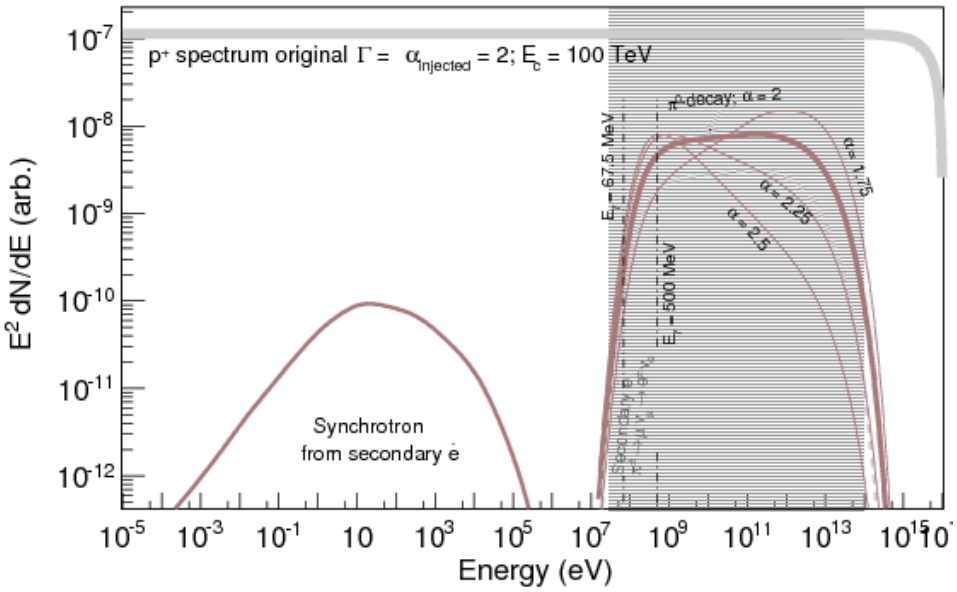


FIGURE 3.2: Spectrum of gamma rays produced by Galactic hydrogen as result of inelastic collision and decay of daughter particles. Figure from [Funk, 2015]

Differently from the molecular counterpart, HI emits at the well known 21 cm wavelength and hence it is directly detectable. The recent HI4PI work [Bekhti et al., 2016] collected many survey and provides the data cubes (v,l,b) of the measured brightness temperature and the recovering formula to get the column density from that. In equation 3.1 is shown the relation between HI column density and, in 3.2, the one for $H_2$ is recalled.

$$n_{HI}[cm^{-2}] = 1.823 \times 10^{18} \int \mathrm{d}v \, T_B(v)[\mathrm{K} \cdot \mathrm{km} \cdot \mathrm{s}^{-1}] \tag{3.1}$$

$$n_{H_2}[cm^{-2}] \approx 10^2 \, n_{CO}[cm^{-2}] \approx 2 \times 10^{20} \int \mathrm{d}v \, T_B^{[CO]}(v)[\mathrm{K} \cdot \mathrm{km} \cdot \mathrm{s}^{-1}] \tag{3.2}$$

From the column density, the gamma-ray flux is calculated in analogy to what was done in chapter 2, starting from the emissivity $\phi(E_\gamma)$ as defined in 2.9:

$$F(E_\gamma) = \int \frac{dV}{4\pi r^2}\phi(E_\gamma) = \int \frac{dV}{\cancel{4\pi r^2}}\cancel{4\pi} n \int J(E_p)\frac{d\sigma}{dE_\gamma}dE_p \tag{3.3}$$

$$= \int \frac{\cancel{r^2}}{\cancel{r^2}} n \cdot dr \int d\Omega \int J(E_p)\frac{d\sigma}{dE_\gamma}dE_p \tag{3.4}$$

$$= n_{col} \int d\Omega \int J(E_p)\frac{d\sigma}{dE_\gamma}dE_p \tag{3.5}$$

where here we wrote the the volume element as $dV = r^2 dr\ d\Omega$ assuming a spherical geometry and used the fact that $n \cdot dr$ is exactly the column density. The total column in hydrogen (taking into account both molecular and atomic contribution) is calculated as $n_{col} = n_{HI} + 2n_{H_2}$.

The neutral and molecular hydrogen are confined to the plane of the Galaxy but they have a different radial distribution. The first one extends from $\sim$ 3 kpc to $\sim$ 15 kpc from the Galactic Centre, whereas $H_2$ seems to be concentrated in a ring of radii $3 \lesssim r \lesssim 8$ kpc. In figure 3.3 are shown the profiles of HI and H2 along the line of sight corresponding to the coordinates of three molecular clouds of the [Rice et al., 2016] catalog. HI data were recovered from the so-called HI4PI survey, that is an all-sky survey obtained by combining observations of the 21 cm line from LAB, GASS and EBHIS surveys. CO data are instead from the [Dame et al., 2001] collection of observations made with the 1.2 meter Millimeter-Wave Chilean telescope of the Harvard-Smithsonian CfA. It emerges that the atomic hydrogen is spread along the entire LoS, while the molecular hydrogen $H_2$ tends to be concentrated in smaller region. In some cases (like for the cloud in figure 3.3 (d)) there appears to be more than one big object in the same line of sight (LoS); whereas in other cases the considered cloud is the only relevant object in the LoS (as the cloud in fig 3.3 (f)). HI in general will be treated as *background* and then subtracted, because the expected flux is calculated using the mass provided by the catalog that takes into account only $H_2$, even though HI could contribute to the MC gamma-ray emission. Molecular clouds are likely to have an HI halo that prevents UV radiation to penetrate and destroy molecules. The mass of the HI counterpart is calculated from the density profiles and is around 10 % of the total mass. This could be significant in some case for cloud detection and analysis, but as a preliminary step we'll neglect it and consider it as background. Table 3.1 presents as an example the values of the column density of the gas in the considered LoS. It can be seen that clouds are peaks in the $H_2$ distribution whereas they do not significantly contribute to the HI amount.

| MC | l (deg) | b (deg) | v(km/s) | $n_{HI}(cm^{-2})$ | $n_{H_2}(cm^{-2})$ | MC HI % | MC H2 % |
|---|---|---|---|---|---|---|---|
| 292 | 30.49 | -0.04 | 96.04 | $1.99 \times 10^{22}$ | $6.7 \times 10^{22}$ | 12 % | 38 % |
| 800 | 332.28 | -0.07 | -90.82 | $1.83 \times 10^{22}$ | $8.2 \times 10^{22}$ | 10% | 67 % |
| 877 | 333.46 | -0.31 | -49.46 | $1.58 \times 10^{22}$ | $7.8 \times 10^{22}$ | 11 % | 52 % |

TABLE 3.1: Column density of hydrogen from the HI and the $H_2$ contribution in the line of sight of three molecular clouds of the [Rice et al., 2016] catalog. The percentage amount of gas from the two components included in the cloud is also reported. These values were computed from the data of [Bekhti et al., 2016] and [Dame et al., 2001]

Heavier nuclei, mostly helium, are computed to account for the 10% to the gamma emissivity [Huang et al., 2007].

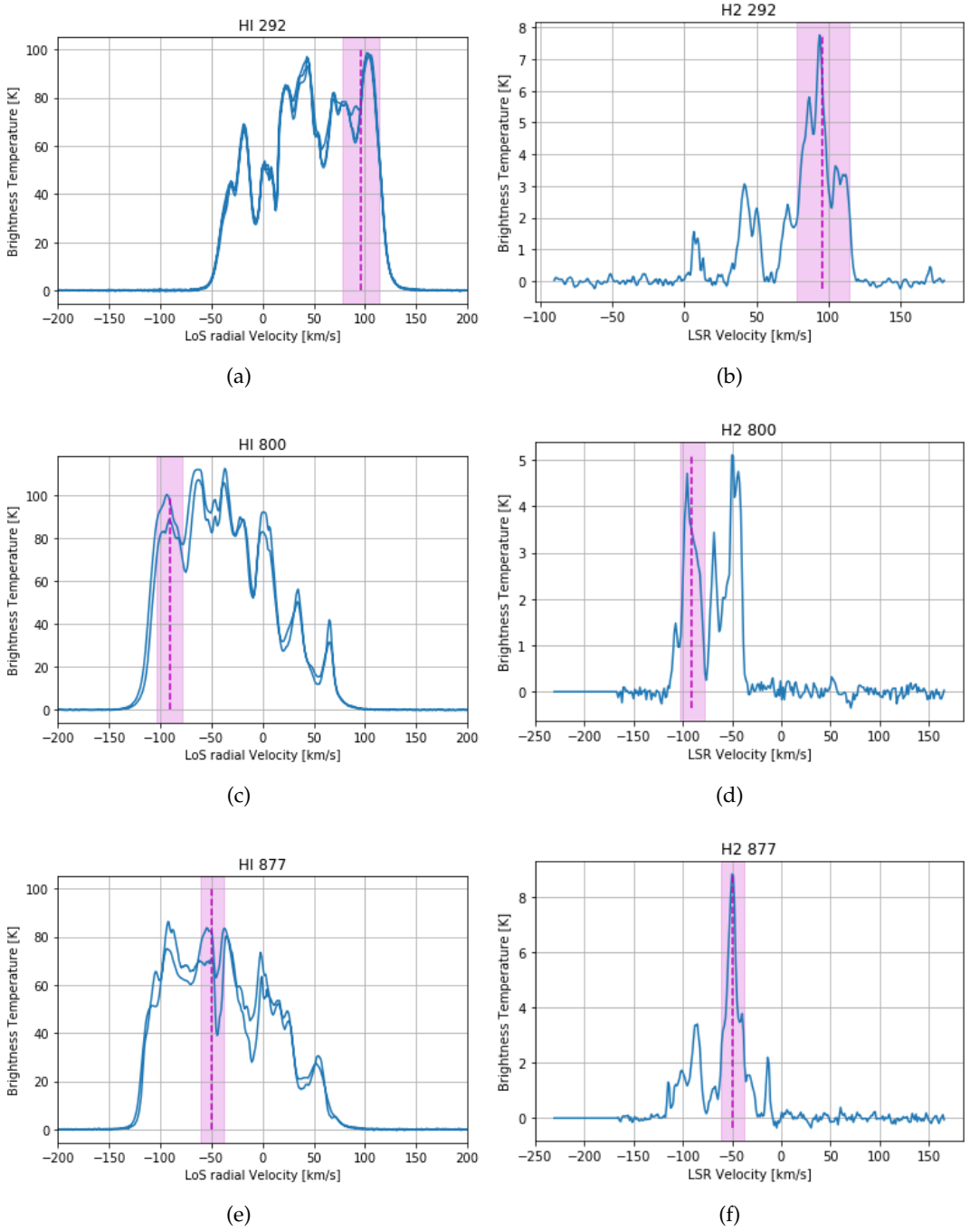


FIGURE 3.3: Brightness temperature profile as a function of the radial velocity for HI (on the left) and CO (on the right) as a proxy of $H_2$ at the line of sight corresponding to three MCs of the CfA catalog. The dashed purple line, that corresponds to the cloud radial velocity and the colored area, that is the corresponding velocity range, as reported in the catalog, individuate the cloud position and extension in the LoS.

### 3.1.2 The electronic component

As well as the protons also the electronic counterpart of the cosmic radiation can source gamma-rays. There exist four processes for the production of HE photons by electrons: inverse Compton (IC) scattering, bremsstrahlung, annihilation of positrons and synchrotron radiation. The first one contributes significantly up to the sub TeV regime, while IC is efficient in almost every energy band. Pair annihilation and synchrotron instead contribute less at very high energies. On the other hand the synchrotron process, forces high energy electron to lose energy, hence it modulates the electrons distribution.

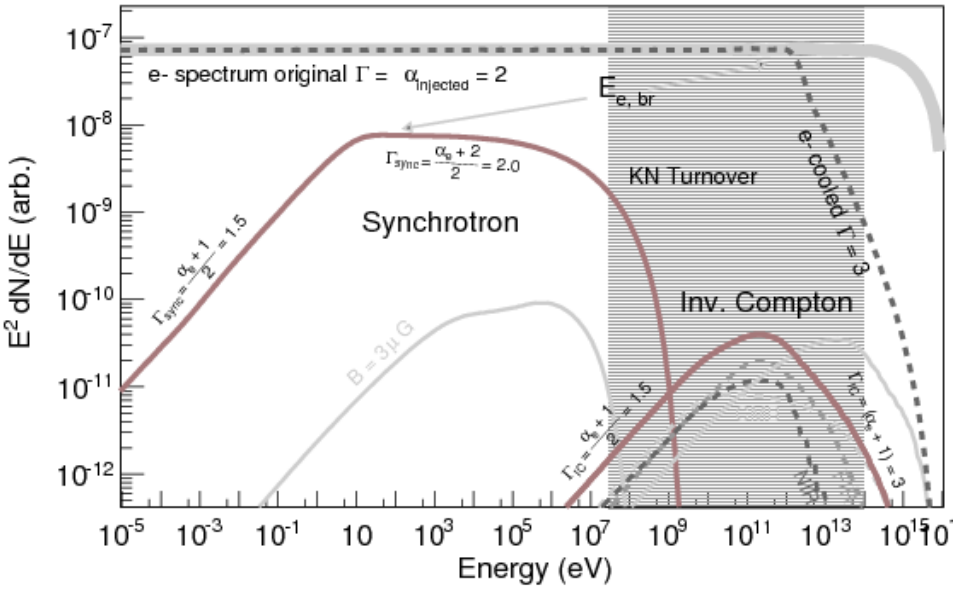


FIGURE 3.4: Spectrum of Galactic electrons derived as result of the main processes cited above. Figure from [Funk, 2015]

#### The inverse Compton emission

One of the principal channel of production of cosmic gamma-rays in astrophysics comes from the interaction of the ultra-relativistic particles with the photons field in the so called *inverse Compton scattering*. In this interactions the target photon receives part of the electron energy and is consequently *up*-scattered to higher frequencies. The process cross section is derived in the context of quantum field theory as the interaction of a free electron with a photon field. In analogy to the "direct" Compton scattering, the Klein-Nishina formula holds [Blumenthal and Gould, 1970]:

$$\sigma_{IC}(E_\gamma, \epsilon, \gamma) = \frac{3\sigma_T}{4\epsilon\gamma^2} G(q, \Gamma_e) \text{ cm}^2 \text{ eV}^{-1} \tag{3.6}$$

with

$$G(q, \Gamma_e) \equiv \left[ 2q \ln q + (1+2q)(1-q) + \frac{(\Gamma_e q)(1-q)}{2(1+\Gamma_e q)} \right]$$

and

$$\Gamma_e = 4\epsilon\gamma/(mc^2), \quad q = E_\gamma/[\Gamma_e(\gamma mc^2 - E_\gamma)]$$

whereas $\gamma$ is the initial Lorentz factor of the electron, and $\epsilon$ and $E_\gamma$ stand for the energy of the photon before and after the scattering. Therefore equation 3.6 gives the probability of production of a photon of energy $E_\gamma$, from the interaction of an electron of energy $mc^2\gamma$, with a photon of energy $\epsilon$. $\Gamma_e$ is the so called *Compton parameter* and set the threshold between two

regimes: the Thomson regime ($\Gamma_e \ll 1$) and the Klein Nishina regime ($\Gamma_e \gg 1$). The spectral features of the emitted photons are strongly dependent on this parameter. In particular in the Thomson limit the typical energy of the scattered photon is $\langle E_\Gamma \rangle \sim 4/3\epsilon\gamma^2$ meaning that, with the right combination of $\epsilon$ and $\gamma$, they can cover almost all the electromagnetic spectrum, up to the gamma waveband. In the Klein-Nishina limit the photon energy is close to the electron energy, so the gamma-ray regime can be easily reached. In this regime however the cross section undergoes a lowering due to recoil effects and therefore the IC emission shows a net cutoff.

In order to compute the IC contribution to the gamma-ray emission in the Galaxy one needs to know the energy distribution of the target photons and of the incoming electrons. The photons involved in the Galactic IC come from the 2.7 K Cosmic Microwave Background (CMB) and from the Galactic radiation field: starlight and dust photons at optical-near infrared and far infrared wavelength respectively. Energy density of CMB is universal and is equal to $\approx 0.25$ eV/cm$^3$ (as reported in [Longair, 2011] for example). The Galactic component instead varies from site to site and is rather uncertain. Another troubling uncertainty appears to be in the distribution of high energy electrons. Commonly a uniform distribution of the sources is assumed, but this is rather questionable because it does not take into consideration that to source TeV electrons the accelerator must be quite young ($\approx 10^5$ yr) and very close ($\approx 100$ pc). At least for the inner part of the Galaxy (l> 315°and l<45°) the CR electron spectrum seems to have an index of 2.15 and an energy density $\sim 0.05$ eV/cm$^3$ but this can be significantly different from different side of the Galaxy.

### The bremsstrahlung emission

Bremsstrahlung emission occurs when a free electron interacts with the Coulomb field of an ion and consequently radiates part of its energy. It is then important wherever there are gas concentration. If the gas is neutral it has also to compete with the ionization process and the shielding of the bounded electrons. Very energetic photons can be produced by bremsstrahlung emission, if the electron energy is sufficiently high. The spectrum of pure (where other processes are negligible) bremsstrahlung $\gamma$ rays perfectly reflects the shape of the electron acceleration spectrum, but with $E_\gamma \simeq E_{el}/2$. However, bremsstrahlung emission is suppressed by inverse Compton at energy higher than some TeV and hence will not be taken into consideration in the context of this work.

### The synchrotron energy losses

Synchrotron radiation is the radiation of a relativistic charged particle in a magnetic field of strength $B$ that is uniform on scales much larger than the gyro-radius of the particle (e.g. the radius of the circular trajectory of the particle in a uniform magnetic field of the same intensity, $r_g \equiv mv/qB$). The deflections that the charged particles undergo, induce the emission of electromagnetic radiation, according to the Larmor formula. When this process involves relativistic particles the power emission results peaked in a cone around the velocity direction. The emitted power and the consequent energy losses are influenced by the medium, in this case thermal plasma. The derivation pass through the solution of the transport equation and involves pretty hard calculations, so we refer to the books of Pacholczyk [Pacholczyk, 1977] and Schilickeiser [Schlickeiser, 2013]. The frequency of the emitted radiation depends on the kinetic energy of the electron, and on the strength of the magnetic field as:

$$\langle \nu \rangle \, [\mathrm{MHz}] \simeq 16 \, B[\mu\mathrm{G}] E^2[\mathrm{GeV}]. \tag{3.7}$$

In the interstellar medium $B \sim 3 - 4$ $\mu$G [Shull Jr, 1988], so photons produced via synchrotron radiation difficultly overcome some GHz (1 eV = 2.418 $\times 10^{14}$ Hz), and therefore don't influence the gamma-band observations.

An important role that the synchrotron effect plays instead is to shape the electrons distribution. The energy loss due to this mechanism brakes the particles and this effect is more efficient for the relativistic ones. [Crusius and Schlickeiser, 1988] demonstrated that for relativistic electrons holds the vacuum approximation and therefore the energy loss is given by [Schlickeiser, 2013]:

$$-\frac{dE}{dt} = -mc^2\frac{d\gamma}{dt} = c\frac{\sigma_T}{4\pi}(B\sin\theta)^2\gamma^2 \ \text{erg s}^{-1} \tag{3.8}$$

where $\sigma_T$, as before, is the Thomson cross section $\gamma$ is the Lorentz factor, $B$ is the strength of the magnetic field that bend the particle's trajectory, $\theta$ is the angle between the magnetic field and the velocity of the particle. Whereas at lower energy the losses are reduced by a factor $\exp(-\gamma_R/\gamma\sin\theta)$, that depends also on the electronic density $n_e$ of the medium, since $\gamma_R = 2.1\times10^{-3}(n_e/1\ \text{cm}^{-3})^{1/2}(B/1\ \text{G})^{-1}$ .

### 3.1.3 Unresolved sources

Another component that can be mistaken for diffuse emission are unresolved sources. This component is unpredictable and for this reason the emission from diffuse gas must be evaluated carefully. For example compare the gamma emission with the radio maps of the gas is always a good cross check. Moreover emission from the diffuse is not expected to have a slope harder than 2.4, [1] so for example this could be another discrimination methods.

## 3.2 Gamma-ray sources

The other component of the background is the discrete component, meaning the direct sources of gamma rays. Many astrophysical objects are able to produce gamma rays, via different mechanism. Up to now hundreds of TeV-emitters are known and are listed for example in the on-line retrievable TeVCat. Main sources of high energy gammas can be pulsars, binary systems and micro-quasars.

### 3.2.1 Pulsars, pulsar winds and plerions

Fermi-LAT measured gamma-ray emission from more that a hundred *pulsars* [Abdo et al., 2013]. These objects are rapidly rotating neutron stars that show an impulsive regular signal in different wavebands from radio (the main observational channel of pulsars) to high energy. Pulsars can provide $\gamma$ photons from three different components: (i) from the magnetosphere, (ii) from the pulsar wind or from (iii) their pulsar wind nebula (PWN).

The emission from the magnetosphere is the combined result from their high spin ($P \approx 10^{-3} - 10$ s) and their high magnetic field ($B \approx 10^{12} - 10^{15}$ G ). Charged particles that leave the surface of the pulsar follow the magnetic field lines and emit radiation for curvature deceleration. The radiation is confined in a conic beam, so that the emission appears to be fan-like (see for example [Longair, 2011]). The gamma beams are expected to be wider and not necessarily correlated to the radio ones, so it can happen, like in the Geminga case [Bignami and Caraveo, 1996], that the pulsar shows gamma emissivity without a radio counterpart. The responsible of particles acceleration is the electric field, that results in a magnetize object by means of the generalized Ohm equation:

$$\frac{\vec{J}}{\sigma} = \vec{E} + \frac{\vec{v}\times\vec{B}}{c} \tag{3.9}$$

[1] These consideration comes from the study of gamma ray emission from the diffuse, as discussed in [Yang et al., 2016]

with $J$ the electric current density and $\sigma$ the conductibility, that, for a perfect conductor $\rightarrow \infty$. Particles accelerated in the direction transverse to the magnetic field rapidly lose energy and fall back onto the pulsar surface. The only particles that can escape the pulsars and produce an observable emission are the ones accelerated parallel to the magnetic field lines. In general the condition $B \cdot E = 0$ is fulfilled, except for two cases: close to the surface of the neutron star or outside at a distance comparable to the light cylinder (an imaginary cylindric surface, whose edges correspond to the limit where the rotation velocity equal the speed of light), where the charges change sign and are no more able to shield the electric field. Independently on the region of production, photons of energy higher than some tens of GeV are not expected from pulsars magnetosphere. This is because high energy photons are heavily absorbed or they create couples $e^+ - e^-$ before they can escape [Caraveo, 2014]. Exceptions can come from millisecond pulsars (MSP), that have lower magnetic fields. MSP are in fact a special class of neutron stars, since they are old neutron stars, that started to rapidly rotate again thanks to the accretion of matter from a companion.

Anyway what is clear from an observational point of view is that gamma ray spectra of pulsars has a typical shape [Aharonian et al., 2013]:

$$E^{-\Gamma} \exp\left[\left(-\frac{E}{E_0}\right)^b\right] \tag{3.10}$$

that is a power law with an exponential cutoff, typically at $E_0 \approx 1 - 10$ GeV. Most of the sources spectra can be fitted with $b = 1$, in agreement with the curvature radiation models. However in some cases the $b$ parameter deviates from unity, suggesting the presence of other mechanisms that can push photons to higher energies.

For example it has been theorized that multi-GeV and TeV photons may come from a cold wind of charged particles that flows out the pulsar and emits synchrotron radiation or interacts via IC scattering with the X-photons generated in the magnetosphere. Typically this wind terminates around 0.1 pc from the pulsar, where it encounters a reverse shock, residual of the supernova explosion. The shock accelerate particles of the ejected plasma up to even $10^{15}$ eV, but the acceleration mechanism is not clear. Models of this emission want the spectrum to flatten around 1 GeV (due to the decrease of Klein-Nishina cross section at higher energies) and a sharp cut off corresponding to the total kinetic energy of the wind.

Particles escaping the pulsar through the wind can populate the surroundings and emit at the same way. These particles form the so-called *pulsar wind nebulae* (PWNe) or *plerions*.

The Crab nebula[2] is the most famous example of PWN. Its spectrum extend for 21 decades (from radio to gamma); at high energies it was measured from some MeV to hundreds of TeV (as in fig. 3.5), proving that PWNe are efficient emitters of VHE photons. Both synchrotron and IC are responsible for the production of gammas; the spectrum of the Crab, and of other known PWNe result as the superposition of these two emission mechanism. The interpretation of synchrotron responsible for $\geq 100$ MeV, in those condition ($B \simeq 100\mu$G), implies that the energy of the power electron must be of the order of 1 PeV. This proves that PWNe are electron PeVatrons.

Flux of the Crab nebula has now become a reference point in TeV-astronomy, such that an actual unit of measure, the *crab unit*, was introduced: the Crab unit (C.U.). The C.U. is the the flux of the Crab nebula, that is taken as a reference as being one of the most studied objects of the Galaxy. The differential and the integral flux are measured to be respectively [Aharonian et al., 2004]:

$$1 \text{ C.U.} = \begin{cases} 2.83 \times 10^{-11} \left(\frac{E}{TeV}\right)^{-2.62} \frac{1}{cm^2\ s\ TeV} & \text{differential} \\ 1.75 \times 10^{-11} \left(\frac{E}{TeV}\right)^{-1.62} \frac{1}{cm^2\ s} & \text{integral} \end{cases} \tag{3.11}$$

[2]The Crab nebula is the remnant of a supernova explosion recorded by Chinese astronomers in 1054 a.C. [Brecher et al., 1983]. Knowing the age of this object with such accuracy made it be the most studied object in the Galaxy.

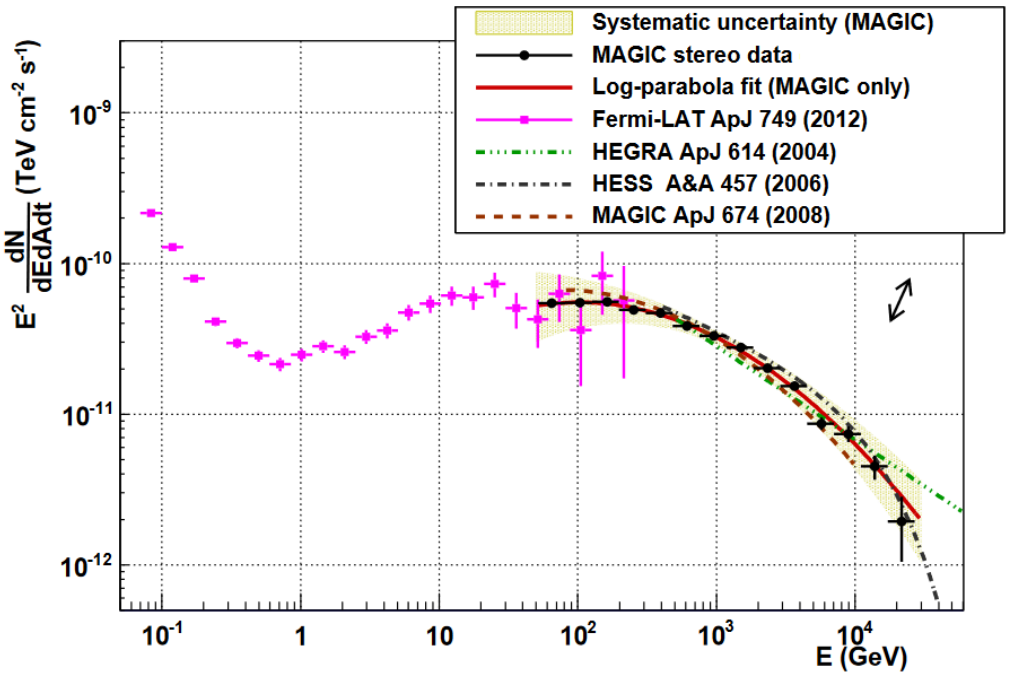


FIGURE 3.5: High energy spectrum of the Crab nebula as measured by the satellite (Fermi-LAT) and ground based (MAGIC,HESS, HEGRA) instruments. The two component of the radiation are well distinguishable: the blue dashed line fits the synchrotron radiation, whereas the other curve are fitting the IC emission for different value of the magnetic field. Figure from [Aleksić et al., 2015]

So clearly pulsars and their nebulae are effective sources of $\gamma$-photons and therefore fall into our definition of background. Luckily most of them have already been discovered and cataloged by Fermi. Moreover, their particular spectral shape (as in equation 3.10) allows, in principle, to distinguish them from our sources of interest: the clouds [3].

### 3.2.2 Binary systems

Binary systems composed at least by one compact object (e.g. a neutron star or a black hole) can result as well as a effective source of gamma photons. In these systems the gravitational energy of the compact object is turned into thermal (typically in the X waveband) emission. They can operate as well powerful particles accelerators. The combination of the two can give rise to a strong IC emission of gamma-rays. Protons can be accelerated as well by binaries, but the pp-production of gamma rays is efficient only in a dense gaseous environment, for example a stellar companion atmosphere. Microquasars or binary pulsar system can then result to be important TeV emitters. The term microquasar observationally labels a source of relativistic jets, commonly produced by an accretion disk around a black hole. In this sense they are similar to quasars, that host massive black holes, whereas microquasars are related to stellar black holes. The power of these jets can eventually overcome the X-ray emission of the black hole itself. These jets are typically trans-relativistic, so the acceleration of particles can proceed at a very high level [Atoyan and Aharonian, 1999]. Despite their potential, microquasars have not been proved yet to be VHE emitters. At a first instant Cyg X-3 or Her X-1 seemed to be TeV emitters, but the claim was not confirmed later on [Aleksić et al., 2010].

[3] Potentially clouds can show an exponential cut off, if there occurs to be a lack of powerful accelerators around them. However they are not expected to show a double components spectrum neither a modulation of the flux around 1 GeV

An other binary system that may be efficient in gamma emission is represented by binary pulsars. Only few of these objects have been detected in the highest energy band, for instance PSR B1259-63/LS 2883 [Abdo et al., 2011]: a pulsar with a massive stellar companion. The source of high energy gamma rays is again the plerion, that emits as described before, but at a higher rate with respect to the isolated case. However, again, also for pulsar binaries the observations don't fit the predictions. Possibly energy losses due to synchrotron, IC or other mechanism are responsible.

Other objects like LS 5039 [Khangulyan et al., 2007], LS I+61 303 [Abdo et al., 2009] and HESS J0632+057 [Hinton et al., 2008], detected in the VHE band, are possible candidates as binary system.

### 3.2.3 Extragalactic sources

High energetic photons may reach our detectors even from extragalactic sources. Fermi-LAT detected more than 1000 extragalactic sources, most of them are *blazars*, while the minority is composed of *starbust galaxies* (SGs) and *radio-galaxies* (RGs).

Blazars are a family of objects that are powered by a massive black hole ($\gtrsim 10^7$ $M_\odot$ ) surrounded by an accretion disk that ejects relativistic jets, almost pointing towards us. This emission is pretty variable spanning from the 1 % of the Crab flux to 15 C.U. . Their SED is characterized by two components one corresponding to synchrotron radiation, the other to IC scattering. Radio Galaxies, are still powered by an active galactic nuclei (AGN), but differently from blazars their jets don't point in the Earth direction. Some of these objects have been detected by Fermi and showed a very hard spectrum $\Gamma \sim 2$.

Besides there is the case of starburst galaxies, that are galaxies that have a localized region of intense star formation. As discussed in the former chapters (§ 1.2) , star forming regions, hosting many SN events, are effective accelerators of particles that can therefore produce cosmic rays, in the same way as in our Galaxy. The spiral galaxy NGC 253, for example hosts a 100 pc wide starburst region, with a 0.03 $yr^{-1}$ SN rate. It has been observed VHE emission from NGC 253, with a hard spectrum embedded by a power law of index $\Gamma \sim 2.2$.

Other possible but not yet proved TeV emitters could be Gamma Ray Bursts (GRBs), Clusters of Galaxies (CGs) or Passive Black Holes (PBH). GRBs are intense flashes of gamma-radiation that occur in timescales from some seconds to some hours; actual instrumentation had not a temporal resolution able to constrain these bursts at high energy. On the other hand CGs are the nest of many AGNs, that can boost particles in the inter cluster medium and source then gamma-rays from leptons or hadrons via the main known process. Finally PBHs, e.g. massive black holes with a very low luminosity at low frequencies could hypothetically sources high energetic and ultra energetic photons by the mean of their magnetic properties. Evidences for these source are still expected to come.

## 3.3 Atmospheric gammas

Gamma rays can be produced as well in our atmosphere by the incoming cosmic rays. Charge particles of the CR, like protons, interact with the atmospheric nuclei by creating pions, kaons, and other nuclei. Most of these mesons are unstable and produces lighter particles, mainly pions, that decay in two gamma photons. This gammas are indistinguishable from the ones produced in the outer space. Their contribution is assumed to be isotropically spread onto the camera of the detectors and is hence measured offset and then subtracted from the source. Another more deep approach is to run Monte Carlo simulations. However hadron decays are not easy to model, since they have to appeal to Quantum Chromo Dynamics.

# Chapter 4

# The Cherenkov Telescope Array

Our atmosphere is not transparent to $\gamma$ radiation: high energy photons are easily absorbed by molecules (mostly $O_3$) in its outermost layers. A direct observations of HE photons is possible only in the open space, by making use of satellites like *Fermi*. Since the spectrum of gamma rays drops very quickly, the flux of VHE photons is weaker compared to the low energy one, so a large collecting area is needed to detect them. Satellites have to deal with width limitations ($\lesssim 1\ m^2$) that prevent them to observe photons more energetic than some hundreds of GeV. Ground-based observatories instead can perform deeper, even though indirect, measurements of the HE particles, by observing their daughter particles, with Extensive Air Shower (EAS) detectors, or their *Cherenkov light*, by means of Imaging Atimospheric Cherenkov Telescopes (IACT). The Cherenkov Telescope Array (CTA) belongs to the latter category. The array will start operating between 2020 and 2025 and is promising to be the major instrument of its kind. With the cooperation of more than one hundred telescopes of different sizes CTA will cover an energy range from 30 GeV to 300 TeV. The improved sensitivity of CTA is believed to be sufficient to detect objects as faint as 1% of the Crab flux and its large field of view (7-10 degrees) will make it an optimal instrument to detect extended sources. This will open up new interesting opportunities to study non-thermal processes related to objects like Supernova remnants, Pulsar Wind Nebulae, Giant Radio Lobes of Radiogalaxies, Clusters of Galaxies and above all Molecular Clouds.

This chapter then goes over the main characteristic of ground based detectors, with the specific focus on the CTA project.

## 4.1 Ground based detectors

High energy photons, when they come in contact with the atmosphere[1], initiate an Extensive Atmospheric Shower (EAS), that means that they are triggered to produce pairs of charged particles, mainly $e^+$ and $e^-$ that quickly undergo bremsstrahlung braking and consequently produce other HE photons, that generate new pairs and so on, as shown in figure 4.1. The shower develops until the energy favors bremsstrahlung radiation over other energy losses, that, for a 1 TeV photon occur at $\sim 10$ km above the sea level. The final products are charged particles and lower energy photons, generally in the optical/UV waveband. Ground based detectors study the products of these showers with the aim to deduce informations on the primary particles. They divide into two categories: the EAS detectors and the Imaging Atmospheric Cherenkov Telescopes (IACTs). The first ones are designed for particles and are basically silicon scintillators, located at high altitudes, to encounter the shower at its maximum development. IACTs instead measure the radiation produced in these cascades that, since it is generated by relativistic particles, occurs to be Cherenkov radiation. The Cherenkov light produced here is composed of visible/UV photons, hence IACT detectors are composed of a reflective surface that focus the Cherenkov light into a camera of photomultipliers. This radiation at ground illuminates an area of radius $\sim$100 m, called *light-pool*.

[1]The nuclei in the atmosphere are fundamental to the conservation of momentum in the splitting of the photon, that otherwise would be forbidden

Besides gamma photons flux is rather weak at high energy (∼1 gamma ray photon per $m^2$ per year from a bright source), so the collector must cover a very wide area. It is calculated, see for example [Aharonian et al., 2013], that with an optical reflector of diameter $D \sim 10$ m, a camera with pixel size 0.1-0.2 °and a field of view of $\sim 3°$, primary gamma-rays of energy $\geq 100$ GeV can be collected from distances as large as 100 m, meaning a detection area of $3 \times 10^4$ $m^2$. To extend the effective collection area nowadays IACT telescopes are disposed in arrays. The stereoscopic observations of air showers with two or more 10 m diameter telescopes separated of 100 m provide a quite low energy threshold (∼ 100 GeV) and a very good sensitivity of $10^{-13}$ erg/$cm^2$ around 1 TeV. This approach is currently used by the main three Cherenkov observatories, namely HESS (High Energy Stereoscopic System), MAGIC (Major Atmospheric Imaging Cherenkov) and VERITAS (Very Energetic Radiation Imaging Telescope Array System) and will be extended also to CTA.

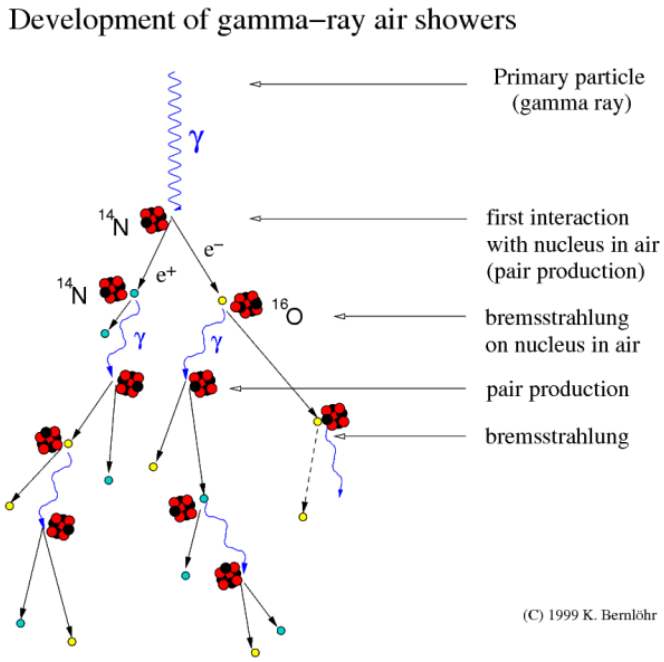


FIGURE 4.1: Extensive atmospheric shower initiated by a gamma-ray. Image from the Max Planck Institute for nuclear physics website

Anyway primaries can be different from gammas, for example cosmic ray protons interact strongly with the atmospheric nuclei creating pions, kaons or other nuclei that keep on interacting with the atmosphere, and eventually create secondaries that in turn generate showers. Charged CRs can usually be distinguished from the $\gamma$ photons because they generate a wider cascade. Moreover $\gamma$ rays are supposed to be aligned with the observed object while CRs in general will have a random distribution. Studying the angular distribution allows to obtain a more refined distinction. The projection of the showers onto the camera plane is an ellipse, and the source stands along its major axis. The angle $\theta$ between the expected source position and the reconstructed position provides informations on the nature of the parent particle; the distribution of this angle, or better of its square $\theta^2$ is expected to be peaked around zero for gammas coming out from the source, and to be flat for background gammas.

## 4.2 CTA

The CTA project will be an array of more than a hundred IACT telescopes, of different sizes: large (LST), medium (MST) and small (SST). They will be divided between two sites: in the Northern and in the Southern hemisphere. The northern site will be in the Canary island of

(a)

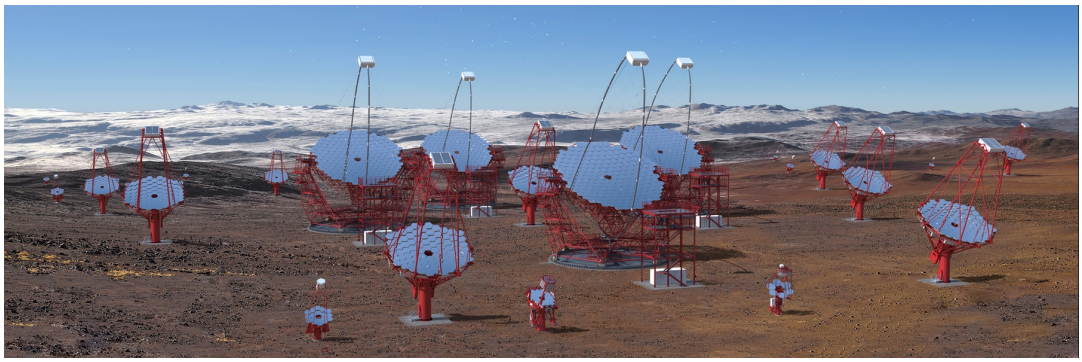

(b)

FIGURE 4.2: Representation of how the two sites of CTA will look like. In (a) the Northern array of La Palma, in (b) the Southern array of Paranal

La Palma, the southern one at Paranal, in Chile. The two sites will have a different configuration due to the different geographical conformations: the northern one will be more limited in size because of the features of the site, and will not have SSTs. In table 4.1 is reported a scheme of the different configuration of the two sites. However this configuration, known as *baseline* configuration is not granted, the CTA community for now guarantees only for a *threshold* configuration, with less telescopes as reported in 4.1.

Large sized telescopes (LST) with their 23-m diameter reflector have the lowest energy threshold among the three kinds of telescoped. The LST is designed to be an alt-azimuth telescope a parabolic reflective surface. Although the LST will stand 45 m tall and weigh around 100 tonnes, it will be extremely nimble, with the goal to be able to re-position within 20 seconds. Both the re-positioning speed and the low energy threshold provided by the LSTs are critical for CTA studies of Galactic transient phenomena, high red-shift active galactic nuclei and gamma ray bursts. Besides the LSTs will stand MSTs that will cover the central energy range from 100 GeV to 10 TeV. They will have a modified Davies-Cotton (e.g. sub-mirrors are disposed in a spherical configuration) mirror of 12 m diameter, with polar mount connected to a camera of 8°of field of view. Finally SSTs will be built and spread into a large area. Due to the power law behavior of the spectrum in fact, the high energy photons flux is lower. With the contribution of these SSTs CTA will extend its energy domain up to 300 TeV. SSTs will have a diameter of 4 m and a field of view of 9°. Probably there will be a mixture of single mirror Davies-Cotton and dual mirror Schwarzschlid-Couder telescopes.

| | | Baseline | | Threshold | |
|---|---|---|---|---|---|
| | Energy range | South | North | South | North |
| LST | 20 GeV -200 GeV | 4 | 4 | - | 4 |
| MST | 100 GeV- 10 TeV | 25 | 15 | 15 | 5 |
| SST | ∼1 TeV - 300 TeV | 70 | - | 50 | - |

TABLE 4.1

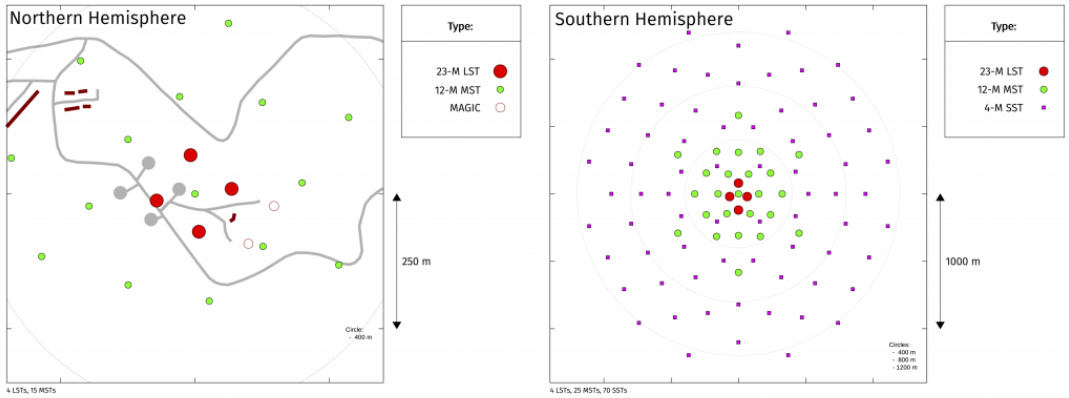


FIGURE 4.3: The two different layouts designed for the Northern and the Southern array of CTA. Image from https://www.cta-observatory.org/

### 4.2.1 CTA performances

For any kind of measurement one has to deal with the instrument capability. As in equation 4.1 the detected signal $e(E', \vec{p}')$ is the result of the convolution between the flux $F(\vec{p})$ of the source and the *instrument response functions* $R(E', \vec{p}'|E, \vec{p})$. Where $E'$ and $\vec{p}'$ label the detected event, and $E$ and $\vec{p}$ the physical one.

$$e(E', \vec{p}') = \int F(\vec{p}) \times R(E', \vec{p}'|E, \vec{p}) d\vec{p}\, dE \tag{4.1}$$

The instrument response functions for CTA comprise the *effective area* $A_{eff}(p, E, t)$, the *point spread function* $PSF(p'|p, E, t)$ and the *energy dispersion* $E_{disp}(E'|p, E, t)$:

$$R(p', E', t'|p, E, t) = A_{eff}(p, E, t) \times PSF(p'|p, E, t) \times E_{disp}(E'|p, E, t) \tag{4.2}$$

where are indicated the dependences on the physical properties of the original event (p,E,t) and of the detected one (p',E',t'). Each of these quantity is computed by simulating showers with Monte Carlo methods. The CTA consortium on their website provides the results of their simulations. [Ambrogi et al., 2016] in their paper modeled the resulting points and derived an analytical parametrization in the energy range from 50 GeV to 100 TeV for a point like source positioned at the center of the field of view (FoV). The plot of the fitted formula for each quantity are reported in 4.4.

### Effective area

For a single telescope the effective area is determined by the radius of the Cherenkov light pool at ground, while for a multi-telescope system is determined essentially by the total geometrical area. CTA bigger array, when completed, will cover an area of $\sim 300$ km$^2$. Particles of different energies create cascades of different area (more energetic particles generate wider showers and vice-versa) that causes an energy dependency of $A_{eff}$. The parametrization of [Ambrogi et al., 2016] for the CTA southern observatory effective area yields:

$$A_{eff}(x) = \frac{A}{1 + B \cdot \exp(-\frac{x}{C})} \tag{4.3}$$

where $x = \log_{10}(E/1\text{TeV})$, $A = 4.36 \times 10^6\ m^2$ is the saturation value of the effective area, whereas $B = 6.05$ and $C = 3.99 \times 10^{-1}$ define the rate of change of $A_{eff}$ with respect to energy.

### Angular resolution

A point like source, when detected from any camera appears not as a point but as a circle with a certain extension. The distribution of the detected photons depends on the instrument, and it is known as point spread function (PSF). In first approximation the PSF is a two dimensional Gaussian:

$$PSF = \exp\left(\frac{x_f^2 + y_f^2}{2\sigma_{PSF}^2}\right) \tag{4.4}$$

where $x_f$ and $y_f$ are the coordinates in the camera focal plane.

The angular resolution in this context is defined as the standard deviation of the gamma ray PSF. The angular resolution depends on the energy, the higher the energy the smaller is the PSF. For CTA a reference value is an angular resolution of 0.05°at 1 TeV, as shown in figure 4.4. The fit of the data points produced the function in 4.5.

$$\sigma_{PSF}(x) = A \cdot \left[1 + \exp\left(-\frac{x}{B}\right)\right] \tag{4.5}$$

here $A = 2.71 \times 10^{-2}$ deg is the best angular resolution achievable with the considered configuration and $B = 7.90 \times 10^{-1}$ is a scaling factor that determines how fast $\sigma_{PSF}$ changes with the energy.

### Energy resolution and energy dispersion

The measure of the gamma photon energies is not direct, it is derived from the energy of the photons generated in the cascades. For this reason it is called *reconstructed* energy and it corresponds to the peak of a probability function, similar to the PSF, known as Point Dispersion Function. The energy resolution, quantifies the ability to distinguish between two energy values and it is defined as the full width at half maximum (FWHM) of the energy distribution centered on the reconstructed energy. CTA energy resolution should reach the level of $\sim$6% above 1 TeV. The parametrization of [Ambrogi et al., 2016] for the energy resolution is given by:

$$\frac{\Delta E}{E}(x) = A \times [(x - B)^2 + (x - B)^4] + C \tag{4.6}$$

with $A = 6.33 \times 10^{-3}$ , $B = 8.34 \times 10^{-1}$ and $C = 6.24 \times 10^{-2}$.

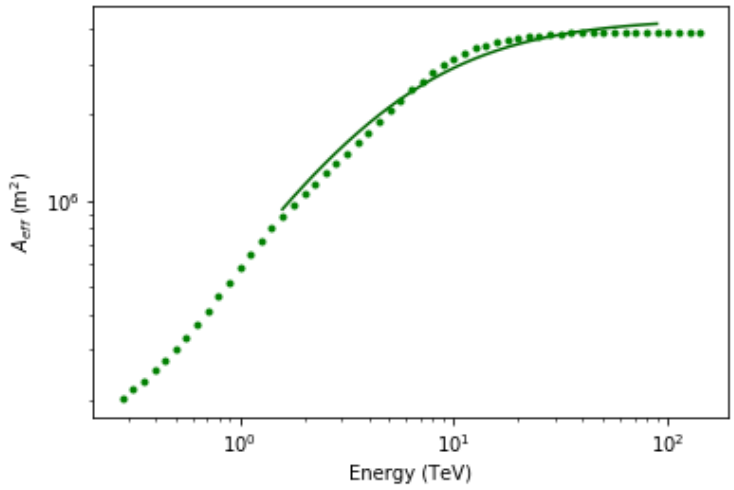


(a)

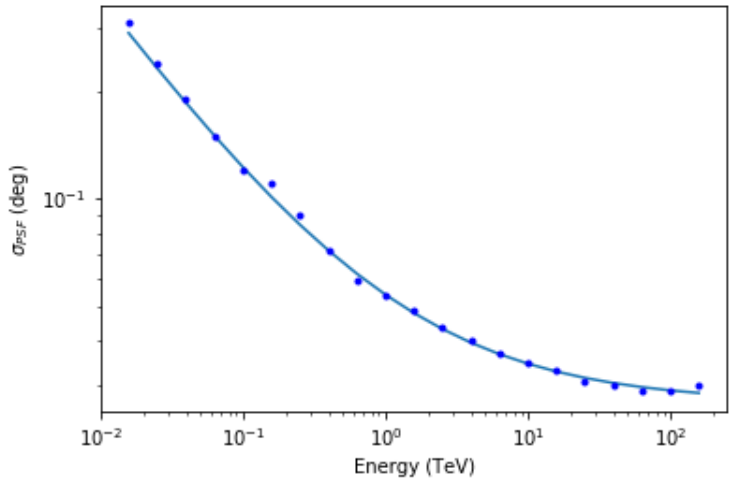


(b)

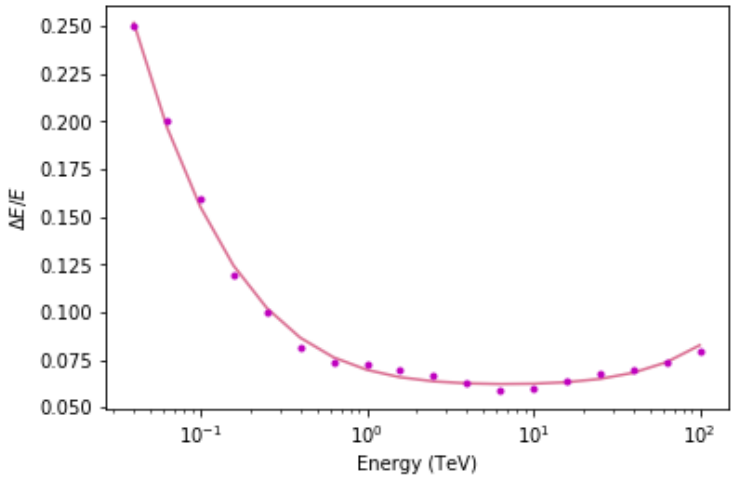


(c)

FIGURE 4.4: Effective area, angular resolution and energy resolution of CTA. The points are taken from the publicly available CTA performances files at https://www.cta-observatory.org/. The solid lines are the best fit function as in [Ambrogi et al., 2016]

### Background rate

The main sources of background for IACT arrays are gammas generated in the atmosphere from the impact of protons and heavier nuclei of the CR, as discussed in 3.3. The CTA-consortium simulates the arrival of these particles, assuming for them a power law spectrum consistent with the satellites measurements. This contribution is influenced by the zenith angle of the observation, since higher zenith angles correspond to more layers of atmosphere that the particles cross, enhancing the chance for interaction. Besides since the final detection products are visible photons, all the sources (both of astrophysical and human origin) of contamination in the optical band have to be taken into consideration. Usually CTA background is evaluated for a dark sky, namely with no moon, and offset from the galactic plane. The electronics noise must be considered as well.

### The Sensitivity

The sensitivity of a telescope is the minimum flux detectable with a required statistical significance, e.g. with enough number of events to distinguish the signal from the background. For CTA the requirements to be fulfilled for each energy bin are:

- at least a $5\sigma$ significance level;
- the presence of at least 10 excess events;
- a signal of at least five times the background systematic error.

The sensitivity is then calculated simulating the flux of a source; for most applications a point source with the spectrum of the Crab nebula is used. Statistical limits are calculated using a maximum likelihood approach, and the background systematics are assumed to have an uncertainty of 1%. The sensitivity of a gamma-ray detector is determined by the effective collecting area, the residual background and the angular resolution and hence depends strongly on the energy. Furthermore different layouts of the array, will give different effective areas, and consequently different sensitivities. The two arrays of CTA will hence have different performances: the northern one will be approximately two times less sensitive than the southern one.

Moreover, these sensitivity curves are background dependent, as one can see from the sensitivity definition itself and hence depends on the zenith angle and other factors that influence the background.

The plots in figure 4.5 show the computed differential sensitivity for a point-like source. Different exposure times and zenith angles were assumed. Different configurations were also tested: it was chosen to consider not only the differences between North and South, but also the difference from the *baseline* configuration, namely the final designed configuration and the *threshold* configuration (as in table 4.1).

For what concerns the extended sources, the question is more delicate. In this case the background rate increases proportionally to the factor $\sqrt{\theta^2 + \sigma_{PSF}^2}$ [Funk et al., 2013], and therefore the sensitivity can be assumed to scale according to the relation:

$$sens_{ext} = sens_{point} \cdot \frac{\sqrt{\theta^2 + \sigma_{PSF}^2}}{\sigma_{PSF}} \tag{4.7}$$

A reference value for CTA differential sensitivity is the sensitivity of a point source observed at low zenith angle ($z \lesssim 20\ ^\circ$) at 1 TeV, with an exposure time of 50 hrs, namely:

$$sens(E = 1\ \mathrm{TeV}, z = 0, t_{exp} = 50\ \mathrm{h}) = 6.55 \times 10^{-14}\ \frac{\mathrm{TeV}}{\mathrm{cm}^2\ \mathrm{s}}$$

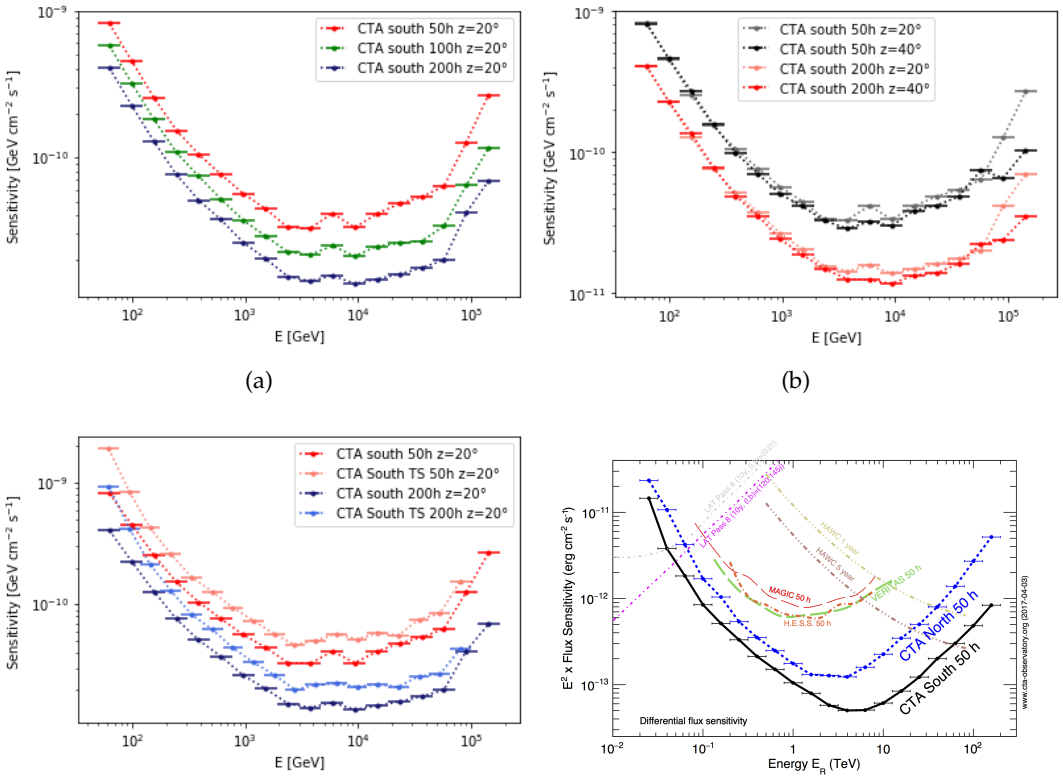


FIGURE 4.5: Comparison of CTA sensitivity for different cases. In (a) sensitivities for the southern array in its definitive configuration for different observation time intervals. In (b) the sensitivity for observation at different zenith angles. In (c) we considered the provisional threshold configuration. Finally in (d) CTA southern and northern arrays are compared with the main current gamma ray detectors. This last figure is from https://www.cta-observatory.org/science/cta-performance/

### 4.2.2 CTA Galactic Plane Survey

CTA is an observatory available for guest observer programs. In addition, the CTA consortium will be granted with a fixed amount of time that will be devoted to sky surveys. One of these so called key science projects (KSP) is a Galactic Plane Survey (GPS). This survey will achieve a sensitivity better than 4.2 mCrab over the entire Galactic Plane and of 1.8 mCrab in the Galactic center and is expected to lead to the discovery of many new VHE objects. The GPS will be divided into two phases: a short term (Years 1-2) preliminary phase, and a long term (Years 3-10) one with a total observing time of 1020 hours with CTA South and 600 hours with CTA North.

The observations will proceed in a scan of the sky, composed of subsequent pointing with a double row strategy with a nominal pointing separation of 3°, like sketched in figure 4.6. The observations will be performed at low zenith angles ($z \lesssim 45$ °) in order to preserve the sensitivity. That will allow to cover the $|b| < 2$°region, where the majority of the known sources, like SNRs and PWNe, is located.

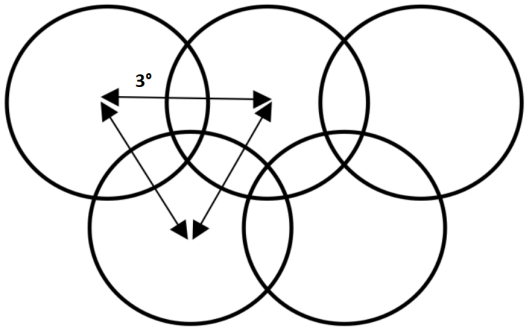


FIGURE 4.6: Double row pointing strategy. The telescope is centered in turn in subsequent points separated by 3 °and disposed in two rows

The GPS is of key importance for studies on cosmic rays. Most of the cosmic rays accelerator s are believed to be in the Plane, both in the arms (OB associations, SNRs) and in the Galactic center (alleged PeVatrons). The existence of PeVatrons will be investigated with this survey and a follow-up specific project. Besides molecular clouds are distributed right in the Galacic plane, so this survey will give us a preliminary overview of our targets, although the scheduled time probably won't be sufficient for MC analysis as suggested by table 4.2.

| | Years 1-2 | | Years 1-10 | |
|---|---|---|---|---|
| Galactic longitude | Sensitivity | Eq. Exposure | Sensitivity | Eq. Exposure |
| **SOUTH** | | | | |
| 300°-60° | 2.7 mCrab | 11.0 h | 1.8 mCrab | 28.6 h |
| 240°-300° | | | 2.6 mCrab | 13.2 h |
| 210°-240° | | | 3.1 mCrab | 8.8 h |
| **NORTH** | | | | |
| 60°-150° | 4.2 mCrab | 6.3 h | 2.7 mCrab | 15.8 h |
| 150°-210° | | | 3.8 mCrab | 7.9 h |

TABLE 4.2

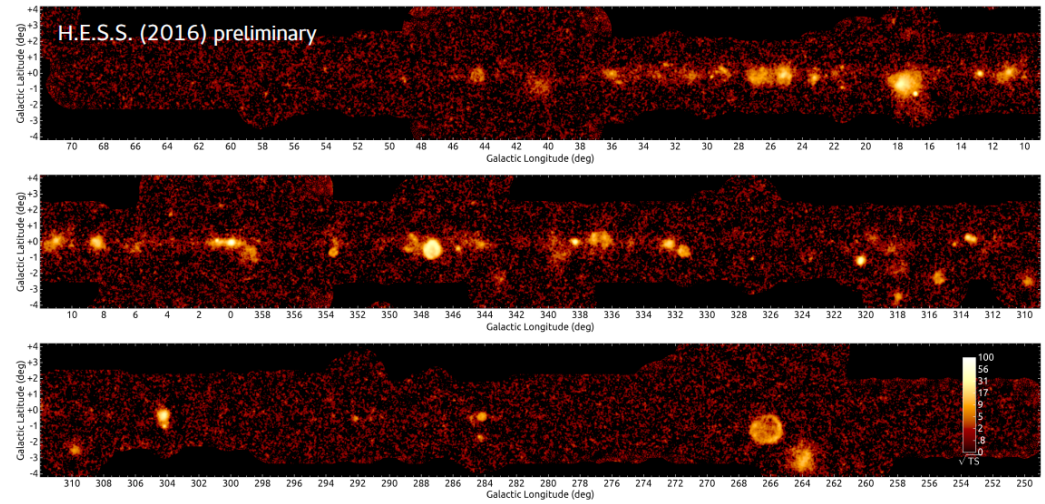


(a)

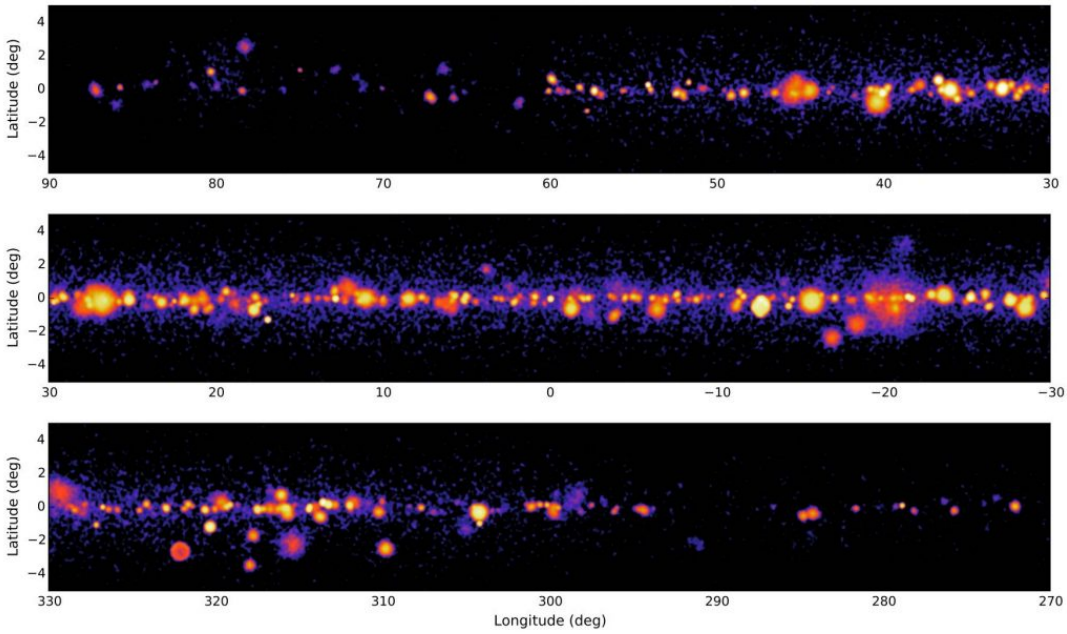


(b)

FIGURE 4.7: (a) Galactic plane sources seen by H.E.S.S. from [Donath et al., 2017] (b) Simulation of the Galactic plane in the region as the result of the proposed GPS. SNR and PWN populations are included

# Chapter 5

# The analysis

The Cherenkov telescope array is scheduled to start operating with the threshold configuration in between 2020 and 2025. Given the huge scientific impact that this instrument will have in pushing forward the understanding of the $\gamma$-ray sky, we found important to study in details its performances. In particular we tried to understand its capability to study molecular clouds.

The goal of this work is to understand if it will be possible to reach a conclusion on the primary CR spectrum, from the data that we will extract from the clouds of the [Rice et al., 2016] catalog.

The starting point is the selection of the clouds to be analyzed. The selection was made accounting for their detectability, that depends on different factors as will be explained in section 5.2.1. Then, to simulate the event, we had to construct the emission model. The cloud emission will depend on the CR primary spectrum that we want to test; we prepared then several different models with different parameters, as presented in section 5.2.2. Section 5.2.3 explains how we built the background template. The methods and the results of the analysis are then reported in 5.2.

## 5.1 Analysis routine

The analysis routine is written using *Gammalib*, a C++ library to handle data from the main gamma-ray detectors, and *ctools* [Knödlseder et al., 2016], a software package developed for CTA analysis. We are here analyzing simulated data, since CTA is not operating yet. In this work we simulate *high level* data, i.e. lists of photons that have passed all the selection cuts. With real data instead one has to undergo some passages: the signal extraction, the calibration, the image cleaning and the background rejection. In few words the incoming Cherenkov photons leave their energy in a photomultiplier tube, that translates it into a current. This signal must be reconverted in energy and calibrated accordingly. Among all pixels that detected a signal it is necessary to distinguish between the ones who actually register a source and the ones who were activated by noise events: this procedure is called image cleaning. Finally one must distinguish and reject the signal that comes from hadronic-initiated cascades. This first part is what we usually call *low level* analysis, and it is not necessary here. At the moment there is no official software to simulate raw data.

Simulating a source consists into randomly generate events that will be produced by that source, assuming for it a precise spatial and spectral model. In the selected region of interest (ROI) may lie already known TeV sources, which should be included in the model since these sources produce photons as well and may contaminate the signal of the source we are studying. The simulation algorithms are implemented in *ctools* and are based on Monte Carlo methods. All the generated events are then weighted with the instrumental response functions in order to estimate the number of events that the instrument will effectively be able to detect. The analysis tools then allow to fit this generated sample of data and to

understand the statistical significance of them. In this way we are able to predict the range of confidence with which the parameter of our model will be constrained.

### 5.1.1 Likelihood analysis

The likelihood $\mathcal{L}$ is defined as the probability of obtaining a certain result starting from an input model. The input model is defined in a ".xml" file and contains a description of the gamma ray sources in the region of interest (ROI). Each source is divided into a *spatial* component, namely the celestial coordinates and the shape of the object and a *spectral* component which provides the energy distribution of the photons. In the input model we choose which parameters to leave *free*, namely which parameters we want to fit. The fit maximizes the likelihood[1]. Besides the statistical errors resulting from the fitting procedure one must account for systematic uncertainties, that can rise from different factors, e.g. weather conditions, the electronics, etc. We assume the systematic uncertainty on the flux will be close to the level of $\sim 15$ %, that is the characteristic value of the current generation of IACT (as H.E.S.S. [Aharonian et al., 2006]) .

The input model $M(E, \vec{p}, t|\alpha)$ will be then the differential flux per unit area in the observed region of the sky as a function of the true energy $E$, the true arrival direction $\vec{p}$ and the time of observation $t$, that is important for variable phenomena. The term $\alpha$ labels the free parameters of the model. Once obtained the number of events, the flux is estimated according to the formula in 5.1:

$$\Phi(E', \vec{p'}|\alpha) = \int dE\ d\vec{p} R(E', \vec{p'}|E, \vec{p}) M(E, \vec{p}|\alpha) \tag{5.1}$$

where $R(E', \vec{p'}|E, \vec{p})$ are the IRFs, as described in §4.2.1.

The more the model resembles the reality, the more probable is to find results that are close to that model, this is the basic concept of a likelihood analysis. In other words $\mathcal{L}$ is a test of the goodness of the model. In case of simulated data, deviation from the model are caused by the statistical fluctuations we injected with the simulations. The point of simulations then is to understand the limits of the detector.

We can choose to perform the analysis in two different ways denoted respectively as *binned* or *unbinned*. In a binned analysis the data collected, either from observations or simulations, are spread in 3D cube in energy and in spatial coordinates. In each bin falls a certain number of counts $n$, according to the distribution we chose, in our case the Poissonian:

$$\mathcal{P}_i(n_i) = \frac{\lambda_i^{n_i}}{n_i!} e^{-\lambda_i} \tag{5.2}$$

where $\lambda_i$ is the number of expected counts for that bin and $i$ labels the bin. The likelihood is computed as the product of the probabilities of observing the detected counts in each bin and can be factorized as following:

$$\begin{aligned}
\mathcal{L} &= \prod_i \mathcal{P}_i(n_i) = \prod_i \frac{\lambda_i^{n_i}}{n_i!} e^{-\lambda_i} \\
&= \prod_i \frac{\lambda_i^{n_i}}{n_i!} \prod_i e^{-\lambda_i} \\
&= e^{-N_{exp}} \prod_i \frac{\lambda_i^{n_i}}{n_i!}
\end{aligned}$$

where $N_{exp}$ is the number of counts that are predicted by the model, and are derived by the integration of 5.1. The likelihood is therefore a product of a factor that depends on the model

[1]The $\chi^2$ is related to the likelihood: $\chi^2 = -2 \log \mathcal{L}$ so maximize the likelihood is equivalent to minimize the $\chi^2$

($N_{exp}$), and a factor that depends on the model ($\lambda$) and on the data ($n$). The choice of the size of the bins influences the accuracy of the analysis, so in principle it is preferable to perform an unbinned analysis. This consists in let the bin size get infinitesimally small so that $n_i$ can be either 0 or 1. This yields to:

$$\mathcal{L} = e^{-N_{exp}} \prod_i \lambda_i$$

where $i$ now labels the counts. The disadvantage of this technique is in the computation time, that for large datasets can become prohibitive.

The model fitting algorithm then accepts as inputs a model and a set of data and returns the parameters with the corresponding errors. The optimization continues for a finite number of iterations and then returns the parameter values that reached a maximum in $\mathcal{L}$. The goodness of the fit is evaluated by the Test Statistic (TS), defined as:

$$\mathrm{TS} = -2 \ \log(\frac{\mathcal{L}_m}{\mathcal{L}_h}) \tag{5.3}$$

where $\mathcal{L}_m$ and $\mathcal{L}_h$ are the maximum likelihood value for two models ($M_h$ and $M_m$) of different number of degrees of freedom $m < h$, for example $M_m$ could be the same model as $M_h$ but with less sources. TS gives an indication of the goodness of the model $M_m$ over another more complicated $M_h$. A theorem (Wilks theorem) states that in case $M_m$ represents at best the data, the TS asymptotically tends to a $\chi^2$ distribution with $h - m$ degrees of freedom. If the functional shape of TS has some fluctuations instead, that may be because of neglected parameters, for example a unknown source in the FoV. A large TS suggests that the $M_m$ is incorrect. Specifically $ctools$ computes TS by making use of the input model and the same model subtracted of a certain number j of parameters.

The main step of a CTA analysis with $ctools$ are then:

- *csobsdef*: creates a .xml file as input model, with the fitting parameters for all sources. The file can be created manually as well
- *ctobssim*: simulates events from the input model and the instrument response functions using a numerical random number generator. Both the astrophysical sources and the background are simulated.
- *ctbin*: (for binned analysis) creates a counts cube map, with a specified number of bins, and fills it with the event from the event list. The counts cube map is a three-dimensional grid that spans in Right Ascension (or Galactic Longitude), Declination (or Galactic Latitude) and reconstructed energy.
- *ctilike*: performs a maximum likelihood model fitting on the data (unbinned) or on the counts cube (binned) and gives the estimation with the relative error of the needed parameters. It additionally computes the TS value, if required.
- *csspec*: extracts the spectrum of a source by fitting the model to the data in a specific set of spectral bins, namely it returns the source differential flux and uncertainty for each bin.
- *ctbutterfly*: compute the envelope that comprises all compatible power law models in a 68% range of confidence with the data.

## 5.2 Our analysis

We followed this routine to perform an analysis on a cloud of the [Rice et al., 2016] catalog. We started with the study of one cloud, namely n. 877 of the above cited catalog, that we considered to be our best candidate. We decided to start with the most promising object in order to understand CTA capabilities in detecting MCs emission. In section 5.2.1 we present the selection criteria that lead us to define this cloud as the best candidate and, in addition,

we provide a list of possible other candidates for future analyses. It is of fundamental importance to have a several targets, possibly distributed in different parts of the Galaxy, if we want to test the Galactic sea of cosmic ray. As explained in 2.2 our final goal is to derive the spectrum of primary cosmic rays in the most different parts of the Milky Way, and a distinct number of clouds in different locations can allow us to have a complete tomography.

To select the clouds, we had first to understand their potential emissivity. We assumed that clouds emit gamma rays as passive emitters by means of interaction with the ambient cosmic ray particles. We assumed that the main channel of production of gammas is the $pp \rightarrow \pi^0 \rightarrow 2\gamma$. The flux depends on the cloud mass and distance and on the ambient cosmic ray density.

We tested different shapes for the primaries CR spectrum: both power law model resembling the local spectrum or with harder slope, and power law with different exponential cut-off, as described in § 5.2.2.

A special section (5.2.3) is dedicated to the modeling of the diffuse background model, as we had to build our own template.

### 5.2.1 Selection of the sample

Among the 1064 clouds of the considered catalog [Rice et al., 2016] we selected the most suitable objects on the basis of:

- Significant emissivity;
- Clear line of sight;
- Number of known bright sources nearby.

As shown in equation 2.11 the cloud differential flux is proportional to the parameter $M_5/d^2_{kpc}$ so a selection made on this parameter is the first step. We computed the sensitivity of CTA and compared it with the expected flux from clouds with different $M_5/d^2_{kpc}$, as shown in figure (a) of 5.1. The sensitivity (as explained in details in $4.2.1$) depends on different factors, here, for selection purpose we considered the sensitivity curve of the Southern array, for an observation of 200 hours at low zenith angles. At a first glance it seems that clouds with $M_5/d^2_{kpc} > 0.5$ are visible and allow a discrete spectral determination. Table 5.1 reports the main characteristics of these clouds: noteworthy the presence of object with mass that reaches $\sim 10^7$ $M_\odot$.

However sensitivity curves are available only for point like sources, that is not the case of MCs, since they are extended sources with an angular width that can reach some degrees. For selection purpose we assumed that the sensitivity of CTA worsen by a factor $\sqrt{\theta^2 + \sigma^2_{PSF}}/\sigma_{PSF}$ (as discussed in 4.2.1), where $\theta$ is the extension of the cloud and $\sigma_{PSF}$ is angular resolution of CTA, that in general depends on the energy. This is just a first approximation, but we decided to stay conservative while waiting for more precise estimation of the sensitivity for extended sources. Comparison between the flux of a cloud with $M_5/d^2_{kpc} = 1$ and the sensitivity convolved with the PSF for different extensions of the source can be found in figure 5.1 (b).

Another point that has been taken into account is the gas on the line of sight (LoS) as it is a source of gamma emission as explained in chapter 4. Even if in principle is not necessary, because this gas is taken into account as background, it is better, where possible, to select clouds with a clear line of sight. That means that there is no more than one cloud in the line of sight and that this cloud is dominant in the LoS.

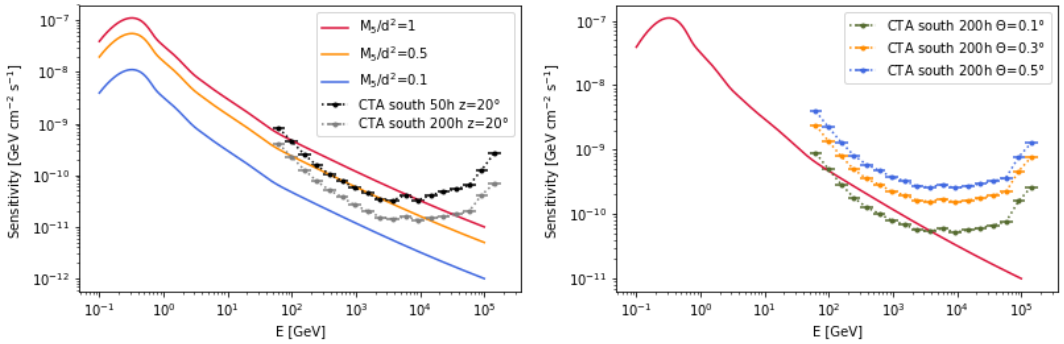


(a) (b)

FIGURE 5.1: (a) CTA differential sensitivity compared to the differential flux of MCs with different ratio $M_5/d^2_{kpc}$. (b) CTA sensitivity for sources of different width compared with the differential flux of a MC with $M_5/d^2_{kpc}$ =1

Finally we explored the known, thus bright[2], TeV sources in an area of 5°around the cloud and discarded clouds with such objects within 1°. Bright sources can, in fact, contaminate the flux of our cloud or create source confusion: if two objects are too close their images on the camera can overlap and in that case it would be impossible to assign the observed photons to a source or to another. Seen the angular resolution of CTA (that is less than 0.1°) probably 1°is an exaggeration, but again we stayed conservative. We referred to the TeVCat [Wakely and Horan, 2008] that includes all the known gamma sources above 50 GeV.

### The first cloud: n. 877

The first cloud chosen according to these criteria was cloud numbered 877 in Rice et al. catalog. This cloud is the one with the highest $M_5/d^2_{kpc}$ parameter, since it is rather massive $M_5$=12.6 and pretty close to us $d_{kpc}$=3.37 (hence $M_5/d^2_{kpc}$=1.1), that means that it has the highest emissivity. Besides it has a relatively small angular size $\theta = 0.33°$(corresponding to $\sim$ 37 pc) and its coordinates (l,b)=(333.46, -0.31) allows to observe it with the southern array, that is the most sensitive one. Moreover the zenith angle of observation has to be taken into account. We calculated it at the moment of culmination, given the latitude of the Paranal observation site $L$= 24°41′ 0.34′ S = -24.68 °and the cloud declination $\delta$= -50.27°:

$$z = L - \delta = -24.68^o + 50.27^o = 25.30^o \tag{5.4}$$

therefore it will be observed above 25°, so we considered the IRFs for z=40°.

Furthermore MC 877 has a rather clear line of sight (as reported in figure 3.3 (b)) and no TeV sources around 1°, as shown in figure 5.2.

The cloud small size prevents us to understand its shape. Dame's [Dame et al., 2001] CO survey has a sensibility of 0.125°so the cloud in this map occupies just few pixels. We decided then to model it as an uniform disk, for now. It is very unlikely that clouds are uniform, spherically symmetric object, rather they are expected to have a central more dense and cold core, whereas the outside part is heated up by UV radiation.

To look for hints of star formation we consulted the map of infrared radiation of the Spitzer Space Telescope [Werner et al., 2004], at 4.5, 8 and 24 $\mu$m. Apparently n. 877 hosts an active

[2]We are considering mainly H.E.S.S. sources. The completeness of the H.E.S.S. array is around ∼10% of the Crab nebula flux, nevertheless it detected more than 50 sources with a flux between 1 and 10% of the Crab flux

| Index | $M_5$ | $d_{kpc}$ | l(deg) | b(deg) | Size (deg) | $M_5/d^2$ |
|---|---|---|---|---|---|---|
| 151 | 2.95 | 2.08 | 16.97 | 0.53 | 0.46 | 0.68 |
| 190 | 4.78 | 2.62 | 34.99 | -0.96 | 0.38 | 0.7 |
| 208 | 7.71 | 3.65 | 16.61 | -0.38 | 0.31 | 0.58 |
| 269 | 55.4 | 10.42 | 23.04 | -0.22 | 0.26 | 0.51 |
| 284 | 11.02 | 4.66 | 28.77 | -0.09 | 0.34 | 0.51 |
| 292 | 65.56 | 8.41 | 30.49 | -0.04 | 0.28 | 0.93 |
| 429 | 10.33 | 3.93 | 109.84 | -0.3 | 0.58 | 0.67 |
| 610 | 0.27 | 0.66 | 142.4 | 1.38 | 0.54 | 0.61 |
| 612 | 0.32 | 0.62 | 126.88 | -0.66 | 0.89 | 0.83 |
| 631 | 0.27 | 0.6 | 110.43 | 1.89 | 0.69 | 0.76 |
| 645 | 0.06 | 0.33 | 124.72 | 3.07 | 0.73 | 0.53 |
| 670 | 1.01 | 1.18 | 224.64 | 1.66 | 0.84 | 0.72 |
| 800 | 90.37 | 9.47 | 332.28 | -0.07 | 0.4 | 1.01 |
| 804 | 24.01 | 5.66 | 328.59 | 0.41 | 0.41 | 0.75 |
| 842 | 56.5 | 9.01 | 320.55 | -0.42 | 0.37 | 0.7 |
| 876 | 60.14 | 10.2 | 323.61 | 0.22 | 0.5 | 0.58 |
| 877 | 12.6 | 3.37 | 333.46 | -0.31 | 0.33 | 1.11 |
| 897 | 28.24 | 7.3 | 309.36 | -0.1 | 0.36 | 0.53 |
| 902 | 115.06 | 12.53 | 340.84 | -0.31 | 0.31 | 0.73 |
| 926 | 4.87 | 2.84 | 326.6 | 0.29 | 0.34 | 0.6 |
| 933 | 29.46 | 6.82 | 305.49 | 0.11 | 0.36 | 0.63 |
| 939 | 5.45 | 2.73 | 343.64 | -0.54 | 0.45 | 0.73 |
| 943 | 2.65 | 2.21 | 322.51 | 0.17 | 0.68 | 0.54 |
| 964 | 2.78 | 1.92 | 345.57 | 0.79 | 0.41 | 0.75 |

TABLE 5.1: Characteristic of the source with $M_5/d^2$ >0.5

star forming region. That is not surprising given its mass, but it is important to take into account this fact, to interpret future data.

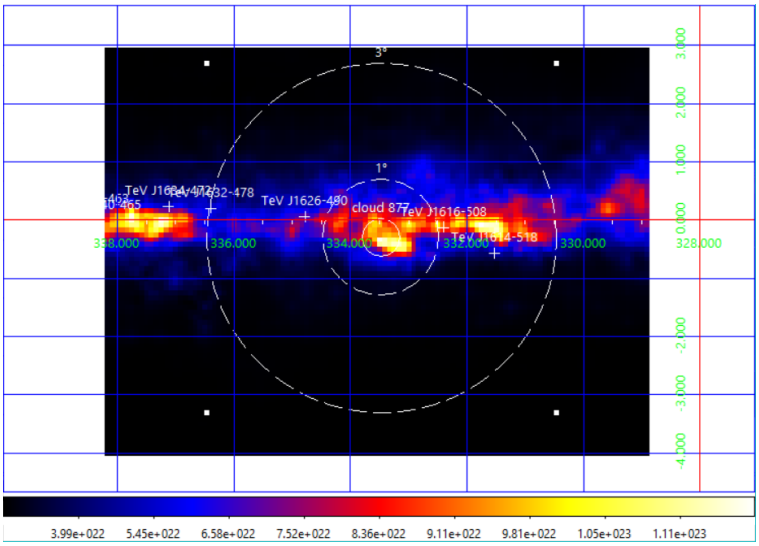


(a)

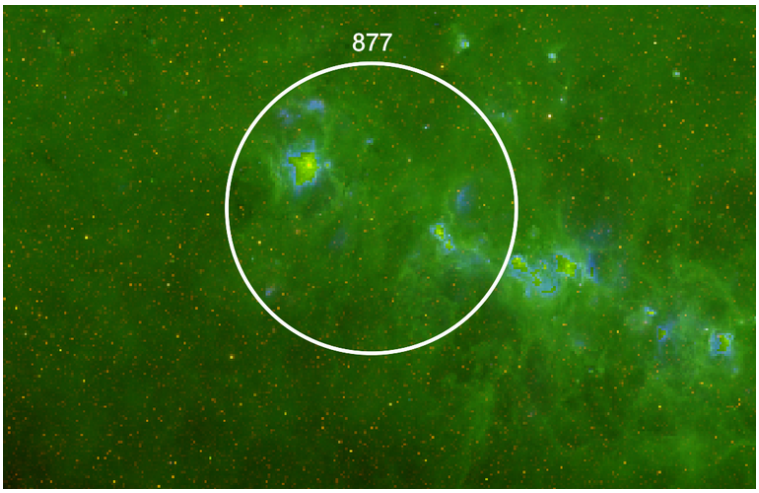


(b)

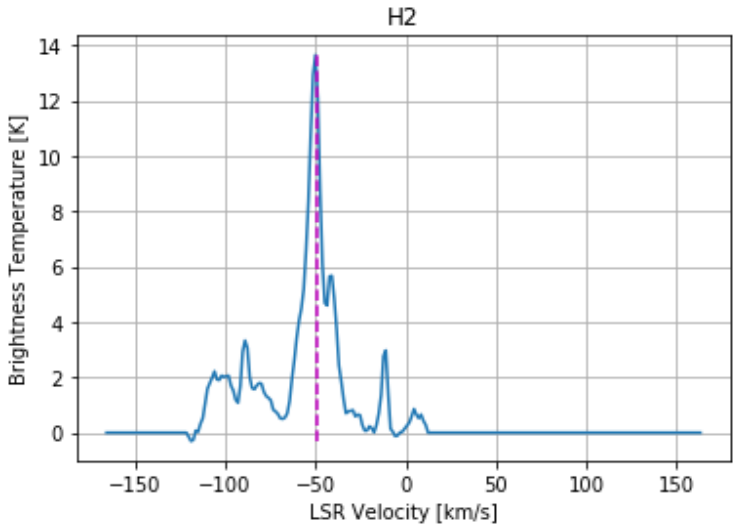


(c)

FIGURE 5.2: Characterization of cloud n. 877. (a) Map of column density of diffuse hydrogen in the region of the cloud. The TeVCat sources are also present, labeled as white crosses. (b) Spitzer map of infrared emission for the same region: these in particular are the superimposition of images at 4.5, 8 and 24 $\mu$m (c) Distribution of the CO in the line of sight centered at the coordinates of MC 877

### 5.2.2 Spectral models for primaries

For what concerns the spectral model, we decided to simulate different spectra. In particular as explained in the former chapters the most interesting model for the spectrum of the parent protons to be tested are:

1. AMS local spectrum;
2. Power law with radial dependence of index;
3. Power law with 2.4 index;
4. Power law with exponential cutoff.

The first one serves to test if the local spectrum is effectively *local* or if it is proper of other regions or even of the entire the Galaxy, hence to test the hypothesis of a *sea* of cosmic rays. The second one was chosen to compare the emission that comes from the cloud from the one that come from the diffuse measured by Fermi at the same distance from the Galactic Center (as in [Yang et al., 2016]). The third one is to take into account the possibility of a powerful CR accelerator inside or nearby the cloud, that hardens the spectrum; we expect for example Giant molecular clouds to host massive star forming region. The last one instead is to test if cut off of the proton spectrum could be appreciated; in particular we simulated a spectrum with four different cutoff: at $10^2$, 500, $10^3$ and $10^4$ TeV. If appreciable, a cutoff in the CR spectrum would let us to set an upper boundary to the power of the proton accelerators, and hence help in the understanding of the underlying mechanism and on their nature.

For spectra 2÷4 it has been assumed the normalization at 1 GeV of 3.24 $\mathrm{GeV}^{-1}\ \mathrm{s}^{-1}\ \mathrm{cm}^{-2}\ \mathrm{sr}^{-1}$ as suggested by the particle data group booklet [Patrignani et al., 2016] and discussed in 1.1. For the cutoff spectrum a 2.6 index was assumed, since it was the intermediate between the considered cases.

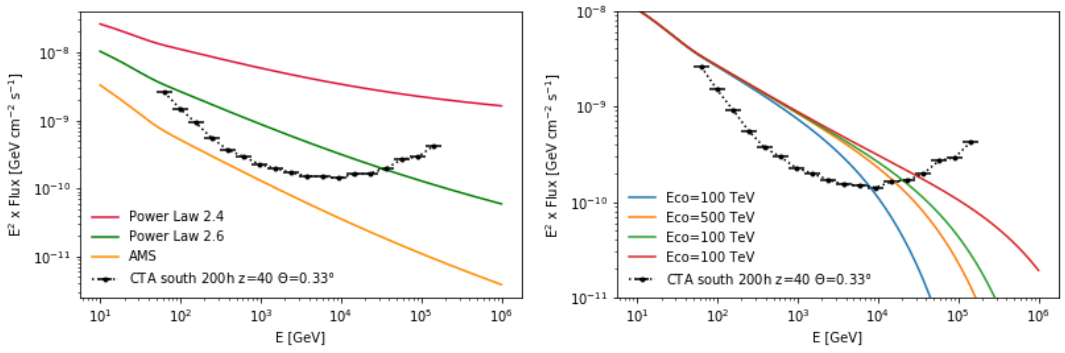


(a) (b)

FIGURE 5.3: Different model simulated with cloud n. 877 compared with sensitivities of CTA and Fermi. Figure (a) shows spectra with different power law index; figure (b) present a power law spectrum with index 2.6 and an exponential cutoff at different value. Values refer to the primary proton spectra. Details in the figure labels.

To derive the expected gamma flux, we performed the calculation reported in 2.11 in which we varied $J(E_p)$ according to these choices.

In figure 5.3 are plotted the modeled spectra for the cloud 877 and the sensitivity of CTA-South computed for 200 hours of observation at z=40°. CTA sensitivity is scaled with the factor $\sqrt{\theta^2 + \sigma_{PSF}^2}/\sigma_{PSF}$ with an energy dependent PSF as in (4.5).

The spectrum of the gamma rays in general resulted a little harder than the parent proton one (as figure 5.4), by means of the little dependency on the energy of the cross section. In order to parametrized it we then performed a fit on the produced point.

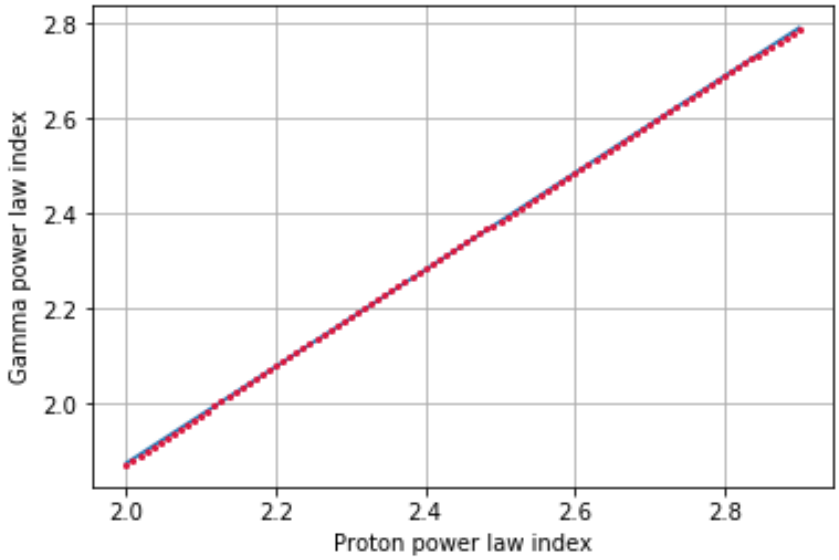


FIGURE 5.4: Relation between the proton power law index and the index of the resulting gamma spectrum

### 5.2.3 The diffuse background model

In order to build the background template we considered the main diffuse sources of gamma rays as in §3.1 and we decided to take into account only the hadronic contribution. We considered in fact that electron emission in this energy range ($\gtrsim$ 100 GeV) is suppressed. Although we do not know the detailed behavior of electrons at those energies, we expect that high energy electrons undergo strong energy losses due to synchrotron emission (eq. 3.8), and that the surviving electrons emit basically via IC scattering in the Klein Nishina regime, namely with a lowered cross section.

For what concern heavy nuclei, we considered their contribution to gamma radiation, estimated to count for $\sim$ 10 % (as[Huang et al., 2007]), is negligible, at least for this preliminary work.

We created then a model of the background gas emission that includes $H_2$ and HI. We started from the map of CO provided by the Smithsonian astrophysical observatory as a tracer for the molecular hydrogen [Dame et al., 2001], and from the HI4PI survey data [Bekhti et al., 2016] for the atomic. We excluded from the cube of CO the pixels corresponding to the cloud under analysis: we cut a box centered at the cloud coordinates (v,l,b) with the width defined as the cloud angular size, for the spatial coordinates, while for the velocity coordinate we chose to consider the given FWHM of the velocity profile, approximated as Gaussian. We then computed the $H_2$ column density from this cut map (as in 3.2) and the column density of HI from the relative data cubes (as in 3.1) and we matched the two maps. Note that we subtracted the cloud just from the $H_2$ map, this is because the mass reported in the catalog takes into account just the molecular hydrogen component, and we used that mass to compute the expected flux. In order to be consistent, we decided then to consider all the HI as background, although we now that it will contribute to the gamma ray emission from the cloud.

At this point we computed the expected gamma ray flux of this component following equation 3.3 in an energetic range from 50 GeV to 300 TeV, assuming an AMS spectrum for the primaries, as a basic hypothesis.

### 5.2.4 The input model for the analysis

The input models of the analysis were then based on the considerations reported above. We considered the diffuse background as in 5.2.3 and all the sources of the TeVCat [Wakely and Horan, 2008] in the considered FoV. We chose to consider a 5°wide region of interest (ROI), that corresponds to the one of the LSTs.

We realized seven different models in each we left unchanged the background sources and the spatial component of our source, while we let its spectral features change. In each model we considered a different gamma spectrum deriving from the different proton spectra discussed before: a AMS like spectrum, a power law 2.6 spectrum, a power law 2.4 spectrum, and a power law 2.6 with exponential cutoff at different energies: 100 TeV, 500 TeV, 1 PeV and 10 PeV.

#### Spatial model

For the spatial model we referred to the relative catalogs of the sources. The only assumption that we made is on the shape of the cloud that we modeled as a uniform disk. Details on the sources are provided in table 5.2

| Source name | Source type | RA [°] | DEC [°] | Spatial model | Extension [ °] |
|---|---|---|---|---|---|
| Rice 877 | MC (signal) | 245.49 | -50.27 | Disk | 0.33 |
| HESS J1640-465 | SNR | 250.18 | -46.53 | Disk | 0.045 |
| HESS J1632-478 | PWN | 248.04 | -47.82 | Gaussian | 0.2 |
| HESS J1634-472 | Unid | 248.74 | -47.27 | Gaussian | 0.1 |
| HESS J1614-518 | Shell SNR | 243.58 | -51.82 | Shell | 0.18-0.24 |
| HESS J1626-490 | Unid | 250.18 | -46.53 | Gaussian | 0.07 |
| HESS J1616-508 | PWN | 244.10 | -50.90 | Gaussian | 0.14 |

TABLE 5.2: Sources in the input of our model. The extension of the sources is evaluated by different parameters depending on the chosen profile function: the radius, for a disk shape, the sigma for Gaussian profiles and the inner and outer radius for shell-type. For the cloud we referred to [Rice et al., 2016], while for the sources to [Wakely and Horan, 2008]

#### Spectral model

For the 1÷3 models in 5.2.2 we considered for the gamma flux a power law shape:

$$\frac{\mathrm{d}N_\gamma}{\mathrm{d}E\,\mathrm{d}A\,\mathrm{d}t} = F_0\left(\frac{E}{E_0}\right)^{-\alpha}$$

and we derived the parameters from a likelihood fit of the point generated with the formula 2.11.

| Primary spectrum | $F_0$ [MeV cm$^{-2}$ s$^{-1}$] | $\alpha$ | $E_0$ [MeV] |
|---|---|---|---|
| (1) AMS | 2.3 $\times 10^{-7}$ | 2.67 | 27.9 |
| (2) PL $\alpha = 2.6$ | 3.69 $\times 10^{-9}$ | 2.40 | 97.2 |
| (3) PL $\alpha = 2.4$ | 2.7 $\times 10^{-9}$ | 2.33 | 209.7 |

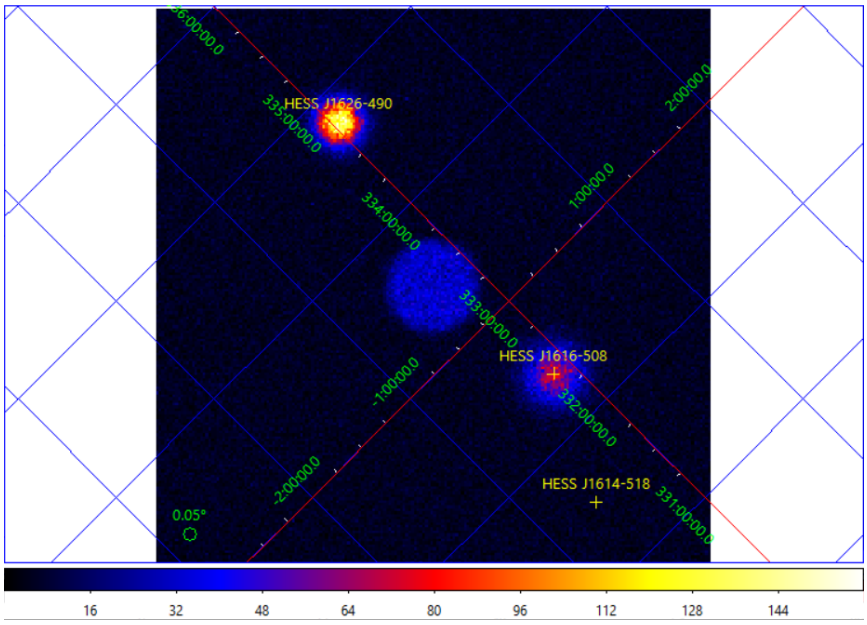


FIGURE 5.5: 2°x2°counts cube map derived from the assumed spatial model as in table 5.2

For the cut off spectra was assumed the shape:

$$\frac{\mathrm{d}N_\gamma}{\mathrm{d}E\,\mathrm{d}A\,\mathrm{d}t} = F_0\left(\frac{E}{E_0}\right)^{-\alpha}\exp\left(\frac{E}{E_{co}}\right)$$

Here $\alpha$ was assumed to be 2.6 and $E_0$=1 GeV. We varied $E_{co}$ between 100 TeV, 500 TeV, 1 PeV and 10 PeV in the parent proton spectra. For this case we chose to give as input a list of points, resulting by the for the simulation and not an analytic parametrization.

### 5.2.5 Results

We performed then the likelihood analysis on the generated events. We decided to follow the binned analysis procedure, with 20 energy bins in a range from 0.05 TeV to 180 TeV. We made use of the most recent IRFs for the southern array in its final configuration for observations at $z = 40°$. We generated then for each model a spectrum, a butterfly diagram, and a residual map. This kind of analysis consider just the statistic errors, namely the statistic fluctuations of our points around the mean value. Systematics are assumed to be $\sim$ 15 % of the flux, according to what is calculated for H.E.S.S [Aharonian et al., 2006].

### 5.2.6 Results from power law spectra

According to figure 5.3 AMS-like spectrum is not detectable (with a $5\sigma$ level of significance), not even in 200 hours. Still, taking into account that the analysis we are performing is more sensitive than the approach used for sensitivity calculation, we simulated the flux for all the cases at 200 hours to check the results. On the other side, figure 5.3 suggested that both the 2.4 and 2.6 spectra should be easily detectable by CTA, since their flux is many order of magnitude larger than the considered sensitivity curve. Therefore we looked for the minimum observation time to detect a *good* spectrum, namely with at least four spectral points with TS>25 each. We tested as the lowest observation time possible a 20 hours interval, that is anyway granted within the key science project of the Galactic plane survey.

We summarize the results in table 5.3, where we report the fitted parameters with the corresponding errors. While the reconstructed spectra are shown in figure 5.6 and in 5.7 for the 200 hours and the 20 hours simulations respectively.

| | 200 hours | | 20 hours | |
|---|---|---|---|---|
| | $F_0$ [MeV$^{-1}$ s$^{-1}$ cm$^{-2}$] | $\alpha$ | $F_0$ [MeV$^{-1}$ s$^{-1}$] | $\alpha$ |
| (1) AMS | $(6.7 \pm 1.8)\times10^{-7}$ | $2.75 \pm 0.03$ | - | - |
| (2) PL $\alpha$=2.6 | $(3.8 \pm 0.29)\times10^{-9}$ | $2.413 \pm 0.008$ | $(3.3 \pm 0.8)\times10^{-9}$ | $2.40 \pm 0.03$ |
| (3) PL $\alpha$=2.4 | $(2.65 \pm 0.03)\times10^{-9}$ | $(2.328 \pm 0.002)\times10^{-9}$ | $(2.5 \pm 0.1)\times10^{-9}$ | $2.321 \pm 0.005$ |

TABLE 5.3: Results from the likelihood fitting of the free parameters

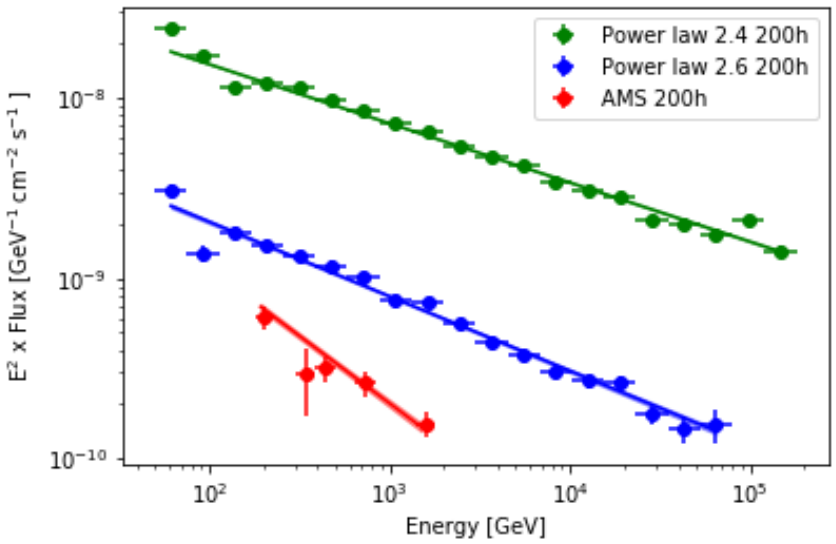


FIGURE 5.6: Comparison between the three different spectra obtained from the three different proton spectra assumed: AMS, power law $\alpha$=2.6 and power law $\alpha$=2.4. From simulation of 200 hours with the baseline configuration

As expected with 200 h the 2.4 and 2.6 power law show an amazing spectrum, with a statistical precision of less than 5%, much lower than the assumed systematic uncertainty. Figure 5.6 shows that with 200 h CTA will be able to detect also a AMS-like spectrum with five significant spectral points.

Looking for minimum observational time, we can infer from table 5.3 and from the plot in 5.7 that 20 hours will already be sufficient to distinguish between a 2.4 and a 2.6 slope, even including a 15% of systematic error and hence it will be possible to confirm or exclude these two models already within the GPS project. On the other hand, the AMS spectrum already showed a poor statistic with a 200 hours time interval and hence is hard to imagine a lower observation time.

We can conclude that CTA will definitely be able to distinguish between the considered spectra with 200 hours of observations. We tested the inclusion of systematic errors of 15% and found that they do not affect this conclusion.

### 5.2.7 Results from cut off spectra

We simulated the gamma ray spectra deriving from four 2.6 power law parent spectra with exponential cutoff at 100 TeV, 500 TeV, 1 PeV, 10 PeV, with the goal to understand if it is possible to recognize a feature of this kind. 200 hours of observations turned out to be necessary

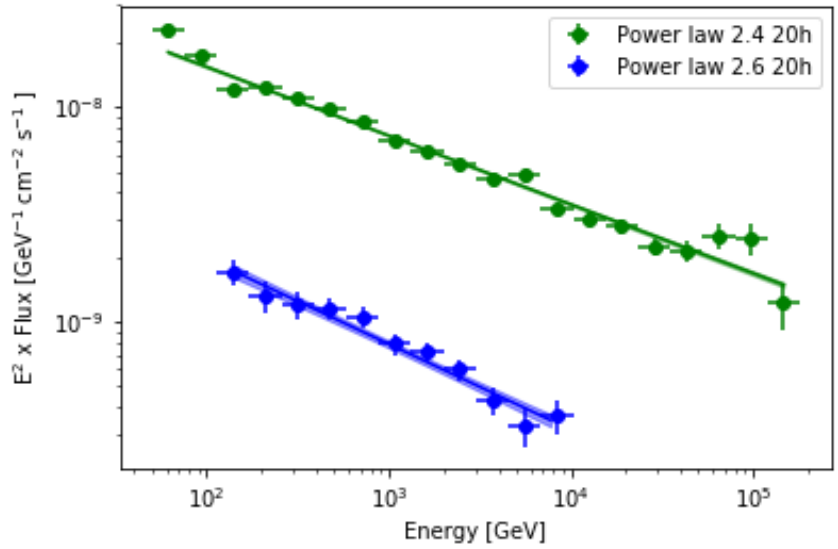


FIGURE 5.7: Comparison between power law spectra with index 2.4 and 2.6, with 20 hours of observation with the baseline configuration

for these studies. The resulting spectra are shown in 5.9 where they are superimposed to a pure power law spectrum. Here systematic uncertainties turned out to be relevant. As it can qualitatively be deived from the plots in fact, a cut off feature at 100 TeV or at 500 TeV is recognizable from a pure power law case, whereas the others are not distinguishable from the power law case.

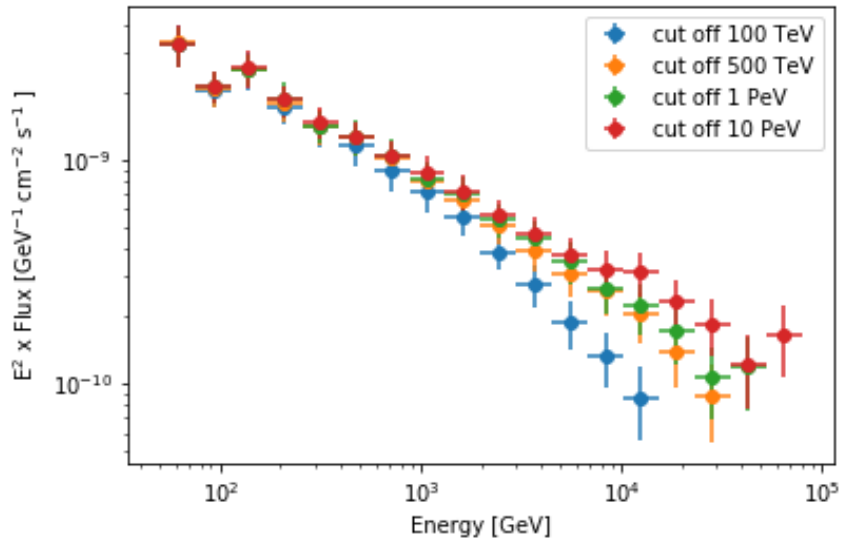


FIGURE 5.8: Resultig spectra from the simulation of parent proton spectra with different cutoff energies

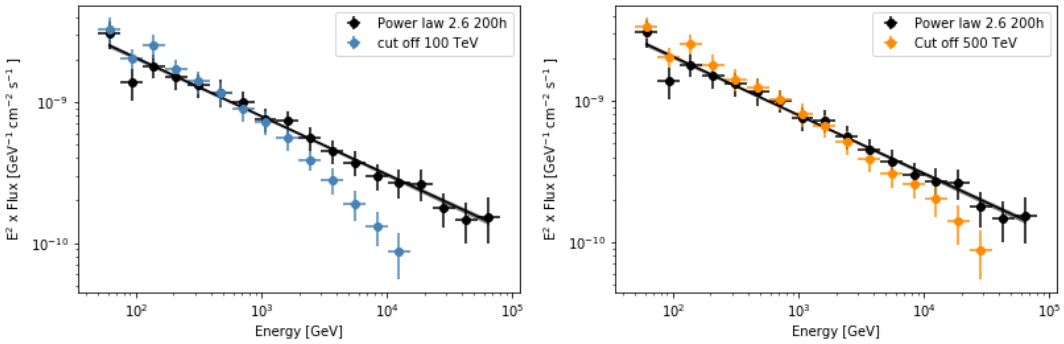


(a)




(b)

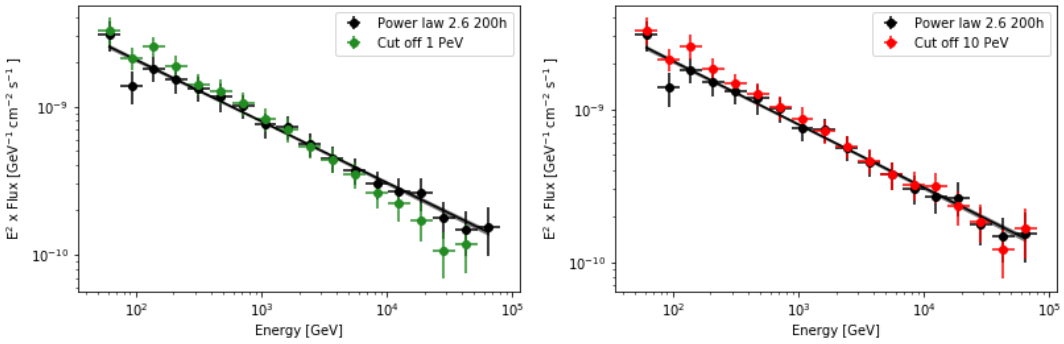


(c)




(d)

FIGURE 5.9: Reconstructed spectra for cloud n. 877 with cut off at different energies: 100 TeV, 500 TeV, 1 PeV and 10 PeV, and the corresponding 2.6 pure power law spectrum. Here the error on the flux is given by the systematic error

# Chapter 6

# Discussion of the results and future outlook

This work was aimed to understand the capabilities of CTA of observing gamma rays coming from giant molecular clouds, and to understand if they can actually be taken as tracers of Galactic Cosmic Rays (§ 2.2). We considered a new catalog of molecular clouds [Rice et al., 2016] and selected our sample after careful considerations. As a first selection criterion we parametrized the flux of the molecular clouds, as function of the parameter $M_5/d_{kpc}^2$ and we compared it with the CTA sensitivity curves. We considered that the sensitivity for an extended source worsen by a factor $\sqrt{\sigma_{PSF}^2 + \theta^2}/\sigma_{PSF}$ with respect to the point-like source sensitivity. As a second step, to avoid source confusion we reconstructed the gas profile along the line of sight (LoS) corresponding to the coordinates of each cloud and chose only the cases in which the cloud was the dominant object, as far as the gas is concerned. Besides we took into account the known bright object of the TeVcat catalog, and chose only the cloud with no such sources within a 1°radius. Out of these criteria, the MC n. 877 turned out to be the best candidate. Although each object must be evaluated case by case, the analysis of the best candidate serves as a reference and as a threshold: bad results with the best candidate would in fact discourage further investigations. We performed then a 3D analysis of simulated high level data, generated with different models for the parent spectra (§5.2.2). In these analyses we included a model of the background that accounted for the contribution to gamma ray emissivity of HI and $H_2$, as explained in detail in § 5.2.3.

From our analyses it resulted that CTA will be largely able to distinguish between the primary spectra that we assumed, namely a power law spectra with index 2.4, a power law spectra with index 2.6, and a AMS-like spectrum. If the proton spectrum is steeper than the local one, CTA will be able to detect the cloud n. 877 with only 20 hours of observations. In particular we showed that 20 hours allow us to disentangle between a 2.4 and a 2.6 power law proton spectrum, even when taking into account extremely conservative systematic uncertainties. The considered 15% relative systematic error is the one estimated for the current generation of IACTs. This means that this result can be obtained even with the observation time already granted to the Galactic Plane Survey Key science project. However much larger observation time is needed to constrain a potential cutoff in the parent spectrum or an AMS-like spectrum. The hypothesis of the cosmic sea requires molecular clouds to show a spectrum like the local one, measured by AMS. Our simulations showed that with 200 hours of observation CTA can reconstruct few significant spectral points in the energy range between 200 GeV and few TeV. This result seems in apparent contradiction with the selection study based on differential sensitivity curves: as shown in 5.3 the AMS-like spectrum lies below the 200 hours sensitivity curve of the Southern array. We believe that this is due to the fact that the 3D analysis, that accounts for both spectral and morphological properties simultaneously, is more sensitive for extended sources than the first approximation approach used for the sensitivity curves. This requires more investigations though and it is one of the main goal of our future work. We would like to underline that this is a preliminary work, produced with a code that is currently under development and has just started to be tested by the CTA community.

For what concerns the hypothesis of a cut-off in the parent spectra, we considered four different values for $E_{co}$: 100 TeV, 500 TeV, 1 PeV and 10 PeV. The analysis of the simulated data showed that in this case the systematic errors are relevant. It turned out in fact that is possible to distinguish if there is a cut-off or not for the simulated cases at 100 TeV and 500 TeV, whereas the higher energies cut-off that we considered are practically indistinguishable from a pure power law. This is consistent with what we expected. If we roughly consider that the gamma rays carry $\sim$ 10-30% of the parent proton energy, a cut-off at 1 PeV of the primary spectrum would be visible at $\sim$ 100-300 TeV in the photon spectra, meaning at the limit of CTA capabilities.

In the view of the goodness of the results with the baseline configuration, we plan to rerun the simulations considering the threshold one. CTA in fact will start operating with a provisional configuration, but these results make us believe that CTA will provide decisive results even with the reduced array.

These results derive from a preliminary analysis, and many more consistency checks are required to reach final conclusion, but anyway they are very promising and invite us to continue and to refine our methods. First of all the background was modeled assuming only the hadronic contribution. We assumed and still believe that the leptonic counterpart will not be significant at TeV energies, and that it will be even less significant in the region of a molecular cloud, where the enhanced proton density favors the $pp \rightarrow \pi^0$ channel. It is important however to perform an analysis to actually evaluate the electronic contribution. We are willing to compute our own model, with the use of GALPROP or DRAGON codes ([Strong et al., 2009] and [Maccione et al., 2011]). The heavier nuclei contribution was considered negligible as well, but for a finer investigation it should be accounted. Furthermore Yang and other authors reported that *Fermi*-LAT observed a radial dependent spectrum of gammas coming from the diffuse gas. If this hypothesis will turn out to be correct also at higher energies, we should not neglect it. We assumed in fact for our background model that the diffuse gas emits as passive emitters when hit by CRs that follow a certain spectrum. In this work we assumed it to be an AMS-like spectrum, or better an extrapolation of the AMS spectrum at high energy, so someone could reasonably argue that this background is model dependent. The solid knowledge of the gas gamma ray emissivity in the Galactic plane that the CTA's GPS will provide, will serve not only to test if the GeV-observed behavior extend also at higher energies, but will help to build a model-independent background too. If the spectrum were harder than the AMS extrapolation, in fact, we might be underestimating its real contribution. In this work, to avoid this problem, we chose a cloud that dominates its line of sight, but with a clear knowledge of the gas emissivity and its distribution, this kind of analysis in principle could be performed for any selected molecular cloud. A refinement should be considered as well in the mass of the cloud, since it determines its flux. In this work we decided to consider the mass reported in the [Rice et al., 2016] catalog, that is derived from $H_2$, but we may want to include the HI fraction of the mass, since it contributes as well to the gamma emissivity and could raise the $M_5/d^2_{kpc}$ of a factor $\sim$0.1-0.15.

Moreover we modeled the cloud as a uniform disk, while there are many reasons to believe that molecular clouds are not uniform nor circular. We expect in fact the cloud to have a hierarchical structure, with a dense core that hosts star formation, and a more tenuous envelope, so maybe a Gaussian profile would result more appropriate. We are wishing to derive more detailed informations from future radio survey of the CO. This may be the case with the release of data from the Mopra Australian telescope [Burton et al., 2013], that is willing to produce a map of the Galactic plane with a spatial resolution of 35", that means twelve times better than the current [Dame et al., 2001] survey (0.125°). A finer map of the gas may lead to recognize the presence of substructures. This would be important for the precision of the analysis but it could allow us also to investigate the CTA capability in performing a spatial dependent spectroscopy. Consider a molecular cloud to be a perfect passive emitter: if a cosmic ray accelerator stands close to the cloud it would *illuminate* it by means of the high energy particles that it injects towards the cloud, and interact with the ambient gas. If the particles energy distribution is uniform in the cloud, there must be a 1:1 correspondence between the density profile of the gas and the gamma ray emissivity. Any discrepancy would

provide important hints on the accelerator location and on the CR propagation mechanism on the cloud size scale.

Any information derived from the clouds with CTA will be of fundamental importance. We are willing then to improve our analyses as suggested and to apply our methods to the other clouds of the catalog. One cloud was a good start to decide if the work was worth it, but we need more objects to strike to a conclusion. The final goal, in fact, is to probe the cosmic ray spectrum in the Galaxy and to understand if CRs are actually distributed in a uniform *sea* that resembles the local one, or if there is a spatial dependency of the CRs density. We want to stress again that molecular clouds above anything else are the perfect objects for this study because they have a higher hydrogen density than the diffuse gas and are restricted in size to some tens of parsecs. We selected several molecular clouds that are located in different part of the Milky Way (see table 5.1) and are promising to give good information on the galactic cosmic ray spectrum. Our analysis showed that CTA is promising to drive to important conclusions on clouds even with few observation hours, at least for the harder spectra. The extension of our study to the other clouds would definitely allow us to have a preliminary overview.

The detection of a spectrum harder than the AMS local in one cloud would mean that in that region there are more energetic particles than in our neighborhood. This could be caused by a nearby or an internal accelerator: for example we discussed that star forming region could be responsible of CRs acceleration. But if this behavior should show up in many other cases, we should maybe consider the idea that the Earth is actually in a special position, where there is a lack of accelerators or a sort of shielding. Clouds at different distances from the Galactic Center would prove or disprove the radial dependency of the CR spectrum,observed by Fermi (as in [Yang et al., 2016]). As the Fermi-LAT claimed, the CRs spectrum should harden toward the galactic center, and hence should be well visible by CTA. On the other hand a failure of CTA in detecting the gamma rays from one molecular cloud in its first operating hours, would suggest the presence there of a steeper spectrum of CRs. More observation hours would be then required for a deeper investigation. As we computed CTA would need at least 200 hours of observation to prove an AMS-like spectrum. More observation hours than the ones scheduled for the GPS project would be anyhow useful in order to test if there is a cut off in the CRs spectrum. We recall that the detection of a cut off at a certain energy would put an upper limit on the CRs energy and hence is of key importance in order to understand this particle origin and acceleration mechanism.

# Bibliography

[Abdo et al., 2011] Abdo, A., Ackermann, M., Ajello, M., Allafort, A., Ballet, J., Barbiellini, G., Bastieri, D., Bechtol, K., Bellazzini, R., Berenji, B., et al. (2011). Discovery of high-energy gamma-ray emission from the binary system psr b1259–63/ls 2883 around periastron with fermi. *The Astrophysical journal letters*, 736(1):L11.

[Abdo et al., 2009] Abdo, A., Ackermann, M., Ajello, M., Atwood, W., Axelsson, M., Baldini, L., Ballet, J., Barbiellini, G., Baring, M., Bastieri, D., et al. (2009). Fermi large area telescope observations of the crab pulsar and nebula. *The Astrophysical Journal*, 708(2):1254.

[Abdo et al., 2013] Abdo, A., Ajello, M., Allafort, A., Baldini, L., Ballet, J., Barbiellini, G., Baring, M., Bastieri, D., Belfiore, A., Bellazzini, R., et al. (2013). The second fermi large area telescope catalog of gamma-ray pulsars. *The Astrophysical Journal Supplement Series*, 208(2):17.

[Abramowski et al., 2016] Abramowski, A., Aharonian, F., Benkhali, F. A., Akhperjanian, A., Angüner, E., Backes, M., Balzer, A., Becherini, Y., Tjus, J. B., Berge, D., et al. (2016). Acceleration of petaelectronvolt protons in the galactic centre. *arXiv preprint arXiv:1603.07730*.

[Acciari et al., 2011] Acciari, V., Aliu, E., Arlen, T., Aune, T., Beilicke, M., Benbow, W., Bradbury, S., Buckley, J., Bugaev, V., Byrum, K., et al. (2011). Discovery of tev gamma-ray emission from tycho's supernova remnant. *The Astrophysical Journal Letters*, 730(2):L20.

[Ackermann et al., 2012a] Ackermann, M., Ajello, M., Allafort, A., Baldini, L., Ballet, J., Barbiellini, G., Bastieri, D., Bechtol, K., Bellazzini, R., Berenji, B., et al. (2012a). Fermi large area telescope study of cosmic rays and the interstellar medium in nearby molecular clouds. *The Astrophysical Journal*, 755(1):22.

[Ackermann et al., 2012b] Ackermann, M., Ajello, M., Atwood, W., Baldini, L., Ballet, J., Barbiellini, G., Bastieri, D., Bechtol, K., Bellazzini, R., Berenji, B., et al. (2012b). Fermi-lat observations of the diffuse $\gamma$-ray emission: Implications for cosmic rays and the interstellar medium. *The Astrophysical Journal*, 750(1):3.

[Adriani et al., 2011] Adriani, O., Barbarino, G., Bazilevskaya, G., Bellotti, R., Boezio, M., Bogomolov, E., Bonechi, L., Bongi, M., Bonvicini, V., Borisov, S., et al. (2011). Pamela measurements of cosmic-ray proton and helium spectra. *arXiv preprint arXiv:1103.4055*.

[Aguilar et al., 2015] Aguilar, M., Aisa, D., Alpat, B., Alvino, A., Ambrosi, G., Andeen, K., Arruda, L., Attig, N., Azzarello, P., Bachlechner, A., et al. (2015). Precision measurement of the proton flux in primary cosmic rays from rigidity 1 gv to 1.8 tv with the alpha magnetic spectrometer on the international space station. *Physical review letters*, 114(17):171103.

[Aharonian, 1991] Aharonian, F. (1991). Very high and ultra-high-energy gamma-rays from giant molecular clouds. *Astrophysics and Space Science*, 180(2):305–320.

[Aharonian et al., 2006] Aharonian, F., Akhperjanian, A., Bazer-Bachi, A., Beilicke, M., Benbow, W., Berge, D., Bernlöhr, K., Boisson, C., Bolz, O., Borrel, V., et al. (2006). Observations of the crab nebula with hess. *Astronomy & Astrophysics*, 457(3):899–915.

[Aharonian et al., 2007] Aharonian, F., Akhperjanian, A., Bazer-Bachi, A., Beilicke, M., Benbow, W., Berge, D., Bernlöhr, K., Boisson, C., Bolz, O., Borrel, V., et al. (2007). Primary particle acceleration above 100 tev in the shell-type supernova remnant rx j1713. 7-3946 with deep hess observations. *Astronomy & Astrophysics*, 464(1):235–243.

[Aharonian et al., 2004] Aharonian, F., Akhperjanian, A., Beilicke, M., Bernlöhr, K., Börst, H.-G., Bojahr, H., Bolz, O., Coarasa, T., Contreras, J., Cortina, J., et al. (2004). The crab nebula and pulsar between 500 gev and 80 tev: observations with the hegra stereoscopic air cerenkov telescopes. *The Astrophysical Journal*, 614(2):897.

[Aharonian et al., 2013] Aharonian, F., Bergström, L., Dermer, C., and Walter, R. (2013). *Astrophysics at Very High Energies*. Springer.

[Aharonian, 2004] Aharonian, F. A. (2004). *Very high energy cosmic gamma radiation: a crucial window on the extreme Universe*. World Scientific.

[Aleksić et al., 2015] Aleksić, J., Ansoldi, S., Antonelli, L., Antoranz, P., Babic, A., Bangale, P., Barrio, J., González, J. B., Bednarek, W., Bernardini, E., et al. (2015). Measurement of the crab nebula spectrum over three decades in energy with the magic telescopes. *Journal of High Energy Astrophysics*, 5:30–38.

[Aleksić et al., 2010] Aleksić, J., Antonelli, L., Antoranz, P., Backes, M., Baixeras, C., Barrio, J., Bastieri, D., González, J. B., Bednarek, W., Berdyugin, A., et al. (2010). Magic constraints on $\gamma$-ray emission from cygnus x-3. *The Astrophysical Journal*, 721(1):843.

[Ambrogi et al., 2016] Ambrogi, L., Wilhelmi, E. D. O., and Aharonian, F. (2016). On the potential of atmospheric cherenkov telescope arrays for resolving tev gamma-ray sources in the galactic plane. *Astroparticle Physics*, 80:22–33.

[Atoyan and Aharonian, 1999] Atoyan, A. and Aharonian, F. (1999). Modelling of the non-thermal flares in the galactic microquasar grs 1915+ 105. *Monthly Notices of the Royal Astronomical Society*, 302(2):253–276.

[Baade and Zwicky, 1934] Baade, W. and Zwicky, F. (1934). Remarks on super-novae and cosmic rays. *Physical Review*, 46(1):76.

[Bekhti et al., 2016] Bekhti, N. B., Flöer, L., Keller, R., Kerp, J., Lenz, D., Winkel, B., Bailin, J., Calabretta, M., Dedes, L., Ford, H., et al. (2016). Hi4pi: a full-sky h i survey based on ebhis and gass. *Astronomy & Astrophysics*, 594:A116.

[Bell et al., 2013] Bell, A., Schure, K., Reville, B., and Giacinti, G. (2013). Cosmic-ray acceleration and escape from supernova remnants. *Monthly Notices of the Royal Astronomical Society*, 431(1):415–429.

[Bignami and Caraveo, 1996] Bignami, G. F. and Caraveo, P. A. (1996). Geminga: its phenomenology, its fraternity, and its physics. *Annual Review of Astronomy and Astrophysics*, 34(1):331–381.

[Binns et al., 2008] Binns, W., Wiedenbeck, M. E., Arnould, M., Cummings, A. C., de Nolfo, G. A., Goriely, S., Israel, M. H., Leske, R. A., Mewaldt, R. A., Stone, E., et al. (2008). The ob association origin of galactic cosmic rays. *New Astronomy Reviews*, 52(7):427–430.

[Blasi, 2013] Blasi, P. (2013). The origin of galactic cosmic rays. *The Astronomy and Astrophysics Review*, 21(1):70.

[Blumenthal and Gould, 1970] Blumenthal, G. R. and Gould, R. J. (1970). Bremsstrahlung, synchrotron radiation, and compton scattering of high-energy electrons traversing dilute gases. *Reviews of Modern Physics*, 42(2):237.

[Bolatto et al., 2013] Bolatto, A. D., Wolfire, M., and Leroy, A. K. (2013). The co-to-h2 conversion factor. *Annual Review of Astronomy and Astrophysics*, 51:207–268.

[Brecher et al., 1983] Brecher, K., Fesen, R., Maran, S., and Brandt, J. (1983). Ancient records and the crab nebula supernova. *The Observatory*, 103:106–113.

[Burton et al., 2013] Burton, M. G., Braiding, C., Glück, C., Goldsmith, P., Hawkes, J., Hollenbach, D. J., Kulesa, C., Martin, C. L., Pineda, J. L., Rowell, G., et al. (2013). The mopra southern galactic plane co survey. *Publications of the Astronomical Society of Australia*, 30.

[Caraveo, 2014] Caraveo, P. A. (2014). Gamma-ray pulsar revolution. *Annual Review of Astronomy and Astrophysics*, 52:211–250.

[Cardillo et al., 2014] Cardillo, M., Tavani, M., Giuliani, A., Yoshiike, S., Sano, H., Fukuda, T., Fukui, Y., Castelletti, G., and Dubner, G. (2014). The supernova remnant w44: Confirmations and challenges for cosmic-ray acceleration. *Astronomy & Astrophysics*, 565:A74.

[Casandjian et al., 2015] Casandjian, J.-M. et al. (2015). The fermi-lat model of interstellar emission for standard point source analysis. *arXiv preprint arXiv:1502.07210*.

[Casanova et al., 2010] Casanova, S., Aharonian, F. A., Fukui, Y., Gabici, S., Jones, D. I., Kawamura, A., Onishi, T., Rowell, G., Sano, H., Torii, K., et al. (2010). Molecular clouds as cosmic-ray barometers. *Publications of the Astronomical Society of Japan*, 62(3):769–777.

[Clemens, 1985] Clemens, D. P. (1985). Massachusetts-stony brook galactic plane co survey-the galactic disk rotation curve. *The Astrophysical Journal*, 295:422–428.

[Crusius and Schlickeiser, 1988] Crusius, A. and Schlickeiser, R. (1988). Synchrotron radiation in a thermal plasma with large-scale random magnetic fields. *Astronomy and Astrophysics*, 196:327–337.

[Dame et al., 2001] Dame, T. M., Hartmann, D., and Thaddeus, P. (2001). The milky way in molecular clouds: a new complete co survey. *The Astrophysical Journal*, 547(2):792.

[Diehl et al., 2006] Diehl, R., Halloin, H., Kretschmer, K., Lichti, G. G., Schönfelder, V., Strong, A. W., Von Kienlin, A., Wang, W., Jean, P., Knödlseder, J., et al. (2006). Radioactive 26al and massive stars in the galaxy. *arXiv preprint astro-ph/0601015*.

[Donath et al., 2017] Donath, A., Brun, F., Chaves, R. C., Deil, C., Marandon, V., Terrier, R., and collaboration, H. (2017). The hess galactic plane survey. In *AIP Conference Proceedings*, volume 1792, page 040001. AIP Publishing.

[Drury, 1983] Drury, L. O. (1983). An introduction to the theory of diffusive shock acceleration of energetic particles in tenuous plasmas. *Reports on Progress in Physics*, 46(8):973.

[F. Hess, 1912] F. Hess, V. (1912). Über Beobachtungen der durchdringenden Strahlung bei sieben Freiballonfahrten. *Physikalische Zeitschrift*, 13:1084–1091.

[Funk, 2015] Funk, S. (2015). Ground-and space-based gamma-ray astronomy. *Annual Review of Nuclear and Particle Science*, 65:245–277.

[Funk et al., 2013] Funk, S., Hinton, J., Consortium, C., et al. (2013). Comparison of fermi-lat and cta in the region between 10–100gev. *Astroparticle Physics*, 43:348–355.

[Gaisser et al., 2016] Gaisser, T. K., Engel, R., and Resconi, E. (2016). *Cosmic rays and particle physics*. Cambridge University Press.

[García et al., 2014] García, P., Bronfman, L., Nyman, L.-Å., Dame, T., and Luna, A. (2014). Giant molecular clouds and massive star formation in the southern milky way. *The Astrophysical Journal Supplement Series*, 212(1):2.

[HESS Collaboration et al., 2016] HESS Collaboration, H., Abdalla, H., Abramowski, A., Aharonian, F., Benkhali, F. A., Akhperjanian, A., Andersson, T., Angüner, E., Arakawa, M., Arrieta, M., et al. (2016). Deeper hess observations of vela junior (rx j0852. 0-4622): morphology studies and resolved spectroscopy. *arXiv preprint arXiv:1611.01863*.

[Higdon and Lingenfelter, 2005] Higdon, J. and Lingenfelter, R. (2005). Ob associations, supernova-generated superbubbles, and the source of cosmic rays. *The Astrophysical Journal*, 628(2):738.

[Hillas, 2005] Hillas, A. (2005). Can diffusive shock acceleration in supernova remnants account for high-energy galactic cosmic rays? *Journal of Physics G: Nuclear and Particle Physics*, 31(5):R95.

[Hinton et al., 2008] Hinton, J., Skilton, J., Funk, S., Brucker, J., Aharonian, F., Dubus, G., Fiasson, A., Gallant, Y., Hofmann, W., Marcowith, A., et al. (2008). Hess j0632+ 057: A new gamma-ray binary? *The Astrophysical journal letters*, 690(2):L101.

[Huang et al., 2007] Huang, C.-Y., Park, S.-E., Pohl, M., and Daniels, C. (2007). Gamma-rays produced in cosmic-ray interactions and the tev-band spectrum of rx j1713. 7-3946. *Astroparticle Physics*, 27(5):429–439.

[Hunter et al., 1997] Hunter, S. D., Bertsch, D., Catelli, J., Dame, T., Digel, S., Dingus, B., Esposito, J., Fichtel, C., Hartman, R., Kanbach, G., et al. (1997). Egret observations of the diffuse gamma-ray emission from the galactic plane. *The Astrophysical Journal*, 481(1):205.

[Jones et al., 2012] Jones, P., Burton, M., Cunningham, M., Requena-Torres, M., Menten, K., Schilke, P., Belloche, A., Leurini, S., Martín-Pintado, J., Ott, J., et al. (2012). Spectral imaging of the central molecular zone in multiple 3-mm molecular lines. *Monthly Notices of the Royal Astronomical Society*, 419(4):2961–2986.

[Kafexhiu et al., 2014] Kafexhiu, E., Aharonian, F., Taylor, A. M., and Vila, G. S. (2014). Parametrization of gamma-ray production cross sections for p p interactions in a broad proton energy range from the kinematic threshold to pev energies. *Physical Review D*, 90(12):123014.

[Keane, 2011] Keane, E. F. (2011). On the birthrates of galactic neutron stars. In *The Transient Radio Sky*, pages 41–59. Springer.

[Khangulyan et al., 2007] Khangulyan, D., Aharonian, F., and Bosch-Ramon, V. (2007). On the formation of tev radiation in ls 5039. *Monthly Notices of the Royal Astronomical Society*, 383(2):467–478.

[Kippenhahn et al., 1990] Kippenhahn, R., Weigert, A., and Weiss, A. (1990). *Stellar structure and evolution*, volume 282. Springer.

[Knödlseder et al., 2016] Knödlseder, J., Mayer, M., Deil, C., Cayrou, J.-B., Owen, E., Kelley-Hoskins, N., Lu, C.-C., Buehler, R., Forest, F., Louge, T., et al. (2016). Gammalib and ctools-a software framework for the analysis of astronomical gamma-ray data. *Astronomy & Astrophysics*, 593:A1.

[Lingenfelter, 2017] Lingenfelter, R. E. (2017). Cosmic rays from supernova remnants and superbubbles. *Advances in Space Research*.

[Longair, 2011] Longair, M. S. (2011). *High energy astrophysics*. Cambridge university press.

[Luna et al., 2006] Luna, A., Bronfman, L., Carrasco, L., and May, J. (2006). Molecular gas, kinematics, and ob star formation in the spiral arms of the southern milky way. *The Astrophysical Journal*, 641(2):938.

[Maccione et al., 2011] Maccione, L., Evoli, C., Gaggero, D., and Grasso, D. (2011). Dragon: Galactic cosmic ray diffusion code. *Astrophysics source code library*.

[Ohm et al., 2013] Ohm, S., Hinton, J., and White, R. (2013). $\gamma$-ray emission from the westerlund 1 region. *Monthly Notices of the Royal Astronomical Society*, 434(3):2289–2294.

[Pacholczyk, 1977] Pacholczyk, A. (1977). Radio galaxies.

[Panov et al., 2009] Panov, A., Adams, J., Ahn, H., Bashinzhagyan, G., Watts, J., Wefel, J., Wu, J., Ganel, O., Guzik, T., Zatsepin, V., et al. (2009). Energy spectra of abundant nuclei of primary cosmic rays from the data of atic-2 experiment: Final results. *Bulletin of the Russian Academy of Sciences: Physics*, 73(5):564–567.

[Patrignani et al., 2016] Patrignani, C. et al. (2016). Review of Particle Physics. *Chin. Phys.*, C40(10):100001.

[Poppel, 1997] Poppel, W. (1997). The gould belt system and the local interstellar medium. *Fundamentals of Cosmic Physics*, 18:1–271.

[Reid et al., 2016] Reid, M., Dame, T., Menten, K., and Brunthaler, A. (2016). A parallax-based distance estimator for spiral arm sources. *The Astrophysical Journal*, 823(2):77.

[Rice et al., 2016] Rice, T. S., Goodman, A. A., Bergin, E. A., Beaumont, C., and Dame, T. M. (2016). A uniform catalog of molecular clouds in the milky way. *The Astrophysical Journal*, 822(1):52.

[Roman-Duval et al., 2009] Roman-Duval, J., Jackson, J. M., Heyer, M., Johnson, A., Rathborne, J., Shah, R., and Simon, R. (2009). Kinematic distances to molecular clouds identified in the galactic ring survey. *The Astrophysical Journal*, 699(2):1153.

[Rosolowsky et al., 2008] Rosolowsky, E., Pineda, J., Kauffmann, J., and Goodman, A. (2008). Structural analysis of molecular clouds: Dendrograms. *The Astrophysical Journal*, 679(2):1338.

[Schlickeiser, 2013] Schlickeiser, R. (2013). *Cosmic ray astrophysics*. Springer Science & Business Media.

[Shull Jr, 1988] Shull Jr, P. (1988). Interstellar magnetic fields: Observation and theory.

[Strong et al., 2009] Strong, A., Moskalenko, I., Porter, T., Johannesson, G., Orlando, E., and Digel, S. (2009). The galprop cosmic-ray propagation code. *arXiv preprint arXiv:0907.0559*.

[Tielens, 2005] Tielens, A. G. (2005). *The physics and chemistry of the interstellar medium*. Cambridge University Press.

[Uchiyama et al., 2012] Uchiyama, Y., FUNk, S., Katagiri, H., Katsuta, J., Lemoine-Goumard, M., Tajima, H., TANAkA, T., and Torres, D. F. (2012). Fermi large area telescope discovery of gev gamma-ray emission from the vicinity of snr w44. *The Astrophysical journal letters*, 749(2):L35.

[Wakely and Horan, 2008] Wakely, S. P. and Horan, D. (2008). TeVCat: An online catalog for Very High Energy Gamma-Ray Astronomy. *International Cosmic Ray Conference*, 3:1341–1344.

[Werner et al., 2004] Werner, M., Roellig, T., Low, F., Rieke, G., Rieke, M., Hoffmann, W., Young, E., Houck, J., Brandl, B., Fazio, G., et al. (2004). The spitzer space telescope mission. *The Astrophysical Journal Supplement Series*, 154(1):1.

[Yang et al., 2016] Yang, R., Aharonian, F., and Evoli, C. (2016). Radial distribution of the diffuse $\gamma$-ray emissivity in the galactic disk. *Physical Review D*, 93(12):123007.

[Yang et al., 2014] Yang, R.-z., de Oña Wilhelmi, E., and Aharonian, F. (2014). Probing cosmic rays in nearby giant molecular clouds with the fermi large area telescope. *Astronomy & Astrophysics*, 566:A142.

[Yang et al., 2015] Yang, R.-z., Jones, D. I., and Aharonian, F. (2015). Fermi-lat observations of the sagittarius b complex. *Astronomy & Astrophysics*, 580:A90.

[Yoon et al., 2011] Yoon, Y., Ahn, H., Allison, P., Bagliesi, M., Beatty, J., Bigongiari, G., Boyle, P., Childers, J., Conklin, N., Coutu, S., et al. (2011). Cosmic-ray proton and helium spectra from the first cream flight. *The Astrophysical Journal*, 728(2):122.

This research made use of ctools, a community-developed analysis package for Imaging Air Cherenkov Telescope data. ctools is based on GammaLib, a community-developed toolbox for the high-level analysis of astronomical gamma-ray data, see http://cta.irap.omp.eu/ctools/

This research made use of Astropy, a community-developed core Python package for Astronomy (Astropy Collaboration, 2013).